CHEMICAL AND BIOLOGICAL TREATMENT OF ACID MINE DRAINAGE FOR THE REMOVAL OF HEAVY METALS AND ACIDITY

Harry R. Diz

Dissertation submitted to the Faculty of the

Virginia Polytechnic Institute and State University

in partial fulfillment of the requirements for the degree of

DOCTOR OF PHILOSOPHY
in
Civil Engineering

John T. Novak, Ph.D., Chair
Donald S. Cherry, Ph.D.
William R. Knocke, Ph.D.
Nancy G. Love, Ph.D.
J. Donald Rimstidt, Ph.D.

August 11, 1997
Blacksburg, Virginia

Keywords: iron biooxidation, iron precipitation, iron removal technology, acid mine drainage

CHEMICAL AND BIOLOGICAL TREATMENT OF ACID MINE DRAINAGE FOR THE REMOVAL OF HEAVY METALS AND ACIDITY

Harry R. Diz

ABSTRACT

This dissertation reports the design of a process (patent pending) to remove iron from acid mine drainage (AMD) without the formation of metal hydroxide sludge. The system includes the oxidation of ferrous iron in a packed bed bioreactor, the precipitation of iron within a fluidized bed, the removal of manganese and heavy metals (Cu, Ni, Zn) in a trickling filter at high (>9) pH, with final neutralization in a carbonate bed. The technique avoided the generation of iron oxyhydroxide sludge.

In the packed bed bioreactor, maximum substrate oxidation rate ($R_{,max}$) was 1500 mg L^{-1} h^{-1} at dilution rates of 2 h^{-1}, with oxidation efficiency at 98%. The half-saturation constant (similar to a K_s) was 6 mg L^{-1}. The oxidation rate was affected by dissolved oxygen below 2 mg L^{-1}, with a Monod-type K_o for DO of 0.33 mg L^{-1}. Temperature had a significant effect on oxidation rate, but pH (2.0 to 3.25) and supplemental CO_2 did not affect oxidation rates.

Iron hydroxide precipitation was not instantaneous when base was added at a OH/Fe ratio of less than 3. Induction time was found to be a function of pH, sulfate concentration and iron concentration, with a multiple R^2 of 0.84. Aqueous [Al (III)] and [Mn (II)] did not significantly ($\alpha = 0.05$) affect induction time over the range of concentrations investigated.

When specific loading to the fluidized bed reactor exceeded 0.20 mg Fe m^{-2} h^{-1}, dispersed iron particulates formed leading to a turbid effluent. Reactor pH determined the minimum iron concentration in the effluent, with an optimal at pH 3.5. Total iron removals of 98% were achieved in the fluidized bed with effluent [Fe] below 10 mg L^{-1}. Further iron removal occurred within the calcium carbonate bed.

Heavy metals were removed both in the fluidized bed reactor as well as in the trickling filter. Oxidation at pH >9 caused manganese to precipitate (96% removal); removals of copper, nickel, and zinc were due primarily to sorption onto oxide surfaces. Removals averaged 97% for copper, 70% for nickel and 94% for zinc.

The treatment strategy produced an effluent relatively free of iron (< 3 mg/L), without the formation of iron sludge and may be suitable for AMD seeps, drainage from acidic tailings ponds, active mine effluent, and acidic iron-rich industrial wastewater.

DEDICATION

It would not have been possible to embark on this project, nor to sustain the effort required to complete it, without the love and support of my wife, Gay. More than five years ago, it was her boldness, her confidence in the future, and her love of live-long learning that led to my embarking on this effort. She has provided greater support and loyalty than was perhaps deserved, and I can only hope to live up to her expectations..

ACKNOWLEDGEMENTS

Additionally, I would like to express appreciation to my major advisor, Dr. John T. Novak, who provided remarkable assistance and support throughout this project, and over the course of the doctoral program. Dr. Novak is an unusual individual who is able to lead without controlling, to inspire without pontificating, and to relate to those less educated and experienced without condescension. His frankness and openness have made it a pleasure to have him serve as major advisor.

I would like to recognize Dr. Donald Cherry for having introduced me to the serious environmental damage caused by acid mine drainage, and for his good-hearted companionship on journeys into the field to investigate those effects.

TABLE OF CONTENTS

LIST OF FIGURES

ix

LIST OF TABLES

Chapter 1 Introduction

Acidic, metal-laden waters are continuously discharged from abandoned mine lands (AML), and active mining sites where the wastes contain iron sulfide minerals. In most cases waters from AML are discharged to the environment with little or no treatment.

A survey of coal mining activities in the eastern US conducted by the USEPA (1976) revealed that acid mine drainage (AMD) contained iron, aluminum, and manganese at concentrations up to 440 mg/L, 270 mg/L, and 125 mg/L, respectively, and sulfate up to 4,000 mg/L, with pH as low as 2.2. There is considerable variation, however, in AMD characteristics from coal and other sources. These dissolved constituents are typically the result of the chemical and biological weathering of sulfide minerals, predominately pyrite and marcasite (FeS_2), but also including pyrrhotite ($Fe_{1-x}S$), chalcopyrite ($CuFeS_2$), and other sulfide mineral salts of heavy metals (Barrett et al., 1993). Pyrite and other sulfides are frequently associated with coal deposits.

In the presence of moisture, abiotic oxidation of pyritic minerals by O_2 and/or ferric iron results in the production of sulfuric acid, and the release of metal ions from the mineral crystal lattice. This process occurs at a higher rate in the presence of certain microorganisms (Nordstrom, 1982). Some species of bacteria are known to obtain energy from the oxidation of ferrous iron.

The pH of AMD may be as low as 2.2 (Hedin and Watzlaf, 1994), and isolated hard rock mine discharges have been measured below that value (Rimstidt, 1995). Organisms exist which survive in these extreme acid conditions, most notably *Thiobacillus ferrooxidans*, which has a pH optimum in the range of pH 1.5 to 3.5, while other microorganisms are known to tolerate low pH conditions (Kuenen et al., 1992).

The most abundant metal released from pyritic minerals in a soluble state is reduced iron, which subsequently oxidizes and precipitates as oxyhydroxides, releasing H^+ and thus creating a second stage of acid generation (Nordstrom, 1982). Iron precipitation generates colloids and fine particulates which settle in aquatic zones of low velocity. Higher stream velocities may carry the precipitates vast distances downstream from the source of the AMD. Certain elements such as arsenic, copper, nickel, and zinc may be present in AMD and are toxic at very low concentrations and/or may bioaccumulate to toxic levels (Pratt, 1990; Mac et al., 1984). Pelagic and benthic organisms are exposed to these metal-rich precipitates by direct physical contact and/or uptake of sediments.

Depending on the pH, dissolved oxygen (DO) concentration, microorganism abundance, and mix of dissolved inorganic species, a wide variety of colors and precipitates may be formed in AMD. It is not uncommon to see bluish-green water some distance downstream from an AMD source with yellow and reddish-brown precipitates. These effects most probably reflect the various oxidation states of iron, and a dynamic flux of compounds formed among iron, aluminum, calcium, and potassium with oxyhydroxides, sulfates, and chlorides.

Iron and manganese oxyhydroxides tend to coat surfaces in stream beds. These oxides are known to be strong scavengers which remove both cations and anions from solution (Singh and Subramanian, 1986). This removal may be reversible, depending on the type and strength of bonds formed between the sorbate and sorbent. For many sorbed species, a subsequent decrease in pH will release cations from the surface (Stumm, 1992). Thus metal-rich sediments may act as sources as well as sinks of heavy metals, even in oxygenated streams.

Various approaches have been used to ameliorate the generation of AMD and its effects. Control at the source has received much attention. The oxidation of pyrite exposed to the atmosphere is strongly favored thermodynamically, and while it is a slow process, attempts to avoid oxidation by preventing moisture, oxygen, and microorganisms from reaching the disturbed pyrite surfaces have met with little success (Unz and Dietz, 1986).

The bulk dumping of limestone in streams was once thought to be capable of neutralizing the acidity of the water, but the limestone became coated with iron oxyhydroxides, slowing its dissolution and thus limiting its effect on stream pH (Hedin and Watzlaf ,1994). It was found that pH neutralization by limestone succeeded so long as the water was anoxic. However, once the neutralized water was exposed to the atmosphere, iron oxidized, hydrolyzed, and acid was generated. Since the iron was left to precipitate in the stream, the lack of an iron removal mechanism was a significant shortcoming of this approach.

When anoxic limestone drains were combined with natural or constructed wetlands, some treatment success was achieved (Wildeman et al., 1994). Properly sized wetlands succeed by maintaining a reducing environment with a population of sulfate-reducing bacteria. Macrophytes contribute by supplying an on-going source of organic carbon for the sulfate-reducers which convert some of the dissolved sulfate to sulfide. The subsequent precipitation of ferrous sulfide results in a decrease in dissolved solids. The generation of ammonia also aids in precipitation of certain heavy metals by elevating pH (Gusek, 1995). However, wetlands have shown a limited ability to cope with intermittent low pH events, and can be overwhelmed by high flow (Tarutis and Unz, 1995). The treatment efficiency of sulfate-reducers is largely a function of the presence of an organic carbon input, appropriate pH (above pH 6), and temperature. Some metals, such as manganese, are not effectively removed by wetlands (Maillacheruvu et al., 1993).

Recent work with algal-cyanobacterial consortia has shown promise in the removal of metals (Vatcharapijarn et al., 1994). Removals appear to be the result of two phenomena: the production of extracellular biopolymers which function by sorption/cation exchange, and/or the creation of micro-environments with locally high dissolved oxygen concentration (DO) and high pH resulting from photosynthesis. These conditions result in the precipitation of oxides of metals which are slow to oxidize under acidic or neutral pH conditions. In particular, Mn(II) will rapidly oxidize to Mn(IV) above pH 9 forming insoluble $MnO_{x(s)}$. An obvious advantage of algal consortia is that they are autotrophs, and thus do not require an input of electron donor or carbon source.

Engineered treatment systems have generally been employed only at active mine sites. These typically consist of pH adjustment with caustic soda (NaOH) or lime (CaO), followed by settling ponds. New source performance standards developed for National Pollutant Discharge Elimination System (NPDES) permits by the USEPA for the coal mining industry stipulate total iron of 3.0 mg L^{-1}, total manganese of 2.0 mg L^{-1}, total suspended solids (TSS) of 35 mg L^{-1}, and pH between 6.0 and 9.0 units (30 day averages) (USEPA, 1976) with similar requirements imposed by The Surface Mining Control and Reclamation Act of 1977.

Work in Great Britain and Japan used combined biological and chemical systems for treatment of acid mine drainage at active or recently abandoned mine sites. An activated sludge system was evaluated in England in the mid-60's with little success (Whitesell et al.*,* 1971). The system relied on heterotrophs and required recycle of sludge with high concentrations of iron and low concentrations of biomass. In Japan, *T. ferrooxidans* was employed at an abandoned mine discharging 20 m^{3}min^{-1} of water with a pH of 1.6 containing 795 mg/L of total iron (Murayama et al.*.* 1987). The bacteria, sorbed to diatomaceous earth, rapidly oxidized ferrous iron in aeration basins with a hydraulic retention time (HRT) of 60 min. Ammonium phosphate was added as a nutrient. Following aeration, settling basins separated the biomass/diatomaceous earth from supernatant with the aid of polymer for biomass recycle. Supernatant containing dissolved ferric iron (pH < 2) was then aerated and neutralized with a calcium carbonate slurry to pH 4. Iron and arsenic compounds precipitated. Effluent contained 13 mg/L total Fe and 0.02 mg/L arsenic (reduced from 5.77 mg/L in the raw water). Total HRT in the system was approximately 8.5 h. The operational cost of treatment was approximately one-third that of the previous all-chemical process.   The cost reported was $0.32 per m^3 treated in 1983 US dollars.

The research described in this dissertation provides the foundation for the development of a new treatment technology (patent pending) for AMD and industrial wastewaters with similar characteristics.   First, the performance of a packed bed bioreactor for the oxidation of ferrous iron was investigated as a first stage in the sequential treatment system. Next, the precipitation kinetics and solubility of ferric sulfate solutions during neutralization with bicarbonate were explored, including the effects of those chemical species normally present in AMD. Insights into the mechanism of iron particle formation were gained, but development of a fundamental model of iron mineral formation was beyond the scope of this engineering study. Finally, the performance of a lab-scale multi-stage system for iron and acidity removal was studied, followed by an evaluation of the system's ability to remove selected heavy metals (Cu, Mn, Ni, and Zn) from solution.

LITERATURE CITED

Barrett, J., M. N. Hughes, G. I. Karavaiko, and P.A. Spencer. 1993. Metal Extraction by Bacterial Oxidation of Minerals. Ellis Horwood. New York. pp. 191.

Gusek, J. J. 1995. Passive-Treatment of Acid Mine Drainage: What is the Potential Bottom Line? Min. Engr. 47(3):250-253.

Hedin, R. S. and G. R. Watzlaf. 1992. The Effects of Anoxic Limestone Drains on Mine Water Chemistry. Proceedings of the International Land Reclamation and Mine Drainage Conference, Pittsburgh, PA. April 24-26, 1994. Pp. 185-194.

Kuenen, J. G. L. A. Robertson, and L. H. Tuovinen.. 1992. The Genera *Thiobacillus*, *Thiomicrospira*, and *Thiosphaera*. in The Prokaryotes, Second Edition. eds. Balows, A., H. G. Truper, M. Dworkin, W. Harder, and K. H. Schleifer. Springer-Verlag. New York. pp. 2638-2657.

Mac, M. J., C.C. Edsall, R. J. Hesselberg, R. E. Sayers, Jr. 1984. Flow Through Bioassay Measuring Bioaccumulation of Toxic Substances from Sediment. EPA-905/3-84-007.

Maillacheruvu, K.Y., G.F. Parkin, C.Y. Peng, W. Kuo, Z.I. Oonge, and V. Lebduschka. 1993. Sulfide Toxicity in Anaerobic Systems Fed Sulfate and Various Organics. Wat. Environ. Res. 65(2):100-109.

Murayama, T., Y. Konno, T. Sakata, and T. Imaizumi. 1987. Application of Immobilized *Thiobacillus ferrooxidans* for Large-Scale Treatment of Acid Mine Drainage. Meth. Enzymol. 36:530-49.

Nordstrom, D.K. 1982. Aqueous Pyrite Oxidation and the Consequent Formation of Secondary Iron Minerals (Chap. 3). in L.R. Hossaer, J. A. Kittrick, and D. F. Faming, eds., Acid Sulfate Weathering, Soil Science Soc. Amer., Madison, WI. pp. 37-56.

Pratt, J.R. 1990. Aquatic Community Response to Stress: Prediction and Detection of Adverse Effects. in Aquatic Toxicology and Risk Assessment: Thirteenth Volume, ASTM STP 1096, W.G. Landis and W.H. van der Schalie, Eds., American Society for Testing and Materials, Philadelphia, pp. 16-26.

Rimstidt, J. D. 1995. personal communication. Department of Geology, Virginia Polytechnic Institute and State University, Blacksburg, VA.

Singh, S.K., and V. Subramanian. 1986. Hydrous Fe and Mn Oxides - Scavengers of Heavy Metals in the Aquatic Environment. CRC Crit. Rev. Environ. Contr. 14(1): 33-90.

Stumm, W. 1992. Chemistry of the Solid-Water Interface. John Wiley & Sons, Inc. New York. pp. 428.

Tarutis, Jr., W. J. and R. F. Unz. 1995. Iron and Manganese Release in Coal Mine Drainage Wetland Microcosms. Wat. Sci. Technol. 32(3):187-192.

Unz, R. F. and J. M. Dietz. 1986. Biological Applications in the Treatment of Acidic Mine Drainages. in Biotechnology for the Mining, Metal-Refining, and Fossil Fuel Processing Industries. H. L. Erhlich and D. S. Holmes, Eds. John Wiley & Sons, Inc. New York. pp. 163-170.

USEPA. 1976. Development Document for Interim Final Effluent Limitations Guidelines and New Source Performance Standards for the Coal Mining Point Source Category. EPA 440/1-76/057a. pp.288.

Vatcharapijarn, Y., B. Graves, and J. Bender. 1994. Remediation of Mining Water with Microbial Mats. in Emerging Technology for Bioremediation of Metals. J. L. Means and R. E. Hinchee, Eds. Lewis Publishers, Boca Raton. pp.124-129.

Whitesell, Jr., L. ., R. L. Huddleston, and R. C. Allred. 1971. Microbiological Treatment of Acid Mine Waters. Water Pollution Control Research Series 14010 ENW 09/71, USEPA. p 78.

Wildeman, T. R., D. M. Updegraff, J. S. Reynolds, and J. L. Bolis. 1994. Passive Bioremediation of Metals from Water Using Reactors or Constructed Wetlands. in Emerging Technology for Bioremediation of Metals. J. L. Means and R. E. Hinchee, Eds. Lewis Publishers, Boca Raton. pp.13-25.

Chapter 2 . Performance of a Packed Bed Bioreactor for the Oxidation of Ferrous Iron in Simulated Acid Mine Drainage

INTRODUCTION

Acid mine drainage (AMD) from working and abandoned mines continues to be an important source of water pollution in the United States and around the world. The primary characteristics of AMD which cause concern are low pH, high specific conductivity, high concentrations of iron, aluminum, and manganese, and the variable presence of toxic heavy metals at trace levels.

Current treatment technologies for AMD are either inadequate or too expensive to be employed at most abandoned mine land (AML) sites which are sources of untreated AMD. Limestone employed for pH adjustment quickly becomes coated with iron oxyhydroxide, drastically reducing its dissolution rate. Constructed wetlands have been relatively successful in locations where topography and space are available, but potentially result in the creation of metal-contaminated soils and groundwater. At working mines, acidic drainage and wash waters are typically neutralized by the addition of sufficient lime or caustic soda to raise the pH above 9 to oxidize and precipitate iron, manganese, and other metals. The precipitated metal hydroxide is then allowed to settle in ponds while supernatant is discharged. Eventually, settling ponds fill with metal sludge and if contaminated with certain heavy metals would require disposal in a hazardous waste landfill. Also, metal hydroxide sludge can be costly to dewater.

A new technology under development (Figure 2.1) removes iron from AMD by means of ferric oxyhydroxide surface precipitation. The unit operations begin with the bio-oxidation of ferrous iron to ferric iron at low pH. The acidic, oxidized iron solution is then circulated through a fluidized bed in such a way as to promote surface precipitation while avoiding the unwanted generation of minute iron particles. The principle source of alkalinity for pH adjustment in the precipitation reactor is a limestone/dolomite bed through which the fluidized bed effluent is circulated to raise pH before re-injection into the fluidized bed. Separately, the iron-free water is re-circulated through a trickling filter with the addition of modest amounts of concentrated caustic soda to oxidize and precipitate manganese. While iron and manganese are typically the only metals included in National Pollutant Discharge Elimination System (NPDES) permits for coal mining operations, the various environments of low and high pH promote the removal of other heavy metals on newly formed iron and manganese-oxide surfaces which are well known to be strong scavengers of heavy metals (Singh and Subramanian, 1986).

In other industrial settings, ferric iron is a useful oxidant in several important industrial processes, such as the leaching of metals from sulfide mineral ores in heap processing, and the removal of hydrogen sulfide from off-gases. In both cases, ferric iron oxidizes reduced sulfur to either elemental sulfur or sulfate, in the process becoming

reduced to ferrous iron. A bioreactor system can be used to regenerate ferric iron from a ferrous sulfate solution.
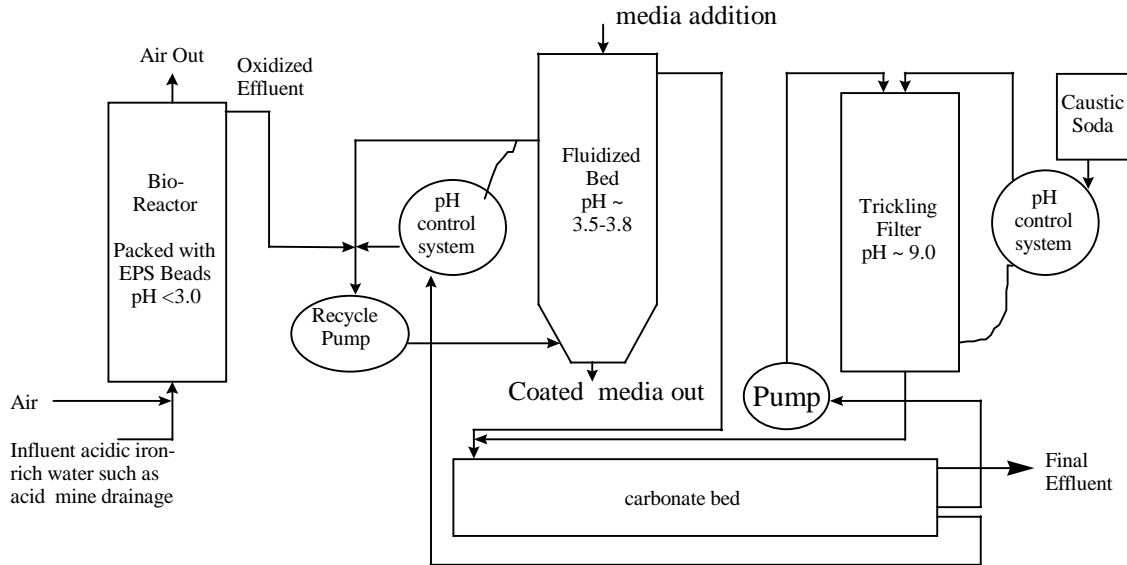
Figure 2.1. Schematic of integrated treatment system for the removal of heavy metals and acidity from acidic iron-rich waters without the formation of metal sludge.

A successful treatment technology for use on AML sites must be compact, inexpensive, and require little operational attention. This paper discusses the performance of the first stage of such a system: a lab-scale bioreactor for the oxidation of ferrous iron, and is one in a series of papers which report the design fundamentals of the prototype AMD treatment system.

BACKGROUND

Abiotic Iron Oxidation

Ferrous iron should not exist in any appreciable concentration in an oxic environment due to highly favorable thermodynamics for its oxidation in the presence of even low DO (Stumm and Morgan, 1981). As with many other natural processes, slow reaction rates rather than equilibrium conditions result in ferrous iron persisting under oxic conditions. Singer and Stumm (1970) found that below pH 3.5, the oxidation rate of ferrous iron by DO is given by the following rate law:

$$-d\,[\Sigma Fe^{2+}]/dt = k\,[\Sigma Fe^{2+}]\,P_{O2} \qquad (2\text{-}1)$$

where ΣFe^{2+} is the sum total of all ferrous species, k is a rate constant (sec^{-1} atm^{-1}), and P_{O2} is the partial pressure of oxygen (atm). In experimental studies, they found k to equal $10^{-8.78}$. Above pH 4.5, they found the rate to be a function of [OH$^-$] as well as P_{O2}.

In subsequent studies by Wehrli (1990) it was found that the oxidation rates of Fe^{2+} and its hydroxo complexes (Fe(OH)$^+$ and Fe(OH)$_2$) differed. As pH is increased and

the relative abundance of these complexes increases, the combined oxidation rate increases. However, in the realm of the current study (below pH 3.5), abiotic oxidation, with a half-life for ferrous iron of well in excess of months, was deemed unimportant.

Thiobacillus ferrooxidans Iron Oxidation

<u>Thermodynamics of Iron Oxidation and Creation of Biomass</u>

Starkey (1945) estimated that it would take 500 parts iron to produce 1 part biomass in autotrophic growth by iron-oxidizing bacteria, a yield of 0.002 g biomass per g iron oxidized. Temple and Colmer (1951) reported that 120 g of ferrous sulfate pentahydrate were consumed to produce 16 mg of fixed carbon. They stated that this was 3.2% energy utilization efficiency, and is equivalent to a yield of 0.00067 mg organic C per mg Fe.

Stumm and Morgan (1970) presented the thermodynamics of oxidation of ferrous iron by autotrophic bacteria. Electrons are transferred to oxygen according to

$$Fe^{2+} + \tfrac{1}{4} O_2 + H^+ = Fe^{3+} + \tfrac{1}{2} H_2O \qquad\qquad (2\text{-}2)$$

The free energy ($\Delta G°$) for this reaction is -10.6 kcal mole^{-1} of Fe II oxidized. Since standard free energies assume $[H^+] = 1$ M, adjustment to the bioreactor pH of 2.3 results in a free energy change of -7.5 kcal mole^{-1} of Fe II. Stumm and Morgan (1970) calculated that the synthesis of organic carbon in the form of glucose from carbon dioxide required 113 kcal mole^{-1} of carbon. They assumed a 36% energy assimilation efficiency and translated this into a yield of about 0.005 g organic carbon synthesized per gram of iron oxidized. If carbon constitutes approximately half the mass of protein, the theoretical yield (Y) for ferrous iron oxidation by an autotroph should be about 0.01 g protein/gram of Fe oxidized. This low yield would result in low biomass production related to iron oxidation. Sludge disposal would therefore not be expected to be an operational requirement.

Monod Kinetics as Applied to a Packed Bed Iron Bioreactor

It has been observed that *T. ferrooxidans* adheres to the surface of mineral particles more strongly than to the surfaces of other cells, and does not produce extra-cellular slimes (Arredondo et al., 1994; Grishin and Tuovinen, 1989; Nikolov and Karamanev, 1990a; Wichlacz and Unz, 1985). Therefore, cell division results in a loss of cells to the liquid medium once a steady state layer has formed on available mineral surfaces. At the high dilution rates anticipated in this series of studies, suspended biomass would be expected to be quite low since cells released from the attached biofilm surface would be removed from the reactor in less than the doubling time of about 7 h reported for these organisms (Silverman and Lundgren, 1959).

The Monod model is a curve fitting procedure using two parameters to define the saturation type function: a maximum rate value (q_{max}), and a half-saturation constant (K_s) which defines the shape of the curve as it transitions from first order to zero order kinetics. Since the configuration of the reactors used in this study did not conform to ideal complete mix designs, and in order not to imply an equivalence to Monod

parameters, the parameters used in this study will be R_{max}, defined as the maximum substrate oxidation rate for the reactor when the asymptotic trend is extrapolated to infinity, and a half-saturation constant, K_s^*, defined simply as that substrate concentration at which the substrate oxidation rate would be one-half of the maximum estimated value. These parameters relate to the reactor performance, and do not imply values corresponding to the intrinsic metabolic capability of individual bacterial cells.

Substrate and Product Inhibition in *T. ferrooxidans*

Jensen and Webb (1995) presented a comprehensive review of studies of inhibition by both ferric and ferrous iron in solution. They reported that Kumar and Gandhi (1990) demonstrated inhibition of Fe(II) oxidation by *T. ferrooxidans* due to high levels (20 g L^{-1}) of ferric iron. LaCombe Barron and Lueking (1990) found that Fe(II) was inhibitory above 2 g L^{-1}. Curutchet et al. (1992) found that Fe(III) concentrations above 2 g L^{-1} inhibited growth. Jones and Kelly (1983) conducted an extensive study of product and substrate inhibition at pH 1.6 and concluded that the kinetics of ferrous iron oxidation were exceedingly complex when influent feed contained 20 mM Fe(II) (1,116 mg L^{-1}) in the presence of 10 to 47 mM of Fe(III) (558 to 2,623 mg L^{-1}). They concluded that substrate inhibition was unlikely below about 100 mM Fe (II), but that competitive product inhibition was "inherent" in chemostat cultures, resulting in an increase in K_s.

Since these studies were restricted to iron concentrations below 10 mM, it was not believed that inhibition would become an important phenomenon.

<center>OBJECTIVES</center>

The goal of this research was to investigate the performance of a packed bed bioreactor for the oxidation of ferrous iron using an open culture of immobilized chemolithotrophic bacteria. The range of physical and chemical conditions typical of AMD sites was studied, including fluctuations in substrate loading, culture pH, dissolved oxygen (DO) concentration, supplementation with carbon dioxide gas, and variation in temperature.

Specifically, the research was intended to answer these questions:

1. What are the loading and detention time limitations for a packed bed bioreactor employing expanded polystyrene (EPS) beads as a surface for immobilization of iron-oxidizing bacteria?
2. Can performance be predicted using a value for maximum ferrous iron oxidation rate and half-saturation constant for this configuration of packed bed bioreactor?
3. Does pH affect kinetics over the range of pH 2.0 to 3.25 expected in a full-scale treatment system?
4. Is temperature an important parameter in predicting oxidation rates? If so, how does it affect the rates?
5. Since the iron-oxidizing organism thought to be most commonly present at AMD sites, *T. ferrooxidans*, is an obligate aerobe, at what point does DO become limiting?

<center>9</center>

6. Since *T. ferrooxidans* is lithotrophic would the addition of carbon dioxide gas to the air supplied to the reactor increase ferrous iron oxidation rates?

METHODOLOGY

Simulated Acid Mine Drainage

For purposes of this study, typical AMD was defined as having the composition shown in Table 2.1 which is based on the results of a USEPA survey of acid-producing coal mine waters (USEPA, 1976). Where appropriate, total iron concentration was varied from 1 mM to 10 mM (56 to 558 mg L^{-1}).

Table 2.1. Simulated AMD (after adjustment to pH 2.3 with H$_2$SO$_4$).

Constituent	Molarity	mg L^{-1}
Iron (ferrous)	0.010	558
Aluminum	0.002	54
Calcium	0.002	80
Magnesium	0.001	24
Sodium	0.0075	175
Potassium	0.0005	20
Ammonium (as N)	0.0005	7
Sulfate	0.025	2400
Phosphate (as P)	0.0005	16

Inoculum

Simulated AMD (0.5 L) was placed in a 1-L flask and inoculated with sediment from a stream draining an acid pool at an AML site near Galax, Virginia. The flask was placed on a magnetic stir plate and aerated. Once the liquid became turbid, the sediment was discarded. Periodically, the culture was centrifuged and decanted, followed by replacement of the simulated AMD. During June, 1996, expanded polystyrene (EPS) beads of approximately 2-3 mm diameter were submerged in the culture medium. The simulated AMD was circulated over the beads with continuous addition of ferrous iron, to encourage the development of a mineral coating. After about two months, a yellow coating had appeared on the beads. Coated beads were maintained submerged in the liquid medium with periodic additions of ferrous iron, until being placed into column reactors for oxidation rate studies. During this start-up period, a mineral sediment accumulated on the bottom of the container in which the beads had been maintained. This sediment, henceforth referred to as a slurry, was removed from that container. The mineral slurry was maintained on a magnetic stir plate in simulated AMD with intermittent feeding of ferrous iron. To prevent the accumulation of dissolved ferric iron to a high level, the bioreactor slurry was periodically centrifuged, decanted, and new

simulated AMD was added. The slurry, whose color remained a bright yellow, was subsequently used in batch kinetic studies as described below. Some of the slurry mineral was rinsed and dried for mineralogical analysis, and was identified by x-ray diffraction to be jarosite $[KFe_3(OH)_6(SO_4)_2]$.

Packed Bed Columns

Mass Transfer Limitation Issues

       While all reactors have mass transfer limitations, biofilm reactors are especially subject to such concerns. However, it is often assumed that mass transfer is not limiting, which greatly simplifies mathematical modeling. Williamson and McCarty (1976) addressed this issue in an attempt to develop a model which accounted for mass transfer in biofilm systems. In their presentation, they developed an expression to estimate whether the electron acceptor or the electron donor was limiting based on stoichiometry, diffusion rates, and molecular weights. They stated that the electron acceptor would be limiting if

$$S_{ea} < S_{ed} (D_{cd}v_aMW_a)/(D_{ca}v_dMW_d) \qquad (2\text{-}3)$$

       where S_{ea} and S_{ed} are the concentrations (mg L^{-1}) of the electron acceptor and electron donor, respectively, D_{ca} and D_{cd} are the diffusion coefficients, v_a and v_d are the stoichiometric coefficients and MW_a and MW_d are the molecular weights for the electron acceptor and donor, respectively. Using equation 2-2 (the reaction of iron with oxygen) for stoichiometry and values for D_{ca} of 1.6 $cm^2 d^{-1}$ (Williamson & McCarty, 1976) and D_{cd} of 1.02 $cm^2 d^{-1}$ (CRC, 1990), it was estimated for this study that oxygen would not be limiting in ferrous iron oxidation so long as the ferrous iron/oxygen mass concentration ratios did not exceed 11. In these studies, the DO was monitored in the effluent from the reactor columns, and was found to remain about 7 mg/L.   So long as ambient [Fe II] concentration remained below about 77 mg/L, it would be expected that ferrous iron rather than DO would be limiting. This was generally the case except at high flow rates and in certain batch studies.

0.1-L Column Reactors

       Small (0.1-L) glass graduated cylinders were equipped with ports top and bottom for continuous flow kinetic studies. The use of a multi-channel peristaltic pump (Masterflex by Cole Parmer Co.) made it possible to maintain constant flow to numerous reactors while introducing different substrate concentrations. Steady state at a given dilution rate (D) was defined as at least 5 HRTs followed by relatively constant substrate concentrations over 3 HRTs. D was computed by dividing the flow rate (L h^{-1}) by the drainable liquid volume, which was about 0.035 L for all 0.1 L columns. The flow rate was adjusted to change D from 1 to 7.4 h^{-1}. Loading rate was calculated by multiplying the flow rate times the influent substrate concentration and dividing by the reactor volume, resulting in a value expressed as mg substrate L^{-1} reactor volume h^{-1}. The

columns were packed with EPS beads (~0.1 L), and restrained with fiberglas screening. Air was passed through a 1 μm filter prior to entering each reactor. Between runs, beads were removed so that reactor surfaces could be cleaned.

<u>1-L Column Bioreactor</u>

A polyethylene graduated cylinder (1 L) was modified to serve as a reactor. A removable perforated plate near the top of the column retained EPS beads below the surface of the liquid. Feed was supplied to the bottom of the column by a peristaltic pump (Masterflex by Cole Parmer Co.). The air supply was passed through a 1 μm filter prior to entering the reactor. An overflow port at the top of the column maintained the liquid level for continuous flow studies. Typically, between 0.5 and 0.7 L of beads were placed in the reactor. Periodically, all liquid was drained and passed through the column several times to remove trapped solids.

Batch Studies for Temperature, pH, DO, and CO_2 Effects

Batch slurry reactors were used to identify the effects of temperature, pH, CO_2, and DO on oxidation rates. With exceptions as noted below, 0.1 L of the mineral slurry mentioned above was added to 250 mL Erlenmyer flasks and placed on magnetic stir plates. Whenever stir plates were used, a piece of corrugated cardboard was placed under each flask to prevent unintended heating of the flask by the stir plate. To begin a study, the desired volume of 0.2 M ferrous sulfate solution was added to each batch reactor. Before reuse, the slurry was returned to the stock container, which was centrifuged, decanted, and new simulated AMD added to prevent the accumulation of ferric iron.

<u>Temperature</u>

For temperatures lower than ambient, the batch reactors were placed with stir plates into a small refrigerator whose temperature could be regulated. The actual temperature of each reactor was measured with a mercury thermometer and recorded at each sampling time. The temperatures investigated were 5°, 7°, 11°, 13°, 14°, 17°, 23°, and 26° C.

<u>Hydrogen Ion Concentration</u>

The pH of various flasks was adjusted with 6 N nitric acid or solid sodium bicarbonate at the beginning of each run, and if necessary after each sampling period. Replicate trials were conducted at several pH values over the range of pH 2.0 to 3.25.

<u>Dissolved Oxygen</u>

Instead of Erlenmeyer flasks, narrow mouth bottles (250 mL) similar in shape to BOD test bottles but with a bottom-located tubing barb were employed. A continuous stream of nitrogen gas was introduced through the bottom tubing to strip oxygen from the slurry which almost filled the bottle. The slurry was kept mixed by magnetic stirrer. A peristaltic pump was connected to a T-connector in the nitrogen line. By varying the pumping speed of the peristaltic pump whose suction end was open to the atmosphere, air

could be added to the nitrogen supply thus controlling the DO level in the reactor. The mouth of the bottle held a one-hole rubber stopper fitted with a short length of narrow gauge vinyl tubing to allow gas to escape while impeding backflow of air. DO was measured by replacing the stopper with a DO probe attached to a YSI Dissolved Oxygen Meter Model 57 such that the end of the probe was immersed in the liquid. The probe shaft sufficiently closed the opening to prevent intrusion of room air while allowing the emerging gas to escape. Due to limitations of apparatus, only one experimental reactor was operated at a time, along with a control reactor containing the same slurry from the stock reservoir. Air was vigorously bubbled through the control reactor. The normal liquid level in the bottles was marked on the bottle wall so that evaporated water could be replaced with deionized water. The DO levels investigated were 0.25, 0.50, and 0.75 mg L^{-1} with controls at 5.0 to 7.5 mg L^{-1}

Carbon Dioxide Partial Pressure

The same apparatus as described above for DO studies was used for CO_2 studies, except that the nitrogen gas tank was replaced with a tank of liquefied CO_2. For metering air and CO_2, two pump heads were mounted onto one peristaltic pump motor. By varying the pump tubing diameter for the CO_2 and air lines, the ratio of CO_2 to air, and thus P_{CO_2}, could be controlled. The combined gases were introduced to the bottom of the reactor which was placed on a magnetic stir plate. Actual flow through each tube for each run was checked by pumping the gases separately into an inverted graduated cylinder filled with water, and measuring water displacement. The continuous flow of air-CO_2 mixture was exhausted through a small opening installed in the mouth of the bottle, which aided in preventing intrusion of room air to the headspace. Three mixtures of CO_2 and air were investigated: 1.6% (v/v) CO_2, 5% (v/v) CO_2, and 9.7% (v/v) CO_2. Controls were supplied with room air, and thus had a P_{CO_2} of about $10^{-3.5}$ atm (about 0.03%). The concentration of CO_2 actually dissolved in the liquid phase was not measured.

Ferrous Iron Determinations

Ferrous iron was determined immediately after sampling and appropriate dilution with acidified deionized water (deionized water to which a few drops of 6 M nitric acid had been added). Acidified deionized water was used for diluting samples before ferrous iron determinations to prevent oxidation of the iron. A DR700 HACH colorimeter was used along with HACH ferrous iron reagent powder pillows (HACH Corporation, Loveland, CO), which conformed to the 1, 10 phenanthroline method (Method 3500-Fe D.) as detailed in Standard Methods for the Examination of Water and Wastewater (APHA, AWWA,WEF, 1992). This method is approved by USEPA. Background color supplied by ferric iron was deducted from readings after blanking with distilled water. The pre-programmed conversion factor of the colorimeter was checked with freshly prepared Fe II standard solutions.

Statistical Methods and Calculations

Where appropriate, means, standard deviations, simple linear regression, and analysis of variance (ANOVA) were computed using the data analysis features of Microsoft Excel 7.0. These calculations were consistent with traditional statistical methods as reported in the literature (Sokal and Rolf, 1995).

RESULTS AND DISCUSSION

Continuous Flow Ferrous Iron Bio-Oxidation Kinetics

0.1-L Reactor Studies

Small reactors (0.1 L) were used to measure the rate of Fe II oxidation when the influent substrate concentration was varied at a selected D. Influent [Fe II] ranged from about 1 mM Fe II (~55 mg L^{-1}) to about 10 mM Fe II (~570 mg L^{-1}) among the five reactors. Once steady state values were obtained at a given D, the flow was increased to increase D. Initially, three dilution rates (1, 1.5, and 2 h^{-1}) were evaluated at room temperature (~25°C). Later, D was increased as high as 7.4 h^{-1}.

While effluent [Fe II] increased in with an increase in influent concentration, removal efficiencies ranged from 96 to 99 % (Figure 2.2). Dilution rate alone up to 2 h^{-1} did not appear to determine effluent ferrous iron concentration.
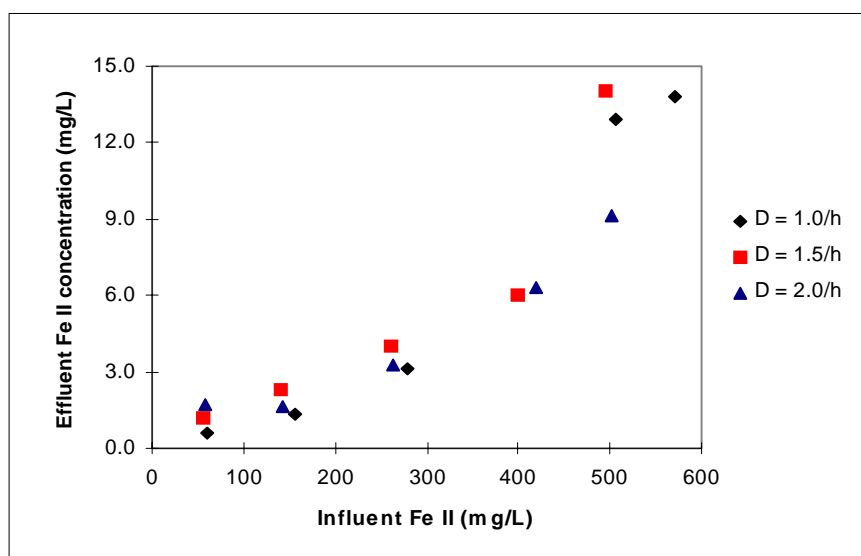
Figure 2.2. Effluent ferrous iron concentration vs influent concentration at 3 dilution rates.

Substrate oxidation rate (R) was calculated by multiplying D times the decrease in [Fe II] (influent [Fe II] - effluent [Fe II]).   When R was plotted as a function of substrate concentration, it showed a saturation effect (Figure 2.3). Using double reciprocal plots, it was estimated that the volumetric substrate oxidation rates (R_{max}) were 750, 1050, and

1575 mg substrate L $^{-1}$ reactor liquid volume h $^{-1}$, for the three dilution rates, respectively. Since there was almost complete oxidation of the influent, these rates represent increased loading due to increased flow rate. The half saturation constant, K_s^*, was estimated to be 6 mg L $^{-1}$ in all three cases. The pattern of the curves in Figure 2.3 closely resembles that shown by Wichlacz and Unz (1985) for treatment of AMD in rotating biological contactors (RBCs) at different flow rates. There are at least two possible explanations for this pattern. The first relates to the thickness of the stagnant liquid layer and mass transfer limitations as discussed by Williamson and McCarty (1976). They found that there were actually two phases to the stagnant layer, which they labeled L_1 and L_2. With adequate shear, L_1 could be reduced to zero thickness, but L_2, the layer immediately adjacent to the surface, could not be eliminated. In the case of an acidic iron bioreactor, the surface is
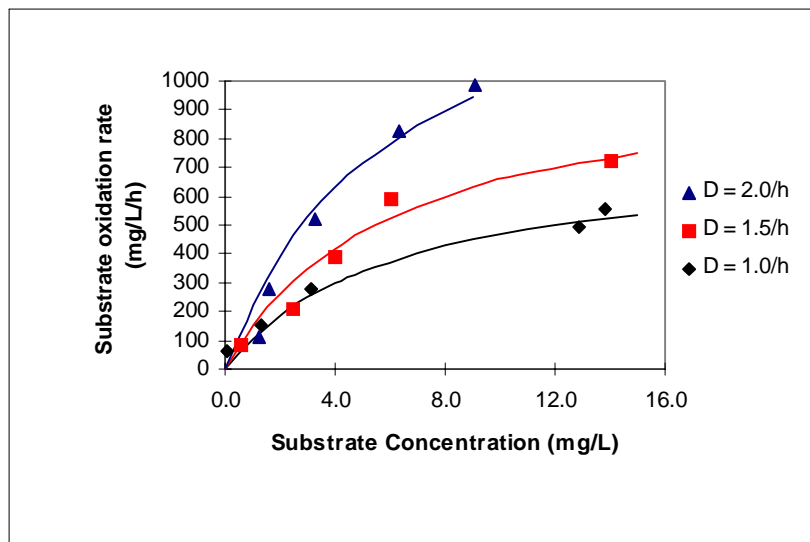
Figure 2.3. Substrate oxidation rate as a function of substrate concentration in EPS packed bed bioreactors at 3 dilution rates.

composed of jarosite to which cells adhere. In scanning electron micrographs, jarosite particles were seen to have high surface area and high porosity (Grishin and Tuovinen, 1988; Lazaroff et al., 1985). The [Fe II] and DO within the pores would be lower than in the bulk liquid due to utilization by cells. Increased flow through the reactor may have decreased the thickness of L_1, thus increasing the driving force moving [Fe II] faster into the pores of the jarosite matrix, resulting in increased rates of oxidation by cells.

There is a second and more compelling explanation for the increase in R_{max} with increased dilution rate. Probably, the columns had significant plug flow character. Since the influent entered the bottom of the reactor, most of the ferrous iron was probably oxidized in the bottom portion of the reactor, and a concentration gradient may have developed up the length of the reactor (Figure 2.4). So long as initial substrate concentration (S_o) $\gg$ K_s^*, the substrate oxidation rate would be zero order in the influent zone of the reactor.
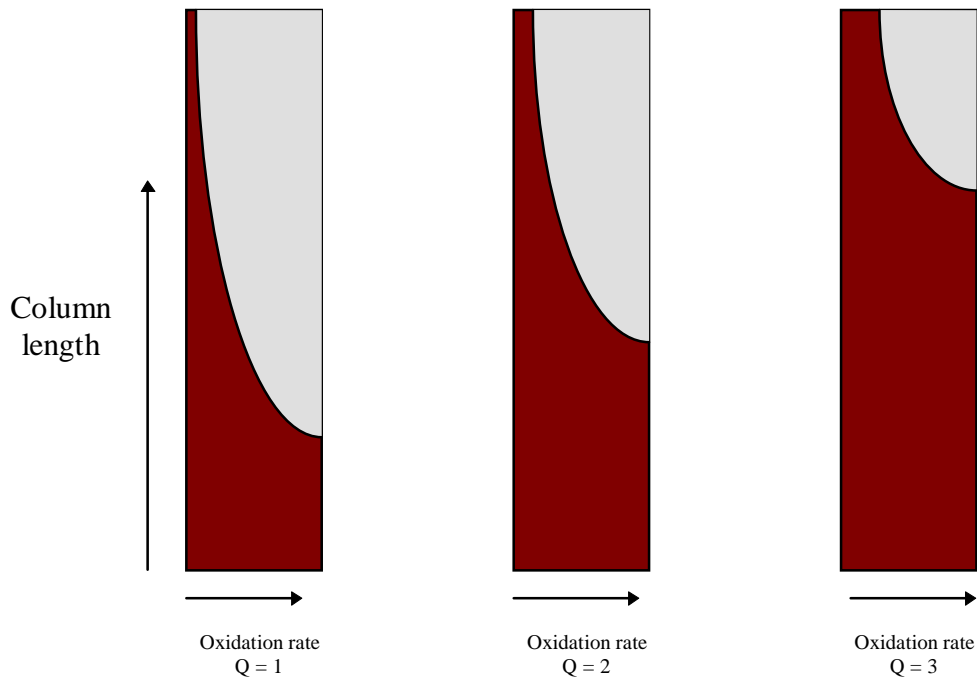
Figure 2.4. Illustration of effect of plug flow character on oxidation rates within
packed bed column reactors. Qs are hypothetical.

A plot (Figure 2.5) of effluent substrate concentration as a function of loading
revealed that un-oxidized substrate increased as dilution rate and loading increased.
(Loading is expressed as mg of ferrous iron L^{-1} reactor volume h^{-1}.) This is consistent
with the idea that once the maximum rate zone had expanded upward incorporating the
entire column due to increased flow rate, effluent substrate concentration would increase
markedly with increased loading.

When substrate oxidation rate was plotted as a function of loading, the effect of
detention time was illustrated clearly (Figure 2.6). Rates at D = 1, 2 and 3.6 h^{-1} were
essentially identical at a given loading rate. There was a marked decrease in rates at D =
7.4 h^{-1}. These results suggest that detention time was an important parameter. In concert
with the oxidation efficiencies presented in Table 2.2, an optimal detention time may be
about 30 min (D = 2 h^{-1}).

Oxidation efficiency (Δ[Fe II]/[Fe II$_o$]) remained high (>98%) until D was
increased above 2 h^{-1}. Above that dilution rate, shorter detention times led to lower
oxidation efficiencies (Table 2.2).
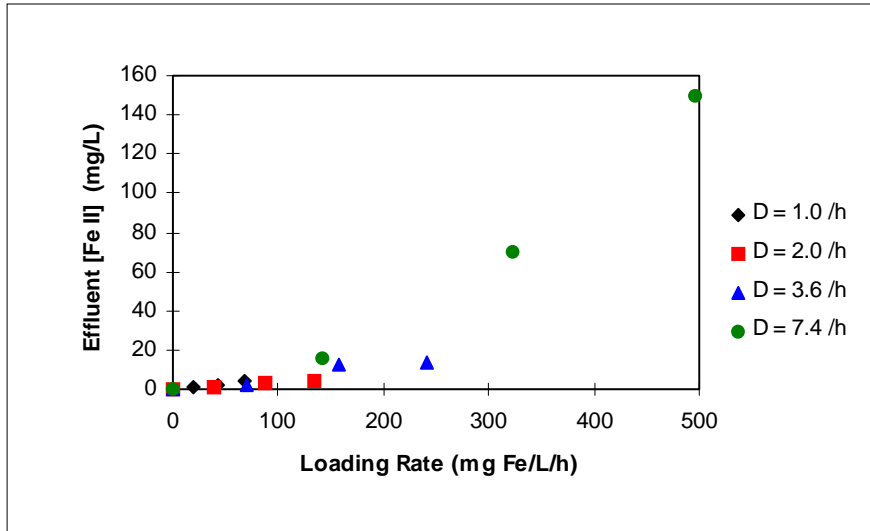
Figure 2.5. Effluent substrate concentration as a function of loading for D = 1 through 7.4 h^{-1}. Loading is expressed as mg ferrous iron L^{-1} reactor volume h^{-1}.
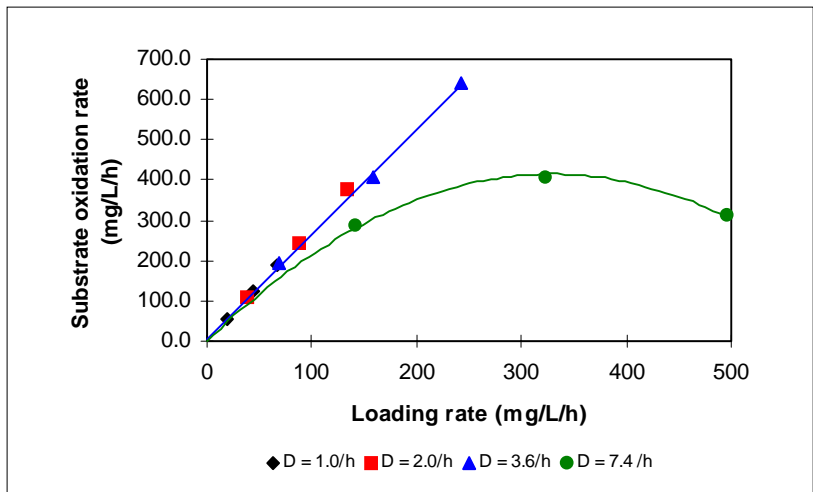
Figure 2.6. Substrate oxidation rate as a function of loading rate at D = 1 to 7.4 h^{-1}. Substrate oxidation rate is expressed as mg ferrous iron oxidized L^{-1} liquid volume h^{-1}. Loading is expressed as mg ferrous iron L^{-1} reactor volume h^{-1}.

Table 2.2. Substrate oxidation efficiency (Δ[Fe II]/[Fe II$_o$]) and loading (mg substrate L^{-1} reactor volume h^{-1}) at 6 influent concentrations and 4 dilution rates.

[Fe IIo]	D = 1 /h		D = 2 /h		D = 3.6 /h		D = 7.4 /h	
mg/L	Ldg	% ox	Ldg	% ox	Ldg	% ox	Ldg	% ox
55	19	98%	39	98%	69	96%	142	71%
125	44	98%	88	98%	158	90%	323	44%
192	67	98%	134	98%	242	93%	495	22%
267	97	99%	184	99%				
501	177	97%	350	98%				
572	200	98%						

1-L Column Bioreactor

A 1-L bioreactor was operated continuously for 30 days. The dilution rate during most of the 30 day period was about 0.3 h^{-1}. About twice a week during that period, the reactor was flushed with reactor liquid to dislodge attached solids and settled sediment to prevent accumulation of minerals and associated biomass not attached to EPS beads. The performance of the reactor over the 30 day period is shown in Figure 2.7. As can be seen, the effluent ferrous iron concentration remained below 10 mg L^{-1} until the ferrous iron loading exceeded 130 mg L^{-1} reactor volume h^{-1}. At a loading of about 225 mg L^{-1} reactor volume h^{-1}, the effluent concentration averaged about 70 mg L^{-1} Fe II. When loading was decreased on day 18, the effluent [Fe II] decreased to a value of about 4 mg L^{-1}. The kinetic behavior of the reactor was very much like that of the 0.1-L reactors. R_{max} and K_s^* were found to be 370 mg L^{-1} h^{-1} and 6 mg L^{-1}, respectively (Figure 2.8).
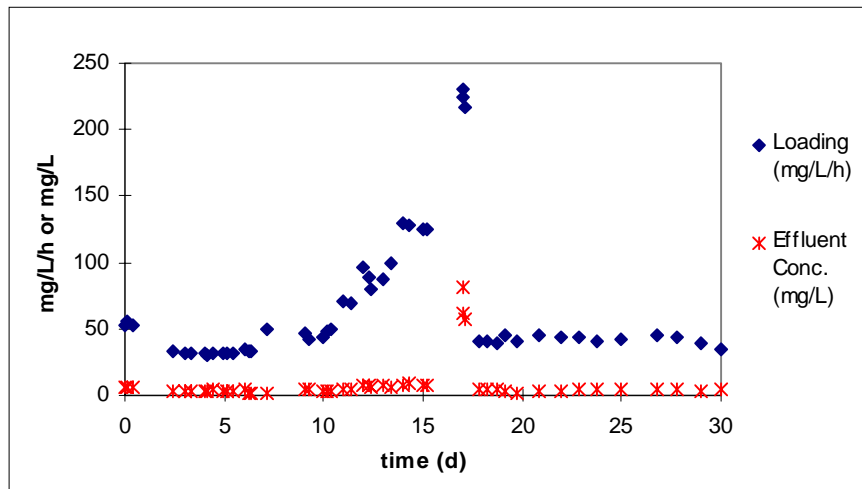
Figure 2.7. Effluent ferrous iron concentration (mg L^{-1}) in a 1-L EPS packed bed bioreactor under varying Fe II loading (mg L^{-1} reactor volume h^{-1}). Substrate oxidation rate is expressed as mg ferrous iron oxidized L^{-1} liquid volume h^{-1}.
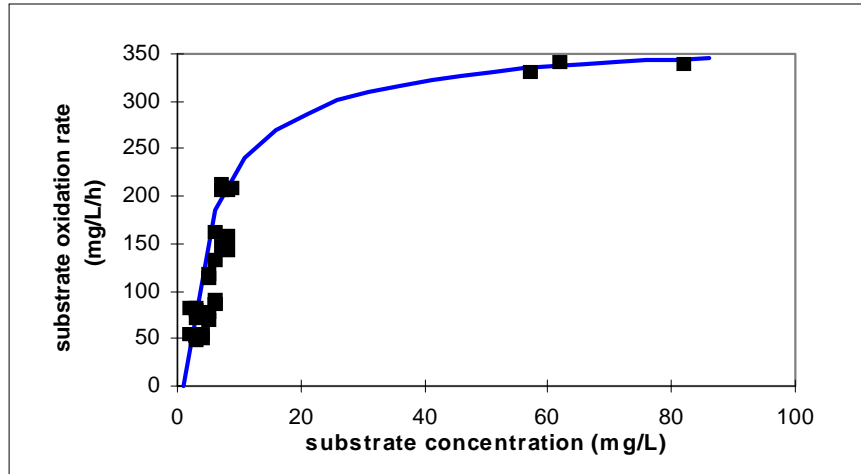
Figure 2.8. Substrate oxidation rate as a function of substrate concentration in a 1-L EPS packed bed bioreactor operated over a 30 day period at various loadings and a dilution rate (D) of about 0.3 h^{-1}; R_{max} = 370 mg L^{-1} h^{-1}, K_s^* = 6 mg L^{-1}. Substrate oxidation rate is expressed as mg ferrous iron oxidized L^{-1} liquid volume h^{-1}.

Influence of Various Factors on Kinetics of Ferrous Iron Bio-Oxidation

Temperature

Temperature had a pronounced effect on oxidation rates over the temperature range of 5° to 26° C. The effect of temperature on rates is most commonly expressed in terms of the Arrhenius equation:

$$r_x = A_o \, e^{-E/RT} \qquad \qquad (2\text{-}4)$$

where r_x is the specific substrate oxidation rate (h^{-1}), A_o (h^{-1}) and E (J mol^{-1}) are coefficients relating to oxidation rate and activation energy, respectively, R is the universal gas constant (J T^{-1} mol^{-1}), and T is temperature in °K. By plotting - ln r_x as a function of T^{-1} (Figure 2.9), values for the coefficients A_o and E were found to be 1.585 h^{-1}, and 183.3 J mol^{-1}, respectively. The expression thus becomes

$$r_x = 1.585 \, e^{-183.3/RT} \qquad \qquad (2\text{-}5)$$
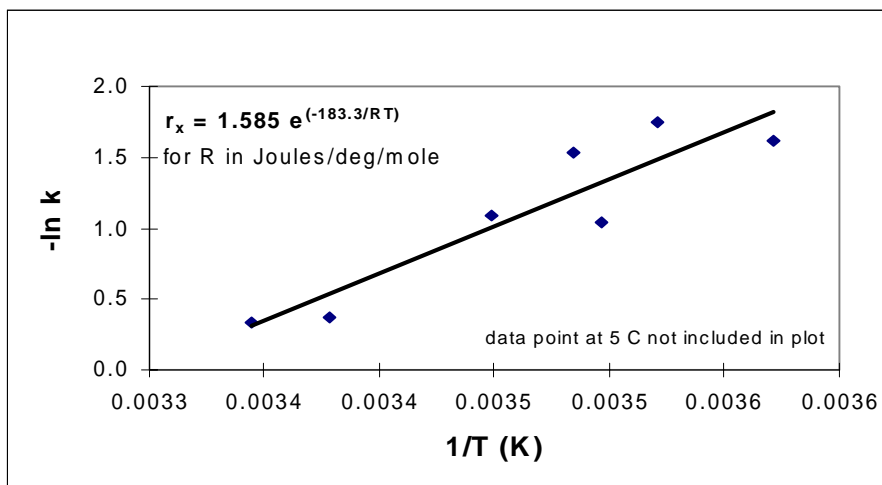
Figure 2.1. Plot of -ln k (specific substrate oxidation rate) as a function of 1/T
gies are either inadequate ous equation coefficients. Temperature range
evaluated was 5 to 26°C.

This finding is in general agreement with Karamanev and Nikolov (1988) who found that the rate began to decrease below 25°C, but they did not explore temperature effects below 15°C. Nakamura et al. (1986) saw no temperature effect in their data on RBCs over the temperature range of 10° to 35° C. However, the data presented in their paper could also be interpreted to show a decrease in rate below 25°C. Unz et al. (1979) and Olem and Unz (1980) observed a decrease in ferrous iron oxidation rates with drop in temperature, but measured greater than 60% oxidation efficiency in RBCs at temperatures below 2° C in lab-scale and pilot-scale experimental systems.

Hydrogen Ion Concentration

The range of pH evaluated was 2.0 to 3.25. Over this range there was no significant effect of pH on the oxidation rate at the $\alpha = 0.05$ level (data not shown). Nakamura et al. (1986) found that rates were constant over the pH range of 1.5 to 2.5, and declining both above and below that range. Karamanev and Nikolov (1988) saw no effect of pH on oxidation rates over the range of 1.3 to 2.2.

Dissolved Oxygen Concentration

The effect of DO on bio-oxidation rates was measured using batch reactors as described above. Preliminary trials (4) were conducted with DO levels below 1.0 mg/L and controls with DO above 6.0 mg/L. Analysis of variance (ANOVA) confirmed that there was a significant effect at the $\alpha = 0.05$ level. Subsequently, single reactors were used to measure the effect of DO at 0.25, 0.50, and 0.75 mg/L, with controls for each maintained above DO = 5 mg/L. The initial [Fe II] was from 220 to 250 mg/L, To facilitate comparisons among several trials, the oxidation rate was expressed in terms of % oxidized h^{-1}. Since rates were constant (zero order) over the range of 0 to 85% oxidized, only data points within that range were used for this analysis. For each trial, 3

to 5 measures were made to establish the rate of oxidation. The coefficient of determination (R^2) for each rate determination varied from 0.881 to 0.999. As shown in Figure 2.10a, the rate for the controls (5.0- 7.0 mg L^{-1} DO) was only slightly higher than the rate at 0.75 mg/L DO. At DO = 0.75 mg L^{-1} and below, there was a gradual decrease in ferrous iron bio-oxidation rate. Using the slopes of the regression lines in Figure 2.10a as the oxidation rates (S/S_o expressed as % change h^{-1}), rate is plotted as a function of DO in Figure 2.10b. The plot shows the classic Monod-type saturation effect. By use of a double reciprocal plot, K_o for oxygen was found to be 0.33 mg/L. The line predicted by this value and a maximum oxidation rate of 17% h^{-1} is shown in Figure 2.10b for comparison with the actual data. A value found in the literature for low DO conditions was Nikolov and Karamanev (1990b), who reported a "limiting" dissolved oxygen concentration of 0.64 mg L^{-1}.
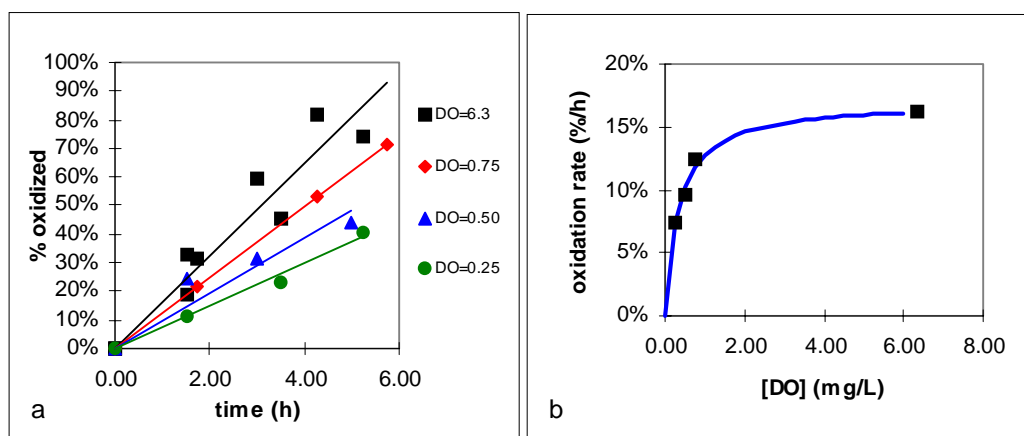
Figure 2.10a, b. Effect of DO on bio-oxidation rate of ferrous iron; the line in (b) is based on values of k=17% h^{-1} and K_o = 0.33 mg/L.

Carbon Dioxide Partial Pressure

Batch oxidation studies with mineral slurries indicated that P_{CO2} did not significantly ($\alpha = 0.05$) affect the bio-oxidation rate when experimental reactors were compared with control reactors receiving air only (Figure 2.11 a, b, and c). It should be noted that dissolved CO_2 ($H_2CO_3^*$) in the reactor liquid was not measured, and thus no statement about transfer efficiency can be categorically made. However, it is reasonable to believe that CO_2 equilibration occurred in these studies which lasted for 10, 30, or 60 hours. Three trials were conducted at 5% and at 9.7% CO_2, while just one was conducted at 1.6% CO_2.

Silverman and Lundgren (1958) found that periodic additions of sodium and calcium carbonate to culture media had no effect on growth. Kelly and Jones (1978) found no effect of CO_2 on growth rate up to 8% CO_2. MacDonald and Clark (1970) investigated the response of *T. ferrooxidans* to supplemental CO_2 in the range of 0.03 to 10%, and found no stimulatory effect.
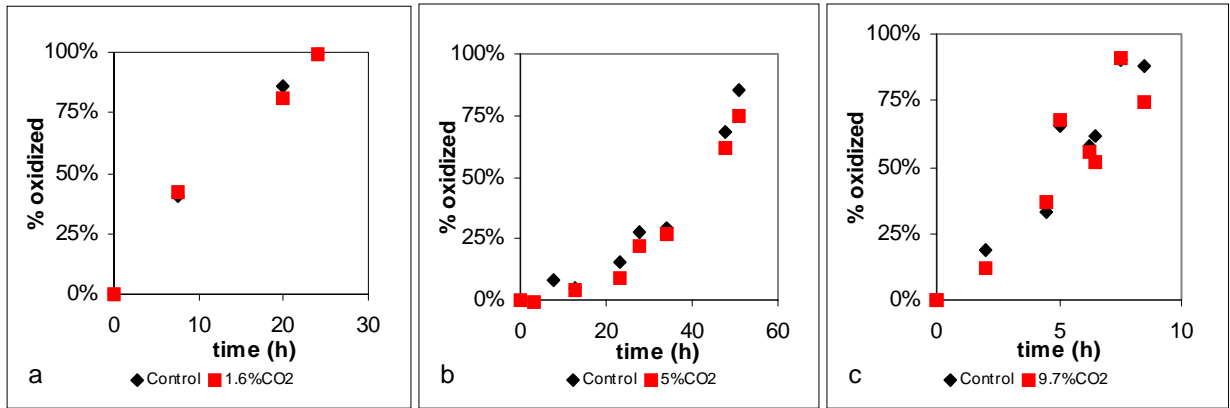
Figure 2.11a,b,c. Effect of supplemental carbon dioxide on bio-oxidation of ferrous iron. Rates are not the same in a, b, and c due to different slurry concentrations used; comparisons are only valid between experimental and controls for each set of trials.

However, LaCombe Barron and Lueking (1990) found that supplemental carbon dioxide did have an effect on growth rates, with a peak growth rate at about 7 to 8% CO_2, with a decline in growth rate both above and below this range. It should be noted that growth rate and oxidation rate may not be absolutely linked together in a 1 to 1 correspondence.

CONCLUSIONS

A packed bed bioreactor using EPS to immobilize bacteria appeared to be practical and useful for the oxidation of ferrous iron in AMD or other waters rich in reduced iron. The production of biomass was low, and thus biosolids disposal would not be expected to be a necessity. Specifically, the objectives of the research project were addressed with the following results:

1. Above a dilution rate of $D = 2 \ h^{-1}$, the substrate oxidation efficiency decreased below 95% as flow rate and loading increased. Good oxidation (98%) occurred at loadings up to 350 mg substrate L^{-1} reactor volume h^{-1} at a dilution rate of $2 \ h^{-1}$.
2. In an EPS packed bed bioreactor for a ferrous iron concentration up to 10 mM, the maximum substrate oxidation rate (R_{max}) was found to be about 1,500 mg L^{-1} liquid volume h^{-1} at $D = 2 \ h^{-1}$. The half-saturation constant K_s^* was found to be about 6 mg L^{-1}.
3. Reactor pH was not an important parameter within the range of pH 2.0 to 3.25.
4. Temperature was a major factor in the bio-oxidation rate of these systems, with a near cessation of oxidation at 5° C. Appropriate design considerations would be necessary to provide for sufficient ferrous iron conversion during winter months in most areas. The coefficients A_o and E for the Arrhenius equation were found to be 1.585 h^{-1}, and 183.3 J mol^{-1}, respectively.

5. Aeration sufficient to provide a DO of 2 mg/L or greater appeared to be adequate to sustain activity, since the K_o for oxygen was found to be 0.33 mg/L.
6. Supplementation of the air supply with CO_2 did not appear to enhance oxidation rates.

LITERATURE CITED

APHA, AWWA, WEF. (1992) Standard Methods for the Examination of Water and Wastewater, 18th Edition. American Public Health Association. Washington, DC.

Arredondo, R., A. Garcia, and C.A. Jerez. 1994. Partial Removal of Lipopolysaccharide from *Thiobacillus ferrooxidans* Affects Its Adhesion to Solids. Appl. Environ. Microbiol. 60(8):2846-2851.

CRC. 1990. Handbook of Chemistry and Physics. CRC Press, Inc. Boca Raton.

Curutchet, G. C. Pogliani, E. Donati, P. Tedesco. 1992. Effect of Iron (III) and Its Hydrolysis Products (Jarosites) on *Thiobacillus ferrooxidans* Growth and on Bacterial Leaching. Biotechnol. Lett. 14(4):329-334.

Grishin, S. I. And O. H. Tuovinen. 1988. Fast Kinetics of Fe^{2+} Oxidation in Packed-Bed Reactors. Appl. Environ. Microbiol. 54:3092-3100.

Grishin, S. I. And O. H. Tuovinen. 1989. Scanning Electron Microscopic Examination of *Thiobacillus ferrooxidans* on Different Support Matrix Materials in Packed Bed and Fluidized Bed Bioreactors. Appl. Microbiol. Biotechnol. 31:505-511.

Jensen, A. B. and C. Webb. 1995. Ferrous Sulphate Oxidation Using *Thiobacillus ferrooxidans:* A Review. Proc. Biochem. 30(3):225-236.

Jones, C. A. and D. P.Kelly. 1983. Growth of *Thiobacillus ferrooxidans* on Ferrous Iron in Chemostat Culture: Influence of Product and Substrate Inhibition. J. Chem. Tech. Biotechnol. 33B:241-261.

Karamanev, D. and L. Nikolov. 1988. Influence of Some Physicochemical Parameters on Bacterial Activity of Biofilm: Ferrous Iron Oxidation by *Thiobacillus ferrooxidans*. Biotechnol Bioeng. 31:295-299.

Karamanev, D. and L. Nikolov. 1991. A Comparison Between the Reaction Rates in Biofilm Reactors and Free Suspended Cells Bioreactors. Bioproc. Eng. 6:127-130.

Kelly, D. P. and C.A. Jones. 1978. Factors Affecting Metabolism and Ferrous Iron Oxidation in Suspensions and Batch Cultures of *Thiobacillus ferrooxidans*: Relevance to Ferric Iron Leach Solution Regeneration, p. 19-44. *In* L.E. Murr, A.E. Troma, and J.A. Brierley (ed.) Metallurgical Applications of Bacterial Leaching and Related Microbiological Phenomena. Academic Press, Inc., New York.

Kumar, S.R. and K.S. Gandhi. 1990. Modeling of Fe^{2+} Oxidation by *Thiobacillus ferrooxidans*. Appl. Microbiol. Biotechnol. 33(5):524-528.

LaCombe Barron, J. and D.R. Lueking. 1990. Growth and Maintenance of *Thiobacillus ferrooxidans* Cells. Appl. Environ. Microbiol. 56(9):2801-2806.

Lasaroff, N., L. Melanson, E. Lewis, N. Santoro, and C. Pueschel. 1985. Scanning Electron Microscopy and Infrared Spectroscopy of Iron Sediments Formed by Thiobacillus ferrooxidans. Geomicrobiol. J. 4(3):231-268.

MacDonald, D. G. and R. H. Clark. 1970. The Oxidation of Aqueous Ferrous Sulphate by *Thiobacillus ferrooxidans*. Can. J. Chem. Engng. 48:669-676.

Nakamura, K. T. Noike, J. Matsumoto. 1986. Effect of Operation Conditions on Biological Fe^{2+} Oxidation with Rotating Biological Contactors. Water Res. 20:73-77.

Nikolov, L. D. and D. G. Karamanev. 1990. Experimental Study of the Inverse Fluidized Bed Biofilm Reactor. Can. J. Chem. Engin. 65:214-217.

Nikolov, L. D. and D. G. Karamanev. 1990. The Inverse Fluidized Bed Biofilm Reactor: A New Laboratory Scale Apparatus for Biofilm Research. J. Ferm. Bioengng. 69(4):265-267.

Olem, H. and R.F. Unz. 1980. Rotating-Disc Biological Treatment of Acid Mine Drainage. J. WPCF 52(2):257-269.

Silverman, M.P. and D.G. Lundren. 1959. Studies on the Chemoautotrophic Iron Bacterium *Ferrobacillus ferrooxidans.* J. Bacteriol. 78:326-331.

Singer, P.C. and W. Stumm. 1970. Acidic Mine Drainage: The Rate-Determining Step. Science 167:1121-1123.

Singh, S.K., and V. Subramanian. 1986. Hydrous Fe and Mn Oxides - Scavengers of Heavy Metals in the Aquatic Environment. CRC Crit. Rev. Environ. Contr. 14(1): 33-90.

Sokal, R. R. and F. J. Rolf. 1995. Biometry: The Principles and Practice of Statistics in Biological Research, 3rd Edition. W. H. Freeman and Company. New York.

Starkey, R.L., 1945. Precipitation of Ferric Hydrate by Iron Bacteria. Science 102:532-533.

Stumm, W. and J. J. Morgan. 1970. Aquatic Chemistry - An Introduction Emphasizing Chemical Equilibria in Natural Waters. Wiley-Interscience. New York.

Stumm, W. and J. J. Morgan. 1981. Aquatic Chemistry - An Introduction Emphasizing Chemical Equilibria in Natural Waters, 2nd Edition. Wiley-Interscience. New York.

Temple, K.L. and A.R. Colmer. 1951. The Autotrophic Oxidation of Iron by a New Bacterium: Thiobacillus ferrooxidans. J. Bacteriol. 62:605-611.

Unz, R. F., H. Olem, P. L. Wichlacz. 1979. Microbiological Ferrous Iron Oxidation in Acid Mine Drainage. Proc. Biochem. 14(6): 2-6.

USEPA. 1976. Development Document for Interim Final Effluent Limitations Guidelines and New Source Performance Standards for the Coal Mining Point Source Category. EPA 440/1-76/057a..

Wehrli, B. 1990. Redox Reactions of Metal Ions at Mineral Surfaces. in Aquatic Chemical Kinetics, ed. W. Stumm . John Wiley & Sons. New York. pp. 311-336.

Wichlacz, P. L. and R. F. Unz. 1985. Growth Kinetics of Attached Iron-Oxidizing Bacteria. Appl. Environ. Microbiol. 50:460-467.

Williamson, K. J. and P. L. McCarty. 1976. A Model of Substrate Utilization by Bacterial Films. J. Wat. Pollut. Contr. Fed. 48(1):9-23.

Chapter 3 - Factors Affecting Precipitation of Ferric Iron in a New System for Removing Iron from Simulated Acid Mine Drainage without the Formation of Iron Sludge

INTRODUCTION

Acid mine drainage (AMD) from working and abandoned mines continues to be an important water pollution problem in the United States and around the world. The primary characteristics of AMD which cause concern are low pH, high specific conductivity, high concentrations of iron, aluminum, and manganese, and the variable presence of toxic heavy metals at trace levels. Current treatment technologies are either inadequate or too expensive; thus, much discharge enters receiving waters with no treatment. This paper presents one of a series of studies intended to develop a new approach to the removal of iron and acidity from this contaminated water. This new approach (patent pending) optimizes the tendency of iron to form coatings while avoiding the formation of dispersed iron hydroxide floc. The requirement for sedimentation basins would thus be eliminated along with the eventual need for disposal of metal hydroxide sludge.

It has been widely observed in natural and engineered situations where dissolved iron is a concern, that iron tends to form coatings of oxyhydroxide minerals on the surfaces over which the iron solution flows. In an AMD contaminated stream, the development of these coatings is dramatic, resulting in the stream beds with bright colors of yellow, orange and reddish brown as the coatings develop and change over time. In addition to the mineral coatings on rocks, gravel, and sand, dispersed iron particulates precipitate from solution and settle to the stream bed, resulting in poor habitat for benthic organisms.

Precipitation of iron is not necessarily instantaneous upon addition of alkalinity to the solution. However, when sufficient base is added to a ferric iron solution to exceed a threshold level, precipitation of iron oxyhydroxides is inevitable, although the time from the addition of the base to the time of appearance of a precipitate, the so-called "induction period", may last from seconds to months (Dousma and de Bruyn, 1976). During the induction period, changes within the solution occur which eventually result in precipitate formation. This process, as will be described in more detail later, appears to involve a reversible increase in polymerization of Fe/OH units, resulting in the formation of many critical-sized entities, termed nucleii. Once critical size is achieved, the nucleii are thermodynamically stable, and continue to grow by incorporation of additional Fe/OH growth units until the concentration of dissolved iron (consisting of sub-critical polymers) becomes so low that the particle growth rate slows appreciably. Collision of independent particles sometimes results in union of the particles due to van der Waals forces. The success of these collisions is a function of repulsive forces due to the presence of a net charge on the particle surface, which is counterbalanced by a diffuse layer formed by

counter-ions from the solution. The intensity of the surface charge, the number and type of counter ions in solution, and thus the thickness of the diffuse layer determines how closely particles may approach and influences the collision efficiency (Weber and Digiano, 1996). This process of small particles uniting is referred to by various terms but here will be called agglomeration. As particles grow in size, particle concentration (# per unit volume) decreases. Once particle concentration decreases to a low level, growth by agglomeration slows and is counter-balanced by agglomerated particle break-up, leading to a terminal size distribution.

It was hypothesized that this sequence leading to the precipitation of iron particles could be interrupted if dissolved growth units and/or very small particles could be removed from solution by exposing the solution at an early stage to an already formed surface. If the growth units and/or very small particles preferentially united with the pre-formed surface, the continued growth and/or agglomeration of the iron nucleii might not occur, thus avoiding the formation of dispersed iron. If dispersed iron formation could be avoided, there would be no need for sedimentation basins for the separation of water from solids, nor for the storage, handling, dewatering, and eventual ultimate disposal of the iron sludge.

Optimal removals of iron would be a balance between minimizing solubility while avoiding such fast precipitation rates that stable particles formed before the iron growth units could contact and attach to the seed particle surfaces. Since AMD typically contains dissolved species other than iron, the effect of those dissolved species on iron solubility and precipitation kinetics would also be important in determining the success of such a treatment system. The major cations present in AMD other than iron are aluminum, sodium, and manganese. Since aluminum and manganese can substitute for iron in the mineral lattice, it was decided to investigate their effect on this process. Sodium would be unlikely to participate in mineral formation under these conditions and was not investigated. Among the anions present, sulfate was considered the most important potential species in influencing solubility and kinetics. It was hypothesized that sulfate would exert a major effect for two reasons. Sulfate has been documented to form aqueous complexes with iron, effectively reducing the concentration of free iron in solution. Sulfate also sorbs strongly to oxide surfaces, reducing the net surface charge and displacing hydroxyl ions in the process. A third and less likely effect by sulfate would be one of pH buffering due to the formation of bisulfate ions.

BACKGROUND

There can be considerable variation in AMD characteristics. However, a survey of coal mining activities in the eastern US conducted by the USEPA (1976) revealed that acid mine drainage (AMD) contained iron, aluminum, and manganese at concentrations up to 440 mg/L, 270 mg/L, and 125 mg/L, respectively, and sulfate up to 4,000 mg/L. The pH of these waters was as low as 2.2. The effects of AMD on aquatic organisms in the receiving water are well known (Newman and McIntosh, 1991), and the presence of heavy metals and sulfate in aquatic water supplies reduces their desirability as potable water sources.

New source performance standards developed for National Pollutant Discharge Elimination System permits by the USEPA for the coal mining industry stipulate total iron of 3.0 mg/L, total manganese of 2.0 mg/L, total suspended solids (TSS) of 35 mg/L, and pH between 6.0 and 9.0 units (30 day averages) (USEPA 1976) with similar requirements imposed by The Surface Mining Control and Reclamation Act of 1977.

Iron Minerals

More than a dozen compounds fit within the designations of iron oxides, hydroxides, and oxyhydroxides (Schwertmann and Cornell, 1991). Some of the most common are ferrihydrite ($Fe_5O_7OH \bullet nH_2O$), goethite (α-FeOOH), lepidocrocite (γ-FeOOH), hematite (α-Fe_2O_3), and amorphous ferric hydroxide ($Fe(OH)_3$). The iron ion is typically six-coordinated in an octahedral pattern with oxygen and/or hydroxide ions. The packing structure may be either hexagonal close-packed (goethite and hematite) or cubic close-packed (lepidocrocite). Additional minerals form when sulfate is present in solution, as it always is at AMD affected sites. These include jarosites [(H,K,Na)$Fe_3(OH)_6(SO_4)_2$], melanterite [$Fe(SO_4) \bullet 7H_2O$], ferric sulfate [$Fe_2(SO_4)_3$], and a recently described mineral, schwertmannite [$Fe_{16}O_{16}(OH)_{12}(SO_4)_2$] (Bigham et al., 1994). These minerals differ in important characteristics, including degree of crystallinity, solubility, and thermodynamic stability. Amorphous ferric hydroxide exhibits no long-range order (and thus no X-ray diffraction pattern), and appears to be the most common initial solid formed when iron(III) precipitates. With time and loss of water, amorphous solids tend to convert to the crystalline forms of goethite and/or to hematite (Schwertmann and Cornell, 1991).

Iron(III) usually has an ionic radius of 0.063 nm in octahedral coordination. Because both Al(III) and Mn(III) are of similar size (0.053 and 0.065 nm, respectively), they may substitute for Fe(III) with little to moderate distortion. Mn(II) on the other hand, has an ionic radius of 0.082 nm (Schwertmann and Cornell, 1991). Stanjek and Schwertmann (1992) suggested that Al for Fe substitution should introduce considerable strain into the lattice structure due to shorter bond lengths with oxygen and result in the inclusion of additional hydroxyl ions.

Aquatic Iron Chemistry

Solubility of Ferrous and Ferric Iron

Since the efficiency of technology would be limited by the effective solubility of iron as a solution moved through the treatment system, an understanding of iron solubility fundamentals is important. Ferric iron is quite insoluble compared to ferrous iron. The K_{sp} for ferrous hydroxide is 4.87 x 10^{-17}, while the K_{sp} for ferrihydrite is 2.64 x 10^{-39} (CRC Handbook of Chemistry and Physics, 71st Edition) and the K_{sp} for amorphous ferric hydroxide is often taken to be 10^{-38} . While there is some dispute among researchers as to the precise K_{sp} for each of the oxyhydroxide forms of Fe(III), there is no disagreement that ferric oxyhydroxides are extremely insoluble, with minerals of increasing crystallinity being more insoluble. Solutions in equilibrium with amorphous ferric

hydroxide have ferric iron concentrations of about $10^{-9.6}$ M from around pH 6.5 to 8.0. At any other pH values, the solubility increases as a result of complexation with the OH^- ligand.

Hydrolysis of Ferric Iron in the Presence of Sulfate

The degree of hydrolysis of ferric ions in aqueous solution is a function of pH. At very low pH (<1.0), the ferric ion coordinates with six water molecules. For convenience, waters of hydration are usually omitted from chemical equations and calculations when water is the solvent. As pH increases, protons are lost to solution in a step-wise fashion. Monomers tend to react to form polymers by olation (the formation of Fe - OH - Fe bonds) followed by oxolation (deprotonation, forming Fe - O - Fe bonds) (Stumm and Morgan, 1996). Figure 3.1 presents the results of a series of runs by the geochemical speciation computer model MINTEQA2 for 10 mM iron in simulated AMD solution (described in the methods section). Solids were not allowed to precipitate in this simulation. Since MINTEQA2 is an equilibrium model and does not account for kinetic factors, if solids had been allowed to precipitate, essentially all of the iron would have precipitated as goethite during the first iteration at pH 2.5, along with 95% of the phosphate. Also, 93% of the potassium and 3.7% of the sulfate would have precipitated with some of the iron as K jarosite. The model was instructed not to allow sorption. Figure 3.1 should thus be viewed as a supersaturated solution in which no solids have formed.
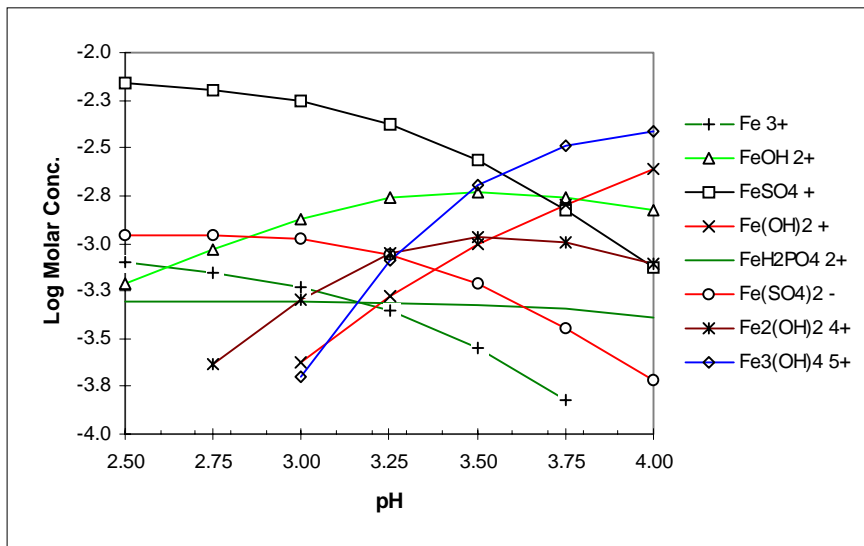
Figure 3.1. Relative abundance of species in a 10 mM Fe_T simulated AMD solution as a function of pH. Values computed by MINTEQA2 with no precipitation allowed.

As can be seen in Figure 3.1, as pH increases above 3.0, Fe/sulfate complexes decrease in abundance along with uncomplexed Fe^{3+}. Above pH 3.5, the trimer $Fe_3(OH)_4^{5+}$ becomes the predominant species, followed in abundance by the monomers

Fe(OH)$_2^+$ and FeOH^{2+}. It appears that hydroxyl ions displace sulfate ions and polymeric iron complexes form by sequential addition of HO-Fe-OH units.

Effect of Sulfate on Precipitation Rates

In their study of the effect of sulfate on iron hydrolysis, Dousma et al. (1979) observed that there was a delay in the iron polymerization process with increasing SO$_4$/Fe ratio below pH 2. They suggested that this was most likely a result of the presence of iron-sulfato complexes. The effect of sulfate on induction times was not reported.

Adsorption of Sulfate on Iron Oxide Surfaces

Parfitt and Smart (1978) provided evidence that sulfate was adsorbed onto iron-oxide surfaces by formation of a binuclear bridge. Adjacent ≡Fe-OH and ≡Fe-OH$_2^+$ groups separated by 0.30 nm provide the active site for adsorption (≡ means surface incorporated). The sulfate ion displaces the hydroxyl and protonated hydroxyl groups forming the ≡Fe-O-S(O)$_2$-O-Fe≡ complex, generating OH$^-$ and H$_2$O. Thus, adsorption results in an increase in pH. They found that sulfate adsorption capacity was 5 times higher for amorphous ferric hydroxide (at pH 4.5) than for goethite (at pH 3.4) on a gram^{-1} basis, while the corresponding surface areas reported were 286 and 90 m^{2}g^{-1} (a ratio of 3.2:1).

Induction Period Studies

The induction period is an operationally defined concept. It is generally defined as that length of time from the addition of a reagent or change in conditions until the time of the detection of a precipitate (Nyvlt et al., 1985). When some property such as a measurable increase in turbidity or a change in conductivity or concentration is used to identify the end of the induction period, the total induction period (t_{ind}) is in fact the sum of the time required to create a stable nucleus (t_i) and the time required for the stable nucleus to grow (t_g) to sufficient size to exert the measured effect (Sohnel and Garside 1992).

Dousma and de Bruyn (1976) used go-stop pH titration and spectrophotometric techniques to study ferric solutions during and after the addition of base. They observed a "pH relaxation" once enough base had been added to exceed a threshold. The "pH relaxation" was a gradual decrease in pH over time after the cessation of the titration accompanied by an increase in optical density. They suggested that initial polymer formation was the result of hydroxo-bond formation. After the threshold pH value had been exceeded, oxolation began in which hydroxo-bonds were converted to oxo-bonds, with the corresponding release of H$^+$. They stated that this was a very slow step compared with monomer and dimer formation reactions.

Dousma and de Bruyn (1979) described the induction period as a "characteristic feature of the aging process." They compared t_{ind} for solutions which had been filtered (0.1 μm) with unfiltered solutions and found no significant difference. Likewise, stirring did not exert an observable effect, and thus bulk diffusion was ruled out as a controlling step. Dousma and de Bruyn measured t_{ind} for ferric nitrate solutions (0.058 M) over the

pH range of 1.85 to 2.22 (equivalent to OH/Fe ratios of 0.49 to 0.89). Induction times ranged from 7 min at pH 2.22 to 47 days at pH 1.85. They concluded that the steps involved in precipitate formation for these solutions were: 1. Hydrolysis of Fe(III) forming monomers and dimers; 2. Reversible formation of polymers; 3. Formation of colloidal-sized nuclei from polymers via a surface-controlled growth process; and 4. Flocculation of colloids resulting in a turbid solution.

Van der Woude and de Bruyn (1983) extended the work of Dousma and de Bruyn (1979) by adding controlled pH studies to free relaxation titrations. Spectrophotometric analysis, pH measurements, and equivalents of base added to maintain pH at a given value were used with ferric nitrate, chloride, and perchlorate solutions ranging in concentration from 0.001 to 0.0625 M. They noted that there was a characteristic color change as the OH/Fe ratio increased, which they ascribed to the increasing degree of polymerization. This was in agreement with a prior study (Dousma and de Bruyn, 1978) of the aging of ferric nitrate solutions where there was a gradual shift in absorbance to longer wavelengths during extended induction times. They observed that Teflon coated vessels did not yield significantly different induction times than did glass containers, and concluded that nucleation on glass surfaces did not control induction period. Their study was limited to the pH range of 1.7 to 2.4 and did not include sulfate solutions. They reported induction periods for a 0.0625 M ferric nitrate solution ranging from less than a minute at pH 2.5 to 1200 hours at pH 2.16.

Dousma and de Bruyn (1979) combined two models presented by Nielsen (1964) for growth of iron oxide coatings: a mononuclear growth model and a polynuclear model. They suggested that the critical nucleus required about 7 to 9 iron atoms joined by olation. A second step involved a structural change due to oxolation, and the growth of the particles by surface-nucleation/precipitation forming goethite-type colloids. These particles then tend to form a precipitate by flocculation. They observed that at room temperature in acid conditions, the particles tended to grow only to an individual size of about 20-40 Å.

In their study of the effect of sulfate on iron oxide formation, Dousma et al.(1979) suggested that the formation of large polymeric complexes was slowed by the complexation of iron by sulfate ions. They noted that at high SO_4/Fe ratios, hematite formation was favored and concluded that sulfate ions somehow prevented the formation of oxo-bridges leading to the formation of goethite (α-FeOOH), but could not describe the mechanism.

Van der Woude and de Bruyn (1983) postulated that induction period and subsequent nucleation was dependent on the formation of a supercritical nucleus from trimers: $Fe_9(OH)_{20}^{7+} + Fe_3(OH)_4^{5+} \rightarrow$ supercritical cluster.

While stating that there are other plausible reaction steps leading to the critical nucleus step, their analysis of optical density changes with increasing polymerization fit well with their conclusion.

Since biological oxidation of iron at low pH can be employed to produce an acidic ferric iron solution from reduced iron in AMD (Chapter 2), carefully controlled pH adjustment in an appropriate reactor environment may lead to iron-oxide surface precipitation on seed particles while avoiding formation of dispersed iron suspensions. If so, a relatively small precipitation reactor might be effective in removing iron from solution without the necessity for sedimentation basins and the formation of iron hydroxide sludge. Coated seed particles which had grown large would be continuously or periodically removed from the reactor system for disposal or reuse for other purposes, and replaced with new seeds. Once iron was removed from solution, neutralization of the effluent could be easily accomplished.

The goal of this phase of the research was to examine the behavior of ferric iron solutions during t_{ind} within the narrow pH range of 2.5 to 4.0. Of particular interest were the effects of sulfate, aluminum, and manganese concentration on t_{ind} since these ions are common in AMD waters. It was considered important to document the length of the induction period for iron concentrations ranging from 1 to 10 mM in solutions typical of AMD to provide guidance for the eventual operation of a prototype treatment system.

Additionally, the following questions were posed.
1. What was the effective iron solubility in typical AMD solutions over the time scale and pH range of interest?
2. Since solubility is related to the mineral phase present, what minerals are precipitated?
3. Does iron concentration affect t_{ind}?
4. Do sulfate/iron ratio, aluminum/iron ratio and/or manganese/iron ratio affect t_{ind}?.
5. Are there detectable changes in solution characteristics during the induction period, such as conductivity and pH, which provide insight into the interaction of sulfate, OH⁻, and iron during precipitation?

METHODOLOGY

Chemicals, Water and Simulated AMD

All chemicals used to prepare solutions were reagent grade except for aluminum sulfate, which was technical grade. Water used was deionized. Solutions were not filtered prior to use. Acids such as nitric, sulfuric and hydrochloric were "Plus" grade by Fisher Chemical Company.

Simulated AMD (Table 3.1) was developed based on the USEPA (1976) findings mentioned above for acid-generating coal mining activities. In a study of the biooxidation of ferrous iron in AMD, reported in Chapter 2, the iron was supplied as ferrous sulfate. Since this study concerned iron precipitation after oxidation, the iron was supplied as ferric sulfate and where appropriate was varied in concentration from 1 to 10 mM.

pH Probe Response and Calibration

The response time of the pH probe/meter (Accumet AP10) appeared to be about 10 s when the probe was immersed in dilute sulfuric acid or an acidic ferric sulfate solution. The probe was periodically cleaned by immersion in a dilute sulfuric acid/hydroxyl amine solution. The probe and meter were calibrated before each set of trials and checked during each session with pH buffers (pH 2.0, 4.0, and 7.0) by Fisher Scientific, Inc. This particular pH meter was selected because it would accept a standard at pH 2.0 in addition to the more commonly used standards.

Table 3.1. Simulated AMD. Concentrations shown are after addition of sulfuric acid to produce pH ~2.3. When used to prepare bicarbonate solution, iron omitted and sulfuric acid replaced with corresponding adjustment to sodium sulfate addition.

Constituent	Molarity	mg L^{-1}
Iron	0.010	558
Aluminum	0.002	54
Calcium	0.002	80
Magnesium	0.001	24
Sodium	0.0075	175
Potassium	0.0005	20
Ammonium (as N)	0.0005	7
Sulfate	0.025	2400
Phosphate (as P)	0.0005	16

Kinetics of Carbonate/Acid Neutralization

Since it was anticipated that the source of alkalinity for the proposed treatment system would be a carbonate mineral, most likely limestone or dolomite, it was necessary to determine if the kinetics of sulfuric acid/bicarbonate neutralization were fast relative to iron precipitation kinetics. A series of trials were conducted by adding a bicarbonate solution to a pH 2.0 sulfuric acid solution. It was observed that the pH reading stabilized within 10 s after the base addition and remained stable. When sufficient base was added to increase pH to about 6, the reading changed from 2.0 to 6.03 in 10 s, then drifted upward over the next 8 min stabilizing at pH 6.71. Thus, the kinetics of bicarbonate/acid neutralization were deemed to be faster than the response time of the probe, at least within the pH range of these studies (pH 2.0 - 4.0).

pH Drift during Titration

A titration experiment was conducted by adding small increments of base solution (0.1 M NaHCO$_3$) to a 0.05 M ferric solution prepared with simulated AMD. After each addition, the pH was measured and recorded every 10 s until the pH remained constant over several successive intervals.

Iron Solubility at Fixed pH

Ferric sulfate solutions (0.01 M Fe) were prepared with simulated AMD, and solid sodium bicarbonate was used to adjust and maintain pH at 2.25, 2.75, 3.00, and 3.20. At various intervals over the next 14 days, samples of solution were removed, filtered through 0.2 μm membrane filters (Supor-200 by Gelman Science, Inc.), and analyzed for dissolved iron. The term "dissolved" is used here with full knowledge that small particles exist which will pass the 0.2 μm membrane. Other definitions are used elsewhere, such as that of Buffle and van Leeuwen (1992) who define three size categories: dissolved (< 1 nm), colloidal (1 nm - 0.45 μm) and particulate (> 0.45 μm). For the purposes of this study it was decided that a 0.2 μm cut-off would be sufficient to provide the necessary information.

Iron Solubility at Fixed Base/Fe Ratio

Equal volumes of 0.01 M Fe (ferric sulfate) and various strength bicarbonate solutions were mixed. The bicarbonate concentrations were selected to produce base/Fe ratios of 0, 1.0, 1.5, 2.0, 2.25, 2.5, 2.75, and 3.0. Samples were removed, filtered through 0.2 μm membrane filters and analyzed for [Fe] over 14 d. The pH was measured and recorded at each sampling time.

Changes in Iron and Sulfate Concentration During Induction and Precipitation

Equal volumes of ferric sulfate solution and bicarbonate solution were mixed in a beaker on a magnetic stir plate and samples of liquid were then withdrawn at specified times for iron and sulfate analysis. The samples were immediately filtered through a 0.2 μm membrane, and preserved with a drop of 6 M nitric acid. Samples were withdrawn at 0.25, 1, 2, 4, 6, and 10 min after mixing.

Induction Period Studies

A technique similar to that suggested by Nyvlt et al.(1985) was employed for induction period studies using ferric sulfate solutions with varying amounts of aluminum, manganese, and sodium sulfate. Iron concentrations studied were 1 mM, 5 mM, and 10 mM. Ten mL of iron solution (at double the desired concentration) were placed in a 100 mL beaker. Ten mL of sodium bicarbonate solution were added quickly by syringe while the contents of the beaker were rapidly mixed by magnetic stir bar.

Upon addition of the base solution, the solution was re-circulated through the optical cell of a spectrophotometer (Beckman DU-640) equipped with a continuous flow pump for 30 seconds, leaving a mixed representative sample in the spectrophotometer's cell . The pH of the solution 10 seconds after addition of the base was recorded. The spectrophotometer was programmed with a kinetic routine to measure absorbance at 650 nm for 0.1 s every 1 s for 10 minutes (Figure 3.2). Prior work revealed that a 10 mM ferric sulfate solution absorbed strongly below 400 nm, but was essentially transparent above that wavelength. Thus, increase in absorbance indicated particulate scattering. The induction period (t_{ind}) was defined as the length of time from the addition of base to the

moment when the absorbance of the sample increased by at least 0.00005 absorbance units per second (abs s[-1]) continuously. To assess the reproducibility of the results of the procedure, 5 trials were conducted with the same mixtures. The measured t_{ind} was found to be reproducible within ± 3 seconds.

Nyvlt et al. (1985) endorsed the use of light scattering (turbidity) measurements when t_{ind} was greater than 10 s. The "induction period" clearly is arbitrary, and includes that time required for the formation of stable nucleii, t_i, and the subsequent growth, t_g, of those nucleii by surface precipitation and/or aggregation.
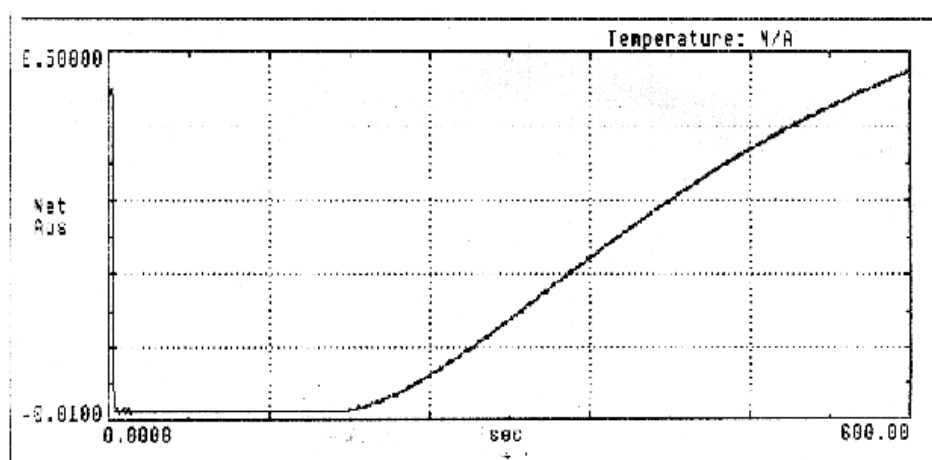
Figure 3.2. Example of induction period scan showing absorbance over a 600 s period. Corresponding tabular values of absorbance were used to determine the end of the induction period. A visible precipitate appeared at about 4 min.

In succeeding trials, the strength of the base solution was altered, thus changing the pH of the resultant solution and t_{ind}. Also, other ions were added to the solutions to measure their effect on t_{ind}. Since aluminum, manganese, and sulfate are the most abundant ions in addition to iron in AMD waters, the effect of these ions on t_{ind} was investigated. A matrix of solution compositions (Table 3.2) was designed to identify the effects of the 3 constituents with minimal experimental trials.

Table 3.2. Solution composition for initial screening study of effects of Al, Mn, and SO_4 on induction period of 1 mM Fe solutions.

Species	low		med		high	
	mg/L	M	mg/L	M	mg/L	M
Al	0	0.0000	135	0.005	270	0.010
Mn	0	0.0000	55	0.001	110	0.002
SO4	144	0.0015	2400	0.025	3840	0.040

Ionic strength was not controlled in these experiments. Ionic strength for the solutions was calculated using MINTEQA2 and found to range from 0.004 to 0.26 M. When t_{ind} data for solutions with the same sulfate concentration but different ionic

strengths were plotted (data not shown), there was no correlation between ionic strength and t_{ind} ($R^2 = 0.07$). Thus any observed effect was not due to increased ionic strength alone.

After initial trials, other combinations of sulfate and aluminum concentrations in iron solutions ranging in concentration from 1 to 10 mM were studied (Table 3.3). In all cases, the concentrations of the iron and bicarbonate solutions were calculated to yield the desired final concentrations after mixing.

Conductivity and pH Measurements During Induction and Precipitation

Concurrent measurements of specific conductivity and pH during induction and precipitation were obtained by positioning the pH probe and conductivity probe (Corning

Table 3.3. Aluminum to iron and sulfate to iron molar ratios in solutions for investigation of induction period effects.

1 mM Fe		5 mM Fe		10 mM Fe	
Ratios		Ratios		Ratios	
Al/Fe	SO4/Fe	Al/Fe	SO4/Fe	Al/Fe	SO4/Fe
0	1.5	0	1.5	0	1.5
0	50	0	10	0	5
0	100	0	20	0	10
5	9	1	3	0.5	2.25
10	16.5	2	4.5	1	3
10	50	2	10	1	5
10	100	2	20	1	10
5	50	1	10	0.5	5

Checkmate Modular meter system with conductivity module) in 50 mL of a 10 mM iron solution in a 250 mL beaker which was rapidly mixed by a magnetic stir plate. At $t = 0$, an equal volume of bicarbonate solution was added to the beaker resulting in a 5 mM iron concentration. Readings of pH and specific conductivity were recorded at $t = 0.25$ min, 0.5 min, and every 0.5 min thereafter for a total time of 10 min. To assess the reproducibility of the conductivity measurement using this procedure, repeated trials were conducted with aliquots of the same solutions. In all, 140 individual measurements were made. For measurements made at a given time interval the mean standard deviation for conductivity was 0.021 mS. Before addition of the base solution, the pH of the iron solution was adjusted to pH 2.34 with 6 M nitric acid for all trials. The bicarbonate solutions used ranged in strength from 4 mM to 10.5 mM. The solution was inspected visually during each trial, and the time of appearance of turbidity within the solution was noted. The induction time determined visually was ± 0.5 min in 7 trials. To explore the changes in behavior due to variations in sulfate concentration, iron solutions and bicarbonate solutions were prepared using deionized water, 50% simulated AMD, and 100% simulated AMD. All glassware and probes were rinsed, carefully cleaned to remove iron deposits, and dried before each trial.

Digestion of Iron Minerals

Precipitates were formed by combining a ferric sulfate solution with varying strength bicarbonate solutions to result in the base/Fe ratios of 1, 2, and 3. The suspensions were centrifuged and washed with deionized water 3 times by repeated centrifugation and decantation. The solids were then allowed to dry at room temperature. Total mineral dissolution was achieved by digestion with hot HCl as recommended by Schwertmann and Cornell (1991). Triplicate samples (~0.1 g) were placed in 15 mL of 6 M hydrochloric acid in test tubes which had been previously acid cleaned. The test tubes were placed in a boiling water bath for 1 h, and stored for later analysis of iron and sulfate.

Oxalate Dissolution of Amorphous Iron Minerals

Oxalate-soluble iron ($[Fe]_o$) is that iron mineral which dissolves when placed in 0.2 M ammonium oxalate acidified to pH 3 with 0.2 M oxalic acid, according to the method of Schwertmann and Cornell (1991). Oxalate solubility is generally presumed to relate to the degree of crystallinity of the mineral; more crystalline iron minerals such as goethite and hematite do not dissolve during this extraction. Triplicate 0.1 g samples were placed in 25 mL of oxalate solution in flasks. The flasks were stoppered, and place on a shaker table in the dark for 2 h. Solution was then removed, filtered through 0.2 μm membranes, and stored for later analysis of iron and sulfate.

Iron Analysis

Total iron was assayed using flame atomic absorption spectrophotometry (Method 3500-Fe B.) as detailed in <u>Standard Methods for the Examination of Water and Wastewater</u> (APHA, AWWA,WEF 1992).

Sulfate Analysis

The presence of iron in all samples made analysis by ion chromatography impractical due to iron precipitation within the column. Therefore, Method 4500-SO_4^{2-} E. (Turbidimetric) as described in <u>Standard Methods for the Examination of Water and Wastewater</u> (APHA, AWWA,WEF 1992) was selected for use. The method used the precipitation of barium sulfate by the addition of barium chloride to create turbidity in the sample, which was measured in a nephalometer (Monitek Model TA1). Samples were diluted prior to addition of the barium chloride based on estimates of sulfate concentration so as to yield acceptable absorbance values. Blanks and standards (Na_2SO_4) were carried through the procedure to generate a standard curve as stipulated in the method.

Ionic Strength and Chemical Speciation Calculations

The computer program MINTEQA2, distributed by the USGS and the Center for Exposure Assessment and Modeling of the USEPA, was used for calculations of ionic strength and speciation.

Statistical Methods and Calculations

Where appropriate, means, standard deviations, simple and multiple linear regression, and analysis of variance (ANOVA) and covariance (ANCOVA) were computed using the data analysis features of Microsoft Excel 7.0. The procedures Best Subset Multiple Regression and Stepwise Elimination were performed by Minitab Release 10X (Minitab, Inc., State College, PA). These calculations were consistent with statistical methods as reported in the literature (Sokal and Rolf, 1995).

RESULTS AND DISCUSSION

Behavior of Ferric Sulfate Solutions Upon Addition of Base

When base was added to a ferric sulfate solution ($SO_4/Fe = 1.5$), the pH increased within a few moments, then drifted as shown in Figure 3.3, an effect referred to by Dousma and de Bruyn (1976) as "relaxation." The initial data point shown in Figure 3.3 is after 1 h. When the base/Fe ratio was less than 3, the pH drifted down over time, and corresponded to a slow decrease in dissolved iron concentration. When sufficient base was added to satisfy the base/Fe = 3 requirement, a drift of pH upward rather than downward resulted. It should be noted however, that the change in pH observed over 14 d for the base/Fe = 3 solution represented a change in $\{H^+\}$ of just 4×10^{-6} M.
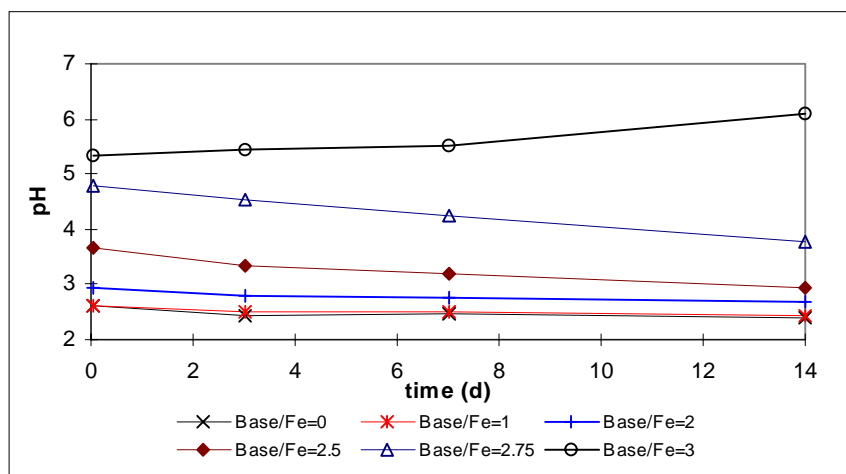
Figure 3.3. pH drift after addition of water or bicarbonate solution to ferric sulfate solution ([Fe] = 5 mM) from 1 h to 14 days.

The ability of acidic ferric sulfate solutions to buffer the addition of hydroxyl ions is illustrated in Figure 3.4, which shows the pH of ferric sulfate solutions over a 14 d time period after various amounts of base were added at t = 0. The pH of the solution changed little until the base/Fe ratio exceeded 2.0. Also as noted above, the pH drifted downward over time except for the base/Fe = 3.0 solution. A possible explanation for this behavior will be presented later.

When [Fe] (operationally defined as that iron which passed a 0.2 μm membrane filter) was plotted as a function of base/Fe and time (Figure 3.5), it was seen that [Fe] decreased over time after dilution with water, and after addition of base. In these figures, the ratio of base/Fe = 0 is used to refer to additions of deionized water containing no added base anions. As discussed in Stumm and Morgan (1981), the dilution of acidic iron solutions with pure water constitutes the addition of base, and may result in the precipitation of iron hydroxide over time. This effect is a function of the initial iron concentration, with more dilute iron solutions unable to buffer the addition of hydroxyls due to dissociation of water.
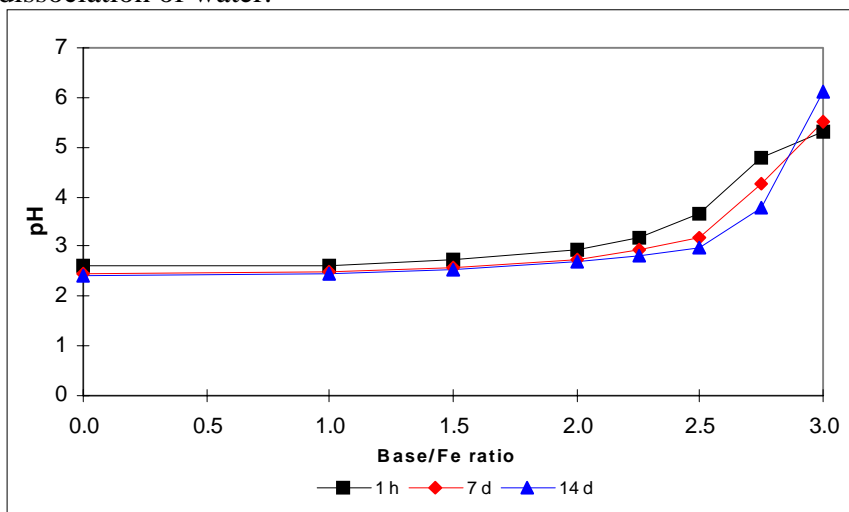
Figure 3.4. Buffer effect (pH response) of ferric sulfate solutions upon addition of base.

In more concentrated iron solutions, iron hydrolysis consumes hydroxyls and results in hydrolyzed iron species which remain stable in solution. It was the author's experience that solutions prepared by the addition of solid ferric sulfate to water where [Fe] ≥ 0.05 M remained stable over long periods of time without precipitation or coating of the glass container walls. More dilute solutions developed coatings and/or visible precipitates within a few days.

As seen in Figure 3.6, iron concentrations decreased quickly at all pH levels until day 3, and then more slowly until day 14. The slope of the solubility curve is steep below pH 3.0 (note that the vertical axis is a log scale), but becomes flat above that value, indicating that increasing the pH from 3.0 to 5.5 would not result much of a decrease in iron concentration over this time period. The importance of kinetics on dissolved iron concentration is evident here, since the thermodynamic solubility of ferric iron in equilibrium with goethite, for example, is on the order of 10^{-9} M at pH 4, five orders of magnitude below that observed over the time frame of these studies.
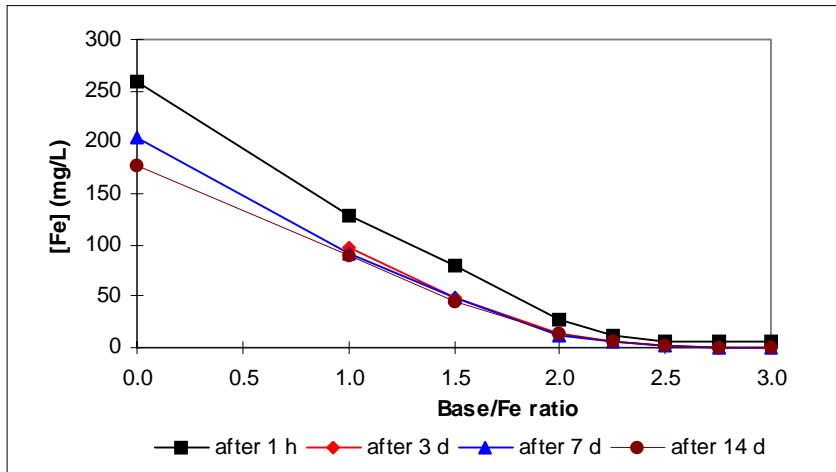
Figure 3.5. Iron concentration as a function of base/Fe ratio and time in SO_4/Fe = 1.5 solutions.
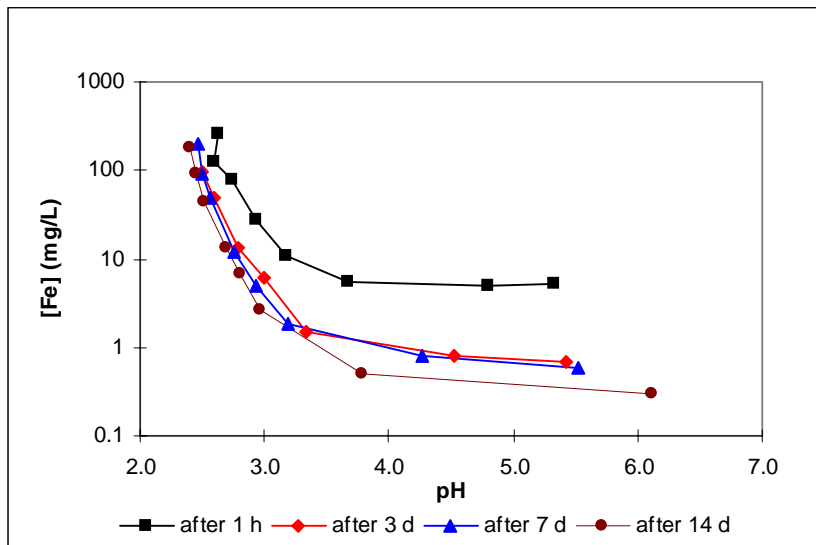
Figure 3.6. Iron concentration as a function of pH and time after base addition in SO_4/Fe = 1.5 solutions.

When 10 mM ferric iron was dissolved in simulated AMD (SO_4/Fe = 2.5), solubility increased and the rate at which equilibrium was approached appeared to slow as illustrated in Figure 3.7. For example, at pH 3.0, dissolved iron in simulated AMD at day 7 was 30 mg/L, which was 13 mg/L above the day 14 value of 17 mg/L. In the simpler ferric sulfate solution discussed above (SO_4/Fe = 1.5), dissolved iron concentration at pH 2.94 was 5 mg/L on day 7, just 2.4 mg/L above the day 14 value of 2.6 mg/L.
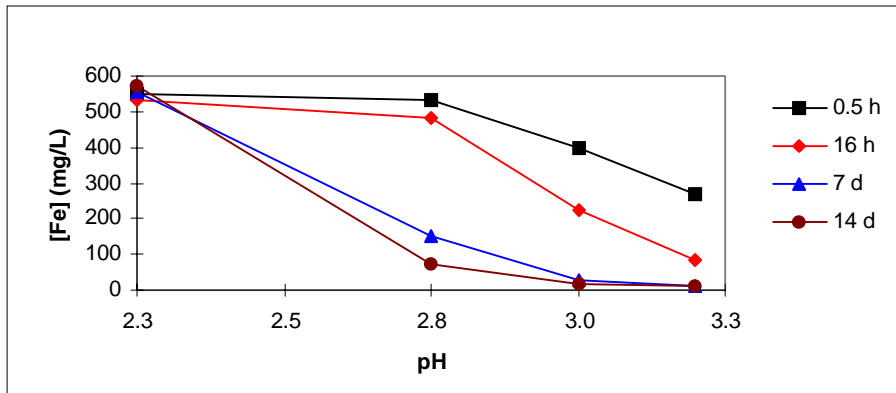
Figure 3.7. Iron solubility as a function of pH and time in simulated AMD (SO_4/Fe = 2.5).

Changes in Iron and Sulfate Concentration During Induction and Precipitation

When weak base was added to a 5 mM iron solution at SO_4/Fe = 1.5, the concentration of iron which passed a 0.2 μm membrane did not change for a period of about 2 minutes (Figure 3.8). After that time, the [Fe] in both of the base/Fe = 0.5 and 0.75 solutions decreased, but it decreased faster in the higher base ratio solution. A visible turbidity was observed in the base/Fe = 0.75 solution at about 2.5 min, while turbidity was observed in the base/Fe = 0.5 at about 5 minutes. When the same base additions were made to solutions which had elevated sulfate concentrations (SO_4/Fe = 5), no turbidity was observed during the 10 minute observation period, and dissolved iron concentration did not change. There were no detected changes in sulfate concentration.
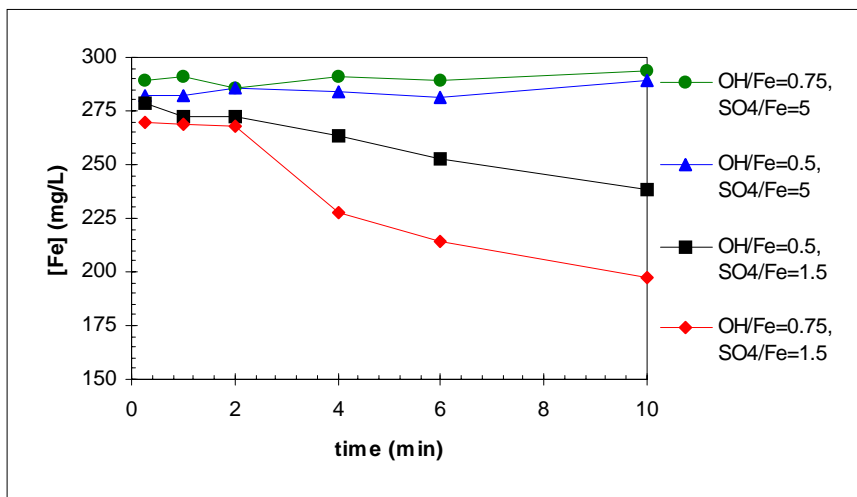
Figure 3.8. Change in iron concentration during induction and precipitation at different base/Fe ratios and SO4/Fe ratios; mean of 2 replicates for each series.

When the higher base/Fe ratio of 2.0 was used in 1 mM Fe solutions which had SO_4/Fe ratios of 1.5 and 10, precipitation occurred almost immediately in both cases, but the iron concentration which passed the 0.2 μm membrane varied slightly. As can be seen in Figure 3.9, there was a slight difference in iron concentration due to sulfate

41

concentration in the early phase of precipitation, but by the end of the 10 min period there was little difference in [Fe] in the low and high SO_4/Fe ratio solutions (4.3 and 5.9 mg L^{-1}, respectively). Sulfate concentration was not observed to change in either case during the 10 minute period. Thus, increased sulfate concentration led to slower precipitate formation. A possible mechanism for this effect will be presented later.
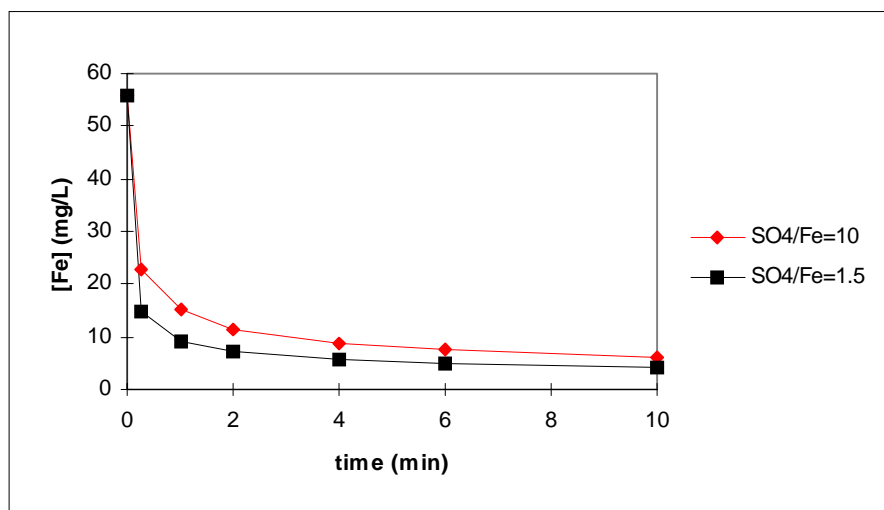
Figure 3.9. Change in iron concentration during precipitation at base/Fe = 2 and SO_4/Fe = 1.5 and 10; initial [Fe] = 1 mM.

Induction Period

Effect of Aluminum and Manganese on Induction Period

Analysis of variance was used to examine the significance of manganese (Mn II) up on induction period to a concentration of 2 mM, and it was found that Mn did not have a significant effect ($\alpha = 0.05$) on t_{ind} in 1 mM Fe solutions. Therefore, it was not investigated further. Aluminum was investigated for its effect on induction period in 1, 5, and 10 mM Fe solutions at Al/Fe ratios up to 10. Using ANCOVA, it was found that Al did not exert a significant effect at the $\alpha = 0.05$ significance level.

Effect of Sulfate on Induction Period

Sulfate exerted a significant effect on t_{ind} as is seen in Figure 3.10a, b, and c for iron concentrations 1 mM, 5 mM, and 10 mM, respectively. Regression lines were calculated for each of the sets of data points in each figure (Table 3.4). There were statistically significant differences ($P < 0.05$) between all groups of data as measured by Students t-Test for closest pairings of groups in the 1 mM Fe solutions. Differences were statistically significant ($P < 0.05$) for all groups in the 5 mM Fe series except between the SO_4/Fe = 1.5 and 3 groups, and for all groups in the 10 mM Fe series except between the SO_4/Fe = 2.25 and 3 groups.

42
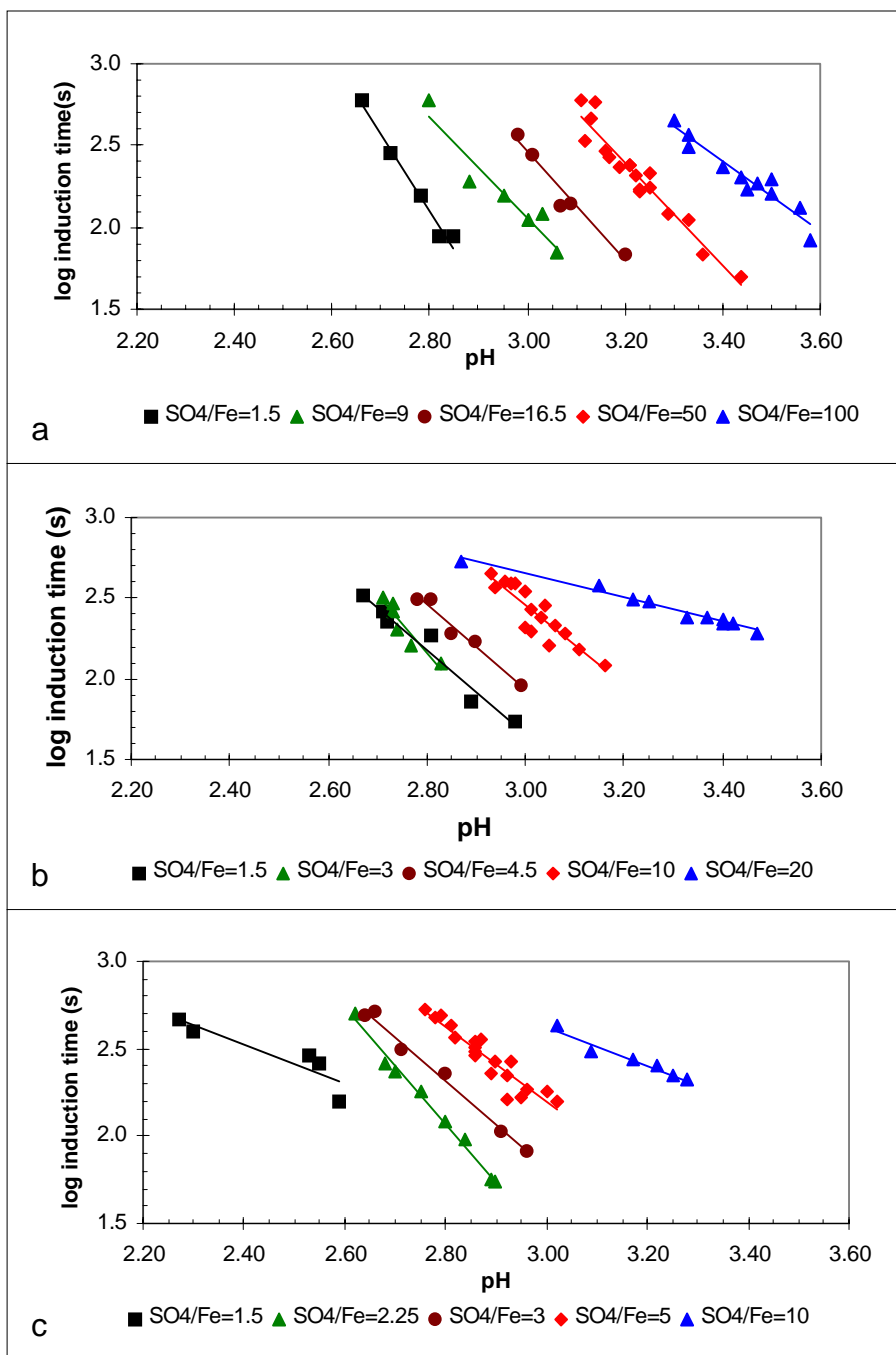
Figure 3.10a,b,c. Effect of sulfate on induction time of (a) 1 mM Fe, (b) 5 mM Fe, and (c) 10 mM Fe solutions with different SO_4/Fe ratios. Each data point represents an individual measurement.

From a visual inspection of the data in these figures, there appeared to be a complex relationship among t_{ind}, the SO_4/Fe ratio, iron concentration, and pH. A higher SO_4/Fe ratio required higher pH to produce the same t_{ind}. Correspondingly, at the same pH, higher SO_4/Fe ratio generally resulted in longer t_{ind}. To investigate this relationship

43

further, the regression lines presented in Table 3.4 were used to estimate the pH associated with t_{ind} of 100 s, 200 s, 300 s, and 400 s for each SO_4/Fe ratio in each iron concentration. The corresponding $\{H^+\}$ were then plotted as a function of log SO_4/Fe ratio.

Table 3.4. Regression coefficients for log induction period (s) as a function of pH for 1, 5, and 10 mM Fe for various SO4/Fe ratios

For 1 mM Fe Solutions				For 5 mM Fe Solutions				For 10 mM Fe Solutions			
SO4/Fe	Slope	Intercept	R^2	SO4/Fe	Slope	Intercept	R^2	SO4/Fe	Slope	Intercept	R^2
1.5	-4.590	14.960	0.979	1.5	-2.612	9.495	0.955	1.5	-1.089	5.135	0.811
9	-3.065	11.257	0.908	3	-3.516	12.007	0.902	2.25	-3.276	11.246	0.991
16.5	-3.333	12.457	0.963	4.5	-2.644	9.867	0.964	3	-2.517	9.361	0.989
50	-3.147	12.469	0.929	10	-2.567	10.037	0.801	5	-2.194	8.774	0.876
100	-2.117	9.599	0.923	20	-0.745	4.887	0.980	10	-1.102	5.933	0.948

When the t_{ind} = 100 s lines were plotted for each of the 3 iron concentrations on the same figure (Figure 3.11a), an interesting result was observed. At a log SO_4/Fe ratio of about 0.5 (SO_4/Fe = 3.16), the three trend lines met, suggesting that at that SO_4/Fe ratio, iron concentration had little effect on the $\{H^+\}$ required for t_{ind} = 100 s. The same was observed (Figure 3.11b, c, and d) for t_{ind} = 200 s, 300 s, and 400 s, respectively, except that with increasing t_{ind}, the point appeared to move slightly to the right, to about log SO_4/Fe = 0.7 (SO_4/Fe = 5). It was also clear that the effect of iron concentration was greater for shorter values of t_{ind} for a given SO_4/Fe ratio.

The relationship between t_{ind} and SO_4/Fe ratio can also be presented by calculating constant pH lines (iso-pH), and then plotting log t_{ind} verses log SO_4/Fe. For each [Fe], the iso-pH lines appear to converge (Figure 3.12a-c). Within the range of log SO_4/Fe ratios investigated, increasing pH led to shorter t_{ind} at all SO_4/Fe ratios, but with a decreasing effect: the presence of sulfate ions slowed the effect of increased hydroxyl ion concentration. While the iso-pH lines appeared to converge, the point of convergence was well beyond the range of SO_4/Fe values investigated, and no conclusions are drawn here as to any significance attached to this observation.

Multiple Linear Regression

Based on the above observations, it was hypothesized that the factors of pH (or its corollary, pOH), iron concentration, and sulfate concentration would be significant predictors of precipitation rate, and thus induction time. These factors as well as others such as base/Fe ratio and SO_4/Fe ratio were evaluated for their ability to predict induction time by means of multiple linear regression. Using Best Subset Regression and Stepwise Multiple Regression, it was found that the factors of pH, log [Fe], and log [SO_4] were the best predictors of log induction time. An iterative process was used to improve the data set by eliminating outliers identified by the statistical program (Minitab Release 10X) which exerted a large influence on the regression. After eliminating outliers, there remained 93 observations. This resultant data set yielded a multiple R^2 of 0.84 with a high level of significance ($P < 0.001$). Multiple R^2 is the Coefficient of Multiple

Determination, and indicates the extent to which the combination of factors predicts the dependent variable (Sokal and Rolf, 1995). A summary of the multiple regression results is presented in Table 3.5. None of the factors produced a significant R^2. The predictive equation for log induction time (s), with standard errors in parentheses, was

$$\log t_{ind} = 6.7(\pm0.30) - 1.29(\pm0.10)pH + 0.94(\pm0.07)\log [SO_4] - 0.36(\pm0.05)\log[Fe]$$

The regression coefficients imply that pH had the largest individual effect on induction time with an increase in pH decreasing t_{ind}, consistent with increased hydrolysis of iron ions. Sulfate concentration was the second most important predictor, with increased $[SO_4]$ lengthening t_{ind}, possibly due to the inner-sphere sorption of sulfate ions on active sites of the oxide surface blocking the attachment of Fe/OH growth units. Increased [Fe] would lead to shorter t_{ind} as the likelihood of effective collisions increased.
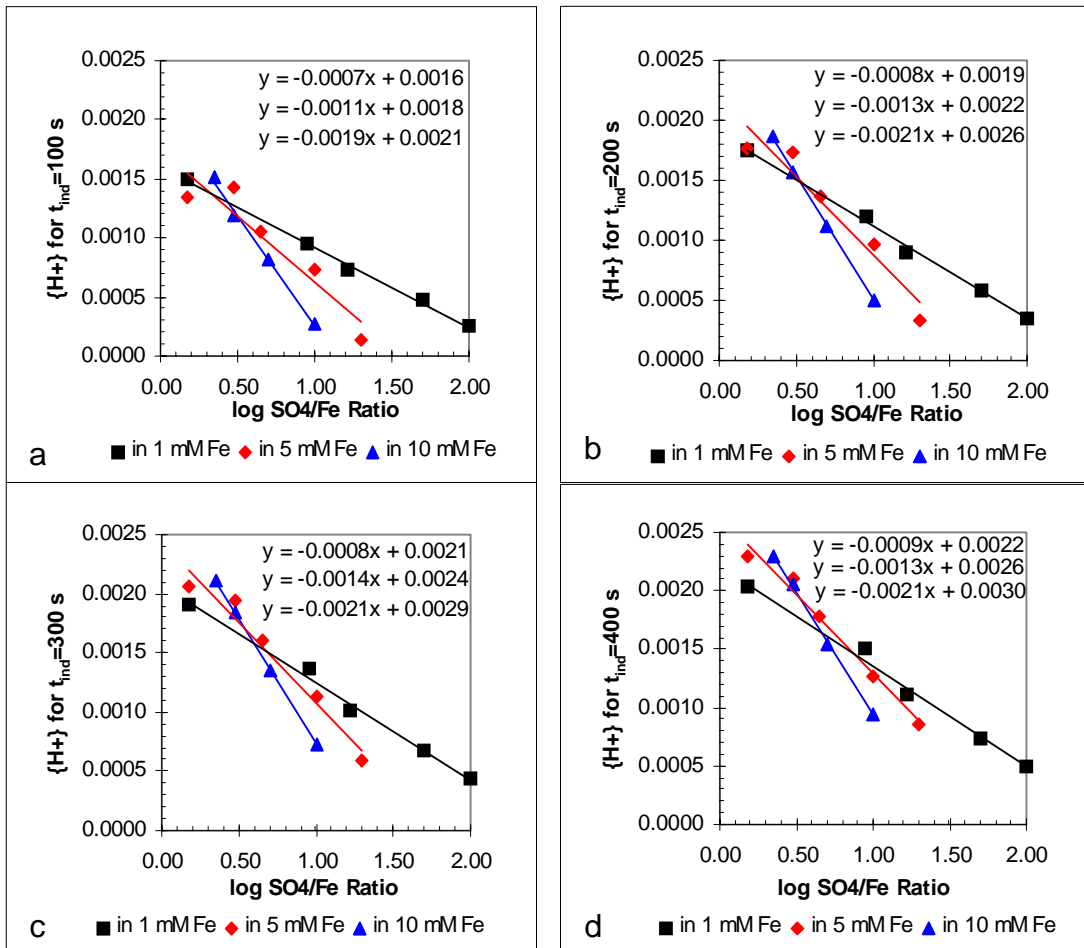
Figure 3.11a, b, c, d. Plot of $\{H^+\}$ associated with t_{ind} of (a) 100 s, (b) 200 s, (c) 300 s, and (d) 400 s as a function of log SO_4/Fe ratio and iron concentration.
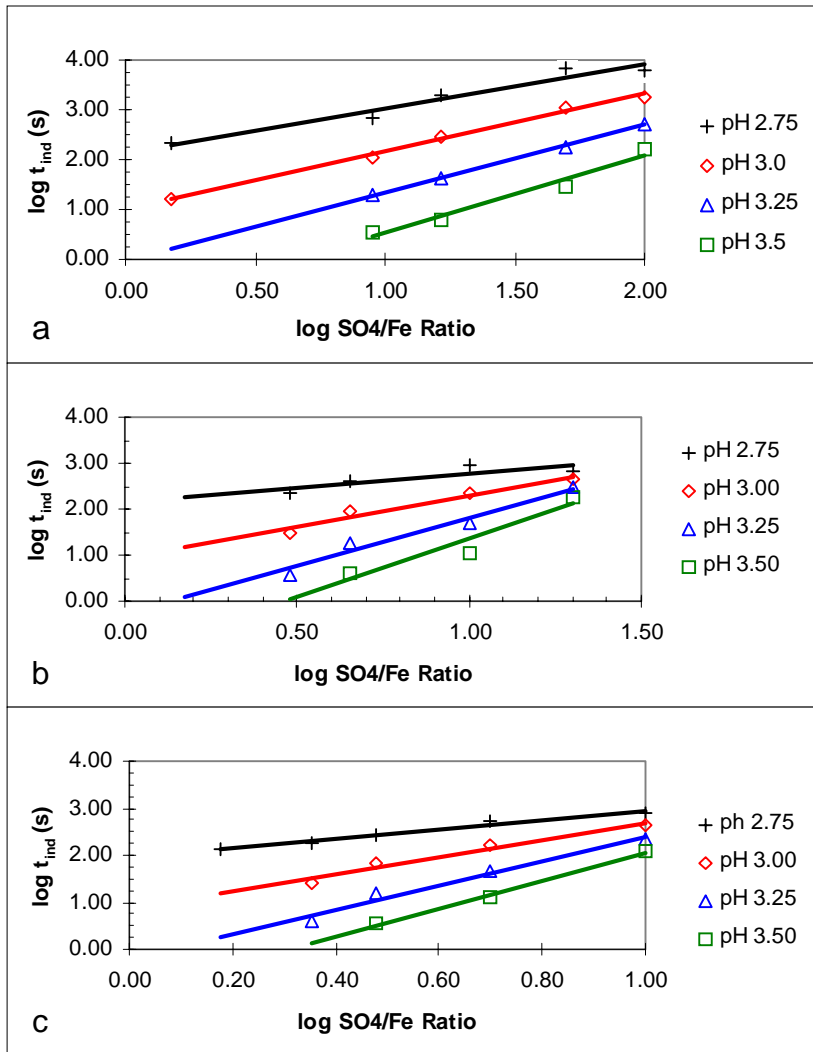
Figure 3.12a, b, c. Induction time as a function of log SO4/Fe ratio and pH for (a) 1 mM Fe, (b) 5 mM Fe, and (c) 10 mM Fe

Table 3.5. Summary of multiple regression results for the predictive factors pH, log [Fe], and log [SO$_4$] with log induction time (s) as the response variable.

Regression Statistics		ANOVA	df	SS	MS	F	Significance F
Multiple R	0.844	Regression	3	2.253	0.751	73.56	5.14E-24
R Square	0.713	Residual	89	0.908	0.010		
Adjusted R Sq	0.703	Total	92	3.161			
Std Error	0.101						
Observations	93						

	Coefficients	Std Error	t Stat	P-value	Lower 95%	Upper 95%
Intercept	6.705	0.3018	22.22	4.50E-38	6.106	7.305
pH	-1.291	0.1008	-12.81	6.75E-22	-1.491	-1.091
log [Fe]	-0.363	0.0479	-7.58	3.16E-11	-0.458	-0.268
log [SO4]	0.940	0.0689	13.64	1.60E-23	0.803	1.076

Conductivity and pH Changes during Precipitation

      The use of the operationally defined concept of t_{ind} provided only macroscopic evidence for the changes occurring in the solution after base addition. As mentioned above, Sohnel and Garside (1992) identified two periods which together constitute the time to an observable effect, namely t_i and t_g. Since the appearance of turbidity does not provide information about changes occurring in the solution prior to the growth of particles of sufficient size and number to scatter light, concurrent measurements of conductivity and pH were made for a series of solutions in hopes of learning more about changes within the solution prior to the visual detection of particles.

<u>Changes due to Varying Base Addition</u>

      Typical of the behavior observed are the results shown in Figure 3.13 for a ferric sulfate solution series prepared using deionized water. The data points in (a) represent pH, while the data points in (b) represent specific conductivity measured concurrently. The initial pH of the iron solution was 2.34, its initial specific conductivity was 2.77 mS, and its initial [Fe] was 10 mM. When the iron solution was mixed with a bicarbonate solution, the resultant iron concentration was 5 mM. Since it was only practical to measure changes which occurred slowly, dilute bicarbonate solutions were used, ranging from 4 to 7.5 mM so that t_{ind} would be within the range of 2 to 10 min. The specific conductivity of several standard sodium bicarbonate solutions was recorded: 5 mM $NaHCO_3 = 0.53$ mS, 7.5 mM $NaHCO_3 = 0.72$ mS, and 10 mM $NaHCO_3 = 0.91$ mS.

      Because of practical considerations, the t_{ind} values for these trials were determined by visual inspection only. However, when t_{ind} was measured for certain of the solutions using the spectrophotometer, the times were reasonably close to those determined visually. Referring to the solutions in Figure 3.13a and b, no precipitation occurred in Solution #1 (prepared with 4 mM bicarbonate) which quickly attained a pH of 2.72-2.73 and was maintained for the 10 minute period. The specific conductivity, measured to be 1.531 mS at 0.25 min, decreased quickly for the first minute, then more slowly until reaching a minimum of 1.467 mS at 5.0 min (time of minimum conductivity $= t_{min}$), and then slowly increased to 1.478 mS by the end of the 10 min period. The behavior of Solution #3, to which 7.5 mM base had been added, followed the same pattern, but was more exaggerated. The pH immediately increased to 2.86 were it remained for 30 s, then decreased steadily reaching 2.70 at the end of the 10 min period, slightly lower than that of solution #1. Turbidity was observed in solution #3 after 2.5 min. Conductivity decreased quickly to 1.367 mS at $t_{min} = 1$ min, then increased to 1.575 at the end of the 10 min period. The rate of change of conductivity slowed toward the end of the period, from a high of 0.044 mS min^{-1} just after the minimum to 0.010 mS min^{-1}. Solution #2 had intermediate behavior, with $t_{ind} = 6$ min, not quite so great of a drop in conductivity as solution #3, $t_{min} = 1.5$ min, and an initial pH plateau of 4 min, which was longer than that of solution #3. Other trials not shown were consistent with those presented here.

      These results indicate that increased additions of base (base/Fe ratio) resulted in exaggerated changes in conductivity and pH during the induction period which

corresponded to shorter t_{ind}. Accompanying shorter t_{ind} were shorter t_{min} , a shorter fixed pH plateau followed by a larger drop in pH, a shorter and steeper drop in conductivity followed by a stronger rebound in conductivity. A sharp drop in conductivity was always followed by an increase in conductivity after the initial period. A possible explanation for these conductivity changes will be proposed later.
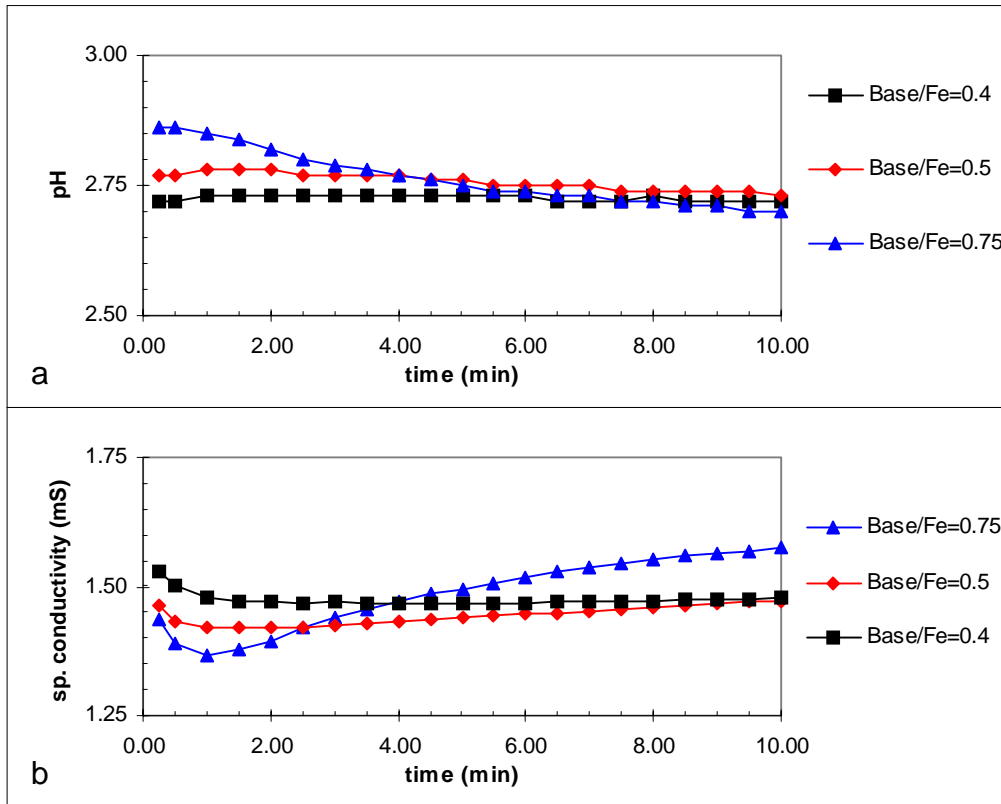
Figure 3.13a, b. Changes in (a) pH and (b) conductivity during induction and precipitation of ferric sulfate solutions after addition of bicarbonate. Solutions were prepared by combining equal volumes of 10 mM ferric sulfate with 4, 5, or 7.5 mM bicarbonate at t=0.

Effect of Sulfate Concentration on Conductivity and pH During Precipitation

To investigate the effect of sulfate on changes in conductivity and pH during induction, a series of trials were conducted using solutions prepared from 50% AMD and 100% AMD in addition to those with deionized water. For purposes of comparison, the pH behavior of trials which resulted in $t_{ind} = 4$ min are presented in Figure 3.14b. The patterns of changes in conductivity (Figure 3.14a) were essentially identical. To achieve the same induction time in the three solutions, higher base/Fe ratios were required in the higher sulfate solutions. As a consequence, the initial pH plateau seen in the low sulfate, base/Fe = 0.65 solution disappeared when the base/Fe ratio was increased to 0.7 and 0.95 in the higher sulfate concentration solutions. Initial pH was also higher in the higher

48

base/Fe solutions, indicating that sulfate did not simply buffer the additional base added by releasing protons from bisulfate ions (HSO_4^{-1}).

In other trials, 10 mM Fe solutions and 7.5 mM bicarbonate solutions (base/Fe = 0.75) were also prepared using deionized water, 50% and 100% simulated AMD. These solutions were combined as described above and pH and conductivity measured. In Figure 3.15a and b, arrows indicate t_{ind}, which were 2.5 min, 3 min, and 9 min for SO_4/Fe ratios of 1.5, 2.5, and 5, respectively. Higher SO_4/Fe ratio slightly increased the t_{min}, from 1 min in SO_4/Fe = 1.5, to 2 min in SO_4/Fe = 5. On a proportional basis, the increase in t_{ind} was 3.6 times the increase in t_{min}. The rate of change in conductivity (ΔmS min^{-1}) was greater in the low sulfate solution, and decreased with increasing sulfate concentration. In spite of the different sulfate concentrations, addition of the same amount of base resulted in almost the same initial pH as shown in Figure 3.15b. At the same base/Fe ratio, there is a greater decrease in pH in the two lower sulfate solutions than in the highest SO_4/Fe solution.
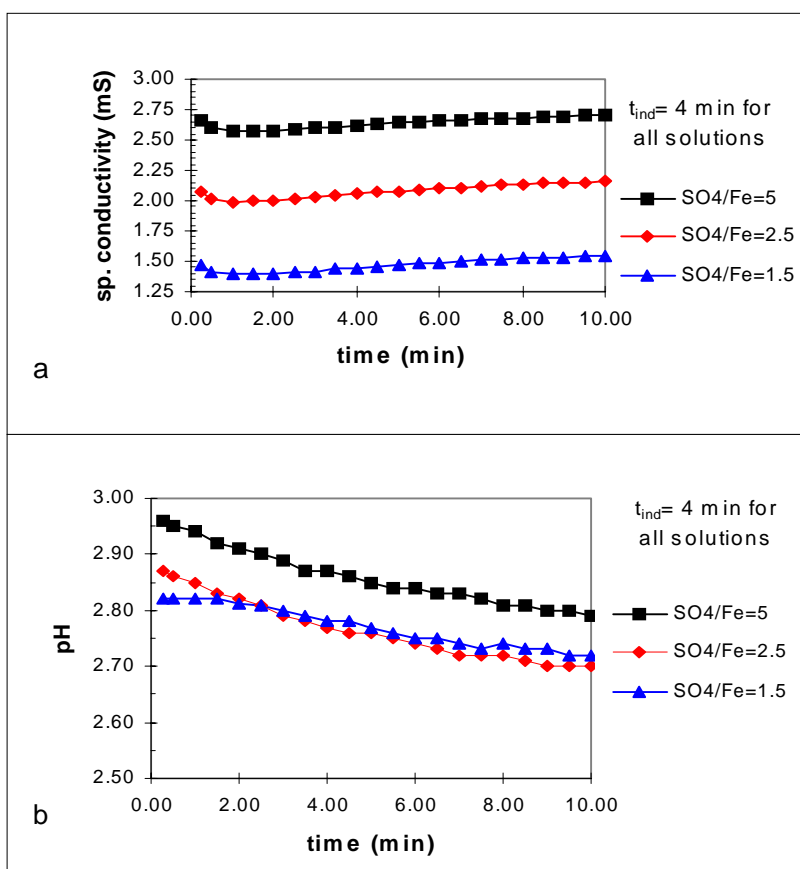
Figure 3.14 a and b. Changes in (a) specific conductivity and (b) pH during induction and precipitation in solutions of different SO_4/Fe ratios which all exhibited a t_{ind} of 4 min; trials were initiated by combining 10 mM iron (ferric sulfate) and various bicarbonate solutions which had both been prepared with deionized water (SO_4/Fe=1.5), 50% AMD (SO_4/Fe=2.5), and 100% AMD (SO_4/Fe=5). Base/Fe ratios were 0.65, 0.70, and 0.95, respectively.
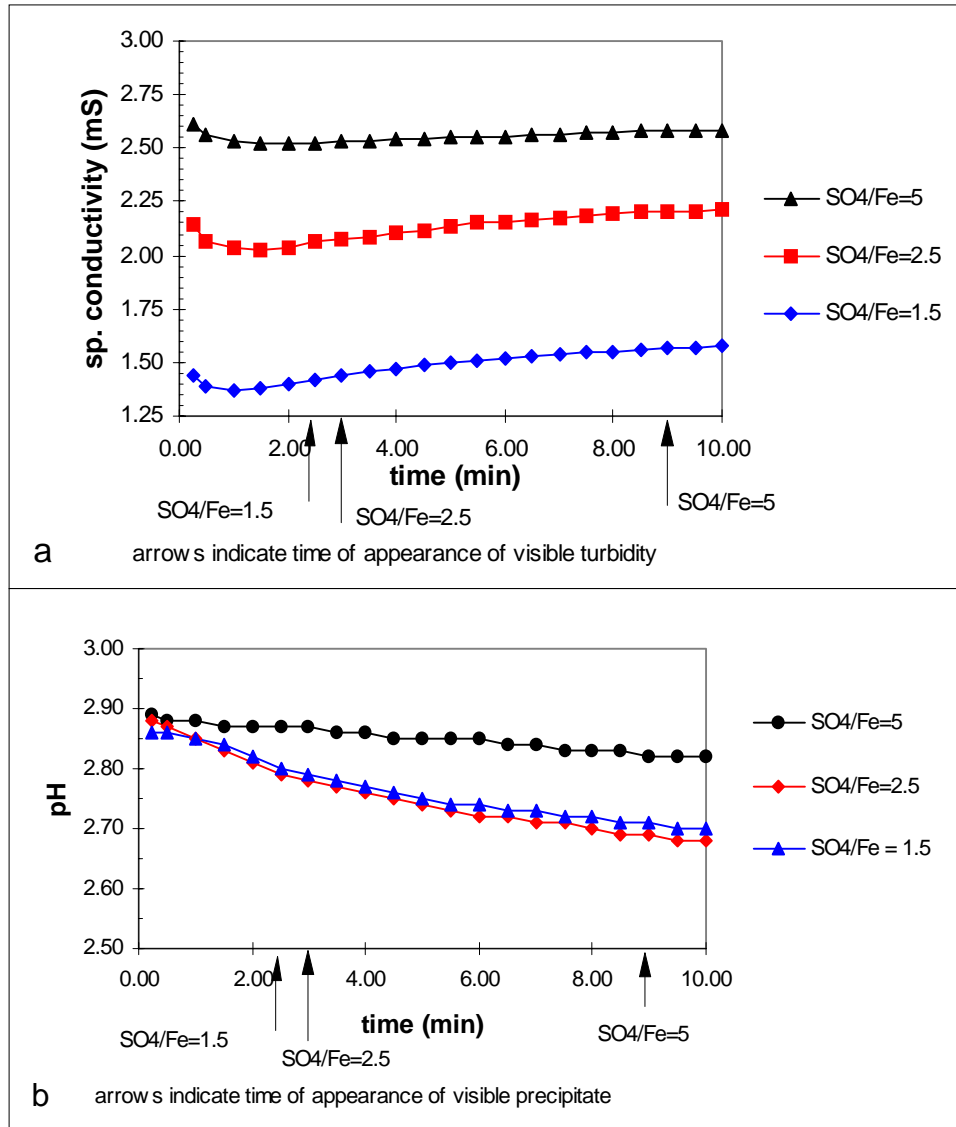
Figure 3.15a and b. Changes in (a) specific conductivity and (b) pH during induction and precipitation with varied SO4/Fe ratios; trials were initiated by combining 10 mM iron (ferric sulfate) and 7.5 mM bicarbonate which had both been prepared with deionized water (SO$_4$/Fe=1.5), 50% AMD (SO$_4$/Fe=2.5), or 100% AMD (SO$_4$/Fe=5).

Thus it was seen that increased sulfate concentration resulted in diminished changes in conductivity and pH during the induction period which corresponded to longer t_{ind}. Accompanying longer t_{ind} were slightly longer times of minimum conductivity, t_{min}, but there was not a one-to-one correspondence.

50

Composition of Minerals Formed By Precipitation

Precipitates were formed by combining a ferric sulfate solution with varying strength bicarbonate solutions to result in the base/Fe ratios of 1, 2, and 3. The minerals were analyzed for iron and sulfate as described in the Methodology section. Iron was found to constitute about 42% by weight of the minerals formed in base/Fe = 1 and 2. For the base/Fe = 3 mineral, iron was about 49% of the total weight. Sulfate was found to make up 14, 16, and 6% by weight of the minerals, respectively. Therefore, the Fe/SO_4 molar ratios were about 5.4:1 and 4.5:1 for base/Fe = 1 and 2, and for the base/Fe = 3 precipitate the Fe/SO_4 molar ratio was about 14:1.

Oxalate solubility is used as an indication of amorphous character, and the ratio of oxalate soluble iron/total iron is a rough indication of the degree of crystallinity (Schwertmann and Cornell, 1991). The base/Fe = 1 mineral was completely oxalate soluble, while the base/Fe = 2 mineral was 55% soluble. The base/Fe = 3 mineral was 48% oxalate soluble. However, none of the minerals exhibited identifiable XRD peaks, which is generally regarded as indicating extremely short range order.

Any sulfate found associated with "perfect" samples of ferric hydroxide, ferrihydrite, goethite, or hematite would be sorbed sulfate as none is represented in the unit formulas of those minerals. Bigham et al. (1996) calculated that full coverage sulfate sorption on goethite would result in an Fe/SO_4 molar ratio of 50. Using values reported by Parfitt and Smart (1978), the Fe/SO_4 molar ratio due to sorption alone for amorphous ferric hydroxide would be 30.

Basic ferric sulfate and jarosites have an Fe/SO_4 molar ratio of 1.5 (Sapieszko et al., 1977), and schwertmannite would have an Fe/SO_4 ratio of 4.5 to 8 (Bigham et al., 1994). Ferric hydroxide, ferrihydrite, and schwertmannite are oxalate soluble, while goethite and hematite are not (Schwertmann and Cornell, 1991). Thus, the minerals formed in this study at low base/Fe ratios were probably schwertmannite. As base/Fe ratio was increased to 3, there was probably little schwertmannite formed, being replaced by ferrihydrite/ferric hydroxide. There may have been some goethite formed also, but there was little confirmation of this other than decreasing oxalate solubility.

<div align="center">

CONCLUSIONS

</div>

The data accumulated in this study is consistent with the model of van der Woude and de Bruyn (1983): an addition of base results in a rapid decrease in the charge per iron atom as nucleation occurs as evidenced by the drop in specific conductivity. The number of nucleii formed, and thus the magnitude of the initial drop in specific conductivity appears to be a function of the initial base addition. Later nucleation appears to be unlikely since the conductivity drop does not continue indefinitely. Size distributions reported for ferric hydroxide precipitates (Dousma and de Bruyn, 1978, Buyanov et al., 1972, Sommer et al., 1973) indicate very small particles. For example, Knight and Sylva (1974) reported the formation of particles 2 - 3 nm, too small to scatter light. They went on to estimate that these stable particles consisted of just 50 iron atoms. This would be

consistent with the observation that conductivity reaches a minimum in less one or two minutes whether precipitation occurred immediately or not at all.

After these first moments, agglomeration probably dominates the next phase rather than continued nucleus growth. Agglomeration rates appear to slow as sizes of about 1 μm are approached. Transmission electron micrographs of schwertmannite (Bigham et al., 1996) showed spherical clusters with radially arranged spikes which ranged in diameter from about 0.4 to 0.6 μm.

There are several factors which might contribute to the slow increase in conductivity after the minimum point is attained: a release of hydrogen ions occurred as oxolation proceeded as suggested by Dousma and de Bruyn (1976); release of sorbed sulfate ions as surface area decreased upon aging of the particles; and continued slow hydrolysis of iron as precipitation slowly continued. The first two possibilities are related and unlikely over the time span considered in these studies. Dousma and de Bruyn examined suspensions over weeks and months, while the time frame here is minutes. The third possibility is a more probable explanation. Continued hydrolysis would be the result of a sequence of chemical events as polymeric iron was removed from solution and equilibrium was restored by the release of iron from the complexes $FeSO_4^+$ and $Fe(SO_4)_2^-$. Those iron ions would hydrolyze, releasing H^+, and slowly become incorporated into the particulate surfaces. The overall reactions of this sort would be

$$3\ FeSO_4^+\ +\ 4\ H_2O\ \rightarrow Fe_3(OH)_4^{5+}\ +\ 4\ H^+\ +\ 3\ SO_4^{2-} \qquad (3\text{-}1)$$

$$3\ Fe(SO_4)_2^-\ +\ 4\ H_2O\ \rightarrow Fe_3(OH)_4^{5+}\ +\ 4\ H^+\ +\ 6\ SO_4^{2-} \qquad (3\text{-}2)$$
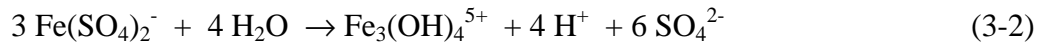
Since the conductivity of a solution is a function of the charge of its ions and their mobility (Reiger, 1994), equations 3-1 and 3-2 show that a greater number of charged species are created than are removed as hydrolysis and slow precipitation of the polymeric iron units proceeds. A release of hydrogen ions occurs as well.

This subsequent precipitation due to the incorporation of polymeric iron into the pre-formed surfaces is slow. The rate would be determined by the saturation factor, π, a ratio of the ion activity product and the solubility product. Since both the concentration of iron is lower than during the initial phase, and the release of H^+ lowers pH, the degree of saturation after the initial phase is lower, and thus the driving force for precipitation is lower. This was reflected in the fast initial decrease in iron concentration, followed a much slower decline in iron concentration over the ensuing hours and days. It is unlikely that this slow decrease is related to a transformation of the mineral, at least over this time frame. A stability study done by Bigham et al. (1996) showed that schwertmannite slowly transformed into goethite over the course of 500 days, with dissolved iron concentration steadily increasing until day 320, and then declining.

Sulfate appears to slow precipitation, but may accelerate agglomeration by reducing surface charge. It seems reasonable to suggest that sulfate exerts two effects on iron oxide growth rates. First, the aqueous complexation reduces the free iron

concentration, and thus lowers the degree of saturation, π. Second, sulfate sorbs to the surface of the nucleii and growing clusters, occupying two active sites each. Bigham et al. (1996) stated that sulfate sorbed to the surface of these small mineral particles appeared to decrease their solubility. Attachment of growth units to those sites occupied by sulfate would likely be inhibited. The eventual displacement of sulfate would be required to permit the continued slow growth of the solid surface.

SUMMARY

It was the purpose of this study to investigate the kinetics of ferric iron precipitation as it related to the design and operation of a treatment system for the removal of iron from acid mine drainage. Therefore, the matrix of ions typically found in AMD was examined for their effects on precipitation kinetics. It was found that iron precipitates rapidly but not instantaneously when less than the stoichiometric requirement of base is added to a sulfate-rich solution. It was concluded that once an oxide surface was formed, the growth of the surface was slowed by the presence of sorbed sulfate ions and by the complexation of dissolved iron with sulfate. It will be the subject of a subsequent chapter to explore how this information can be used in an iron-removal system.

Specifically, the following conclusions were drawn.
1. The effective iron solubility in typical AMD solutions was affected by sulfate concentration. It appears that the dissolved iron concentration attainable within the pH range required to avoid instantaneous precipitation may be about 5 mg/L.
2. The predominant mineral produced by precipitation in acidic iron sulfate solutions was schwertmannite, mixed with ferrihydrite.
3. Iron concentration had a negligible effect on induction period when the SO_4/Fe ratio was low. At higher SO_4/Fe ratios, iron concentration exerted a greater effect when t_{ind} was short, but when long induction periods (>300 s) were considered, iron concentration had a small effect.
4. Within the concentration ranges investigated, aluminum/iron ratio and manganese/iron ratio do not play an important role in determining induction period length.
5. Induction time, and thus rate of precipitate formation, can be predicted based on knowledge of the pH of the reactor environment, iron concentration, and sulfate concentration.
6. Changes in conductivity and pH provide some confirmation of the model of van der Woude and de Bruyn (1983) which suggests that fast nucleation is followed by a growth period lasting no more than a few minutes; particles then agglomerate to form precipitates. These precipitates then grow even more slowly by surface precipitation over hours and days. Sulfate appears to decrease the rate of these processes, particularly the slower phase of surface precipitation.

LITERATURE CITED

APHA, AWWA, WEF. 1992. Standard Methods for the Examination of Water and Wastewater, 18th Edition. American Public Health Association. Washington, DC.

Bigham, J. M., L. Carlson, and E. Murad. 1994. Schwertmannite, a New Iron Oxyhydroxysulphate from Pyhasalmi, Finland, and Other Localities. Mineralog. Mag. 58:641-648.

Bigham, J. M., U. Schwertmann, S. J. Traina, R. L. Winland, and M. Wolf. 1996. Schwertmannite and the Chemical Modeling of Iron in Acid Sulfate Waters. Geochim. Cosmochim. Acta, 60(12):2111-2121.

Buffle, J. and H. P. van Leeuwen. 1992. Environmental Particles, Volume 1. Lewis Publishers, Boca Raton.

Buyanov, R. A., O. P. Krivornuchko, and I. R. Ryzhak. 1972. Kinet. Katal. 13:470.

CRC Handbook of Chemistry and Physics, 71st Edition. 1990. D. R. Lide, Ed. CRC Press. Boca Raton.

Dousma, J. and P.L. de Bruyn. 1976. Hydrolysis-Precipitation Studies of Iron Solutions. I. Model for Hydrolysis and Precipitation from Fe(III) Nitrate Solutions. J. Colloid Interface Sci. 56(3):527-538.

Dousma, J. and P.L. de Bruyn. 1978. Hydrolysis-Precipitation Studies of Iron Solutions. II. Aging Studies and the Model for Precipitation from Fe(III) Nitrate Solutions. J. Colloid Interface Sci. 64(1):154-170.

Dousma, J. and P.L. de Bruyn. 1979. Hydrolysis-Precipitation Studies of Iron Solutions. III. Application of Growth Models to the Formation of Colloidal αFeOOH from Acid Solutions. J. Colloid Interface Sci. 72(2):314-320.

Dousma, J., D. den Ottelander and P.L. de Bruyn. 1979. The Influence of Sulfate Ions on the Formation of Iron (III) Oxides. J. Inorg. Nucl. Chem. 41:1565-1568.

Knight, R. J. and R. N. Sylva. 1974. Precipitation in Hydrolysed Iron (III) Solutions. J. Inorg. Nucl. Chem. 36:591-597.

Newman, M. C. and A. W. McIntosh, editors. 1991. Metal Ecotoxicology, Concepts and Applications. Lewis Publishers, Chelsea Michigan.

Nielsen, A.E. 1964. Kinetics of Precipitation. Pergamon Press, Oxford.

Nyvlt, J., O. Sohnel, M. Matuchova and M. Broul. 1985. The Kinetics of Industrial Crystallization. Elsevier Science Pub. Co. Amsterdam. pp. 350.

Parfitt, R. L. and R. Smart. 1978. The Mechanism of Sulfate Adsorption on Iron Oxides. J. Soil Sci. Soc. Am. 42:48-50.

Rieger, P. H. 1994. Electrochemistry, 2nd Edition. Chapman & Hall. New York.

Sapieszko, R.S., R. C. Patel, and E. Matijevic. 1977. Ferric Hydrous Oxide Sols. 2. Thermodynamics of Aqueous Hydroxo and Sulfato Ferric Complexes. J. Phys. Chem. 81(11): 1061-1068.

Schwertmann, U., and R.M. Cornell. 1991. Iron Oxides in the Laboratory: Preparation and Characterization. Verlagsgesellschaft mbH, Weinheim. pp.137.

Sohnel, O. and J. Garside. 1992. Precipitation: Basic Principles and Industrial Applications. Butterworth-Heinemann Ltd. Oxford. pp. 391.

Sokal, R. R. and F. J. Rolf. 1995. Biometry: The Principles and Practice of Statistics in Biological Research, 3rd Edition. W. H. Freeman and Company. New York.

Sommer, B. A., D. W. Margerum, J. Renner, P. Saltman, and Th. G. Spiro. 1973. Bioinorg. Chem. 2:295.

Stanjek, H., and U. Schwertmann. 1992. The influence of aluminum on iron oxides. Part XVI: Hydroxyl and aluminum substitution in synthetic hematites. Clays Clay Min. 40: 347-354.

Stumm, W. 1992. Chemistry of the Solid-Water Interface. John Wiley & Sons, Inc. New York.

Stumm, W. and J. J. Morgan. 1981. Aquatic Chemistry, An Introduction Emphasizing Chemical Equilibria in Natural Waters, 2nd Edition. John Wiley & Sons, Inc., New York.

Stumm, W. and J. J. Morgan. 1996. Aquatic Chemistry, Chemical Equilibria and Rates in Natural Waters, 3rd Edition. John Wiley & Sons, Inc., New York.

USEPA. 1976. Development Document for Interim Final Effluent Limitations Guidelines and New Source Performance Standards for the Coal Mining Point Source Category. EPA 440/1-76/057a. pp.288.

van der Woude, J.H.A. and P.L. de Bruyn. 1983. Formation of Colloidal Dispersions From Supersaturated Iron (III) Nitrate Solutions. I. Precipitation of Amorphous Iron Hydroxide. Colloids and Surfaces 8:55-78.

Weber, W. J. and F. A. Digiano. 1996. Process Dynamics in Environmental Systems. John Wiley & Sons, Inc., New York.

Chapter 4 -Performance of a Lab-Scale Treatment System for Removal of Iron and Acidity From Acid Mine Drainage Without the Formation of Iron Sludge

INTRODUCTION

Acid mine drainage (AMD) continues to be an important water pollution problem around the world. When pyritic minerals are exposed to the atmosphere, oxidation of sulfide produces sulfuric acid and releases reduced iron and other metals to solution. The characteristics of AMD include low pH, high specific conductivity, high concentrations of iron, aluminum, and manganese, and the variable presence of toxic heavy metals. Current technologies are either inadequate or too expensive; thus, much discharge enters receiving waters with no treatment. This paper presents the results from one phase of the research and development of a new approach to remove of iron and acidity from this contaminated water. This new treatment system (patent pending) takes advantage of the tendency of ferric iron to form mineral coatings and avoids the formation of iron hydroxide sludge (Figure 4.1). The requirement for sedimentation basins would thus be eliminated along with the need for storage and disposal of iron hydroxide sludge.

In its reduced form, ferrous iron (Fe II) is quite soluble, but once exposed to the atmosphere, it will oxidize to the ferric (Fe III) form. At low pH, ferrous iron oxidization is due to microbial activity; above about pH 4.5, abiotic oxidation occurs quickly by reaction with oxygen from the atmosphere. Once oxidized, the very low solubility of ferric iron results in precipitation of oxyhydroxide minerals if pH exceeds 3.0. In a previous phase of the work (Chapter 2), it was shown that ferrous iron, the usual form of iron released from acid generating mine surfaces (pyritic minerals), could be oxidized in a bioreactor while maintaining the iron in the dissolved state since the bioreactor operated below pH 3.0.

The precipitation of ferric iron is not instantaneous upon addition of alkalinity to the solution. However, when sufficient base is added to a ferric iron solution to exceed a threshold level, precipitation of iron oxyhydroxides is inevitable, although the time from the addition of the base to the time of appearance of a precipitate, the so-called "induction period", may last from seconds to months (Dousma and de Bruyn, 1979). During the induction period, changes within the solution occur which eventually result in precipitate formation. This process, described in detail elsewhere (Chapter 3), appears to involve a reversible increase in polymerization of Fe/OH units, resulting in the formation of many critical-sized entities, termed nucleii. Once critical size is achieved, the nucleii are thermodynamically stable, and continue to grow by incorporation of additional Fe/OH growth units until the concentration of dissolved iron becomes low and the rate slows significantly. Over time, small particles may tend to join together, a process referred to by various terms but here called agglomeration (Mullin, 1993). As particles grow in size, the number of particles decreases, and growth by agglomeration slows; precipitation,

usually defined as the appearance of filterable particles, may occur at some point in this process.

media addition
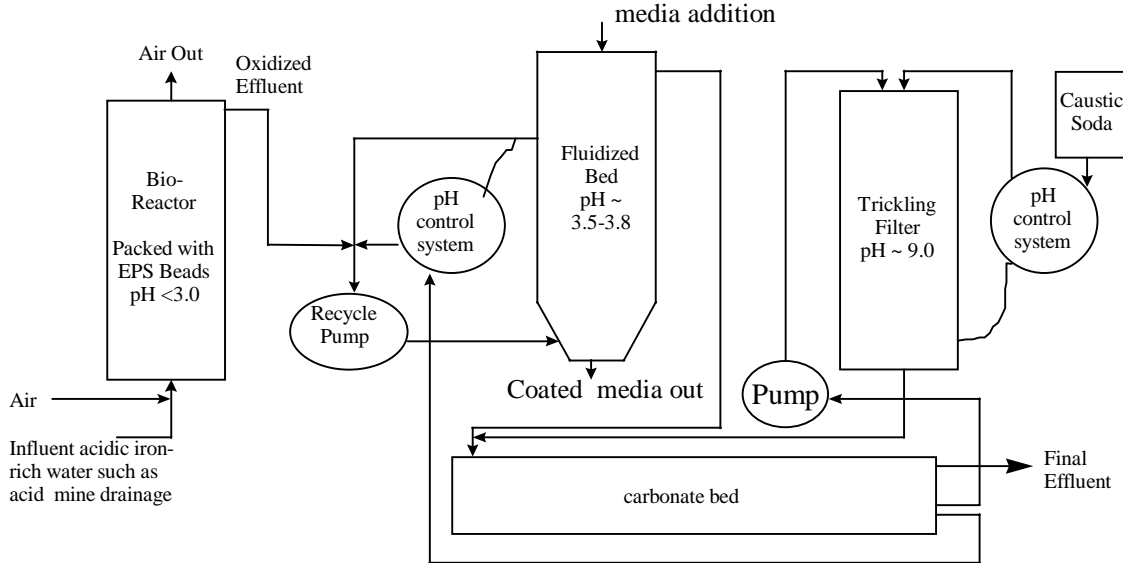
Figure 4.1. Schematic of integrated treatment system for the removal of heavy metals and acidity from acidic iron-rich waters without the formation of metal sludge.

It was hypothesized that this sequence could be interrupted if dissolved iron units and/or very small iron particles could be removed from solution at an early stage by exposing the solution to a mineral surface. If the growth units and/or very small particles preferentially united with the pre-formed surface, the continued growth and agglomeration of the iron nucleii could not occur, thus avoiding the formation of precipitated iron.

Since AMD typically contains dissolved species other than iron, the effect of those dissolved species on iron solubility and precipitation kinetics would be important in determining the success of such a treatment system. In a previous phase of the work (Chapter 3) it was found that aluminum and manganese did not exert any measurable effect on precipitation rates. However, it was found that sulfate exerted a major effect by increasing iron solubility and slowing precipitation rates.

This paper presents the results of the lab-scale evaluation of the multi-stage treatment system for iron and acidity removal. A subsequent chapter will present the results on the system's removal of several heavy metals other than iron.

BACKGROUND

Various approaches have been used to ameliorate AMD and its effects. Control at the source has received much attention but resulted in little progress. The oxidation of pyrite exposed to the atmosphere is strongly favored thermodynamically but is limited kinetically. While oxidation may be a slow process, attempts to prevent moisture,

oxygen, and microorganisms from reaching the disturbed pyrite surfaces have met with relatively little success (Unz and Dietz, 1986).

The bulk dumping of limestone in streams was once thought to be capable of neutralizing the acidity of the water, but typically the limestone became coated with iron oxyhydroxides, slowing its dissolution and thus limiting its effect on stream pH (Hedin and Watzlaf, 1994). It was found that pH neutralization by limestone was successful so long as the water was anoxic. However, once the neutralized water was exposed to the atmosphere, iron oxidized, hydrolyzed, and acid was generated. Since the iron was left to precipitate in the stream, the lack of an iron removal mechanism was a significant shortcoming of this approach.

When anoxic limestone drains were combined with natural or constructed wetlands, some treatment success was achieved (Wildeman et al., 1994). However, wetlands have shown a limited ability to cope with intermittent low pH events, and can be overwhelmed by high flow (Tarutis and Unz ,1995). Some metals, such as manganese, are not effectively removed by wetlands.

Recent work with algal-cyanobacterial consortia has shown promise in the removal of metals (Vatcharapijarn et al., 1994). An obvious advantage of algal consortia is that they are lithoautotrophs, and thus do not require an artificial input of electron donor or carbon source.

Engineered treatment systems have generally been employed only at active mine sites. These typically consist of pH adjustment with caustic soda ($NaOH$) or lime (CaO), followed by settling ponds. New source performance standards developed for National Pollutant Discharge Elimination System permits by the USEPA for the coal mining industry stipulate total iron of 3.0 mg/L, total manganese of 2.0 mg/L, total suspended solids of 35 mg/L, and pH between 6.0 and 9.0 units (30 day averages) (USEPA, 1976) with similar requirements imposed by The Surface Mining Control and Reclamation Act of 1977.

An activated sludge system for treatment of acid mine drainage was evaluated in England in the mid-60's with little success (Whitesell et al., 1971). In Japan, *Thiobacillus ferrooxidans* was employed at an abandoned mine discharging 20 $m^3 min^{-1}$ of water with a pH of 1.6 containing 795 mg/L of total iron (Murayama et al., 1987). Total detention time in the system was approximately 8.5 h. The operational cost of treatment was approximately one-third that of the previous all-chemical process.

A previous phase of this research program had investigated the performance of a packed bed bioreactor using expanded polystyrene beads to immobilize iron-oxidizing chemolithotrophic bacteria (Chapter 2) for the purpose of converting any reduced ferrous iron to the ferric state at low pH (about pH 2.3). It was found that good oxidation efficiency (98 %) could be expected at influent ferrous iron concentrations up to 10 mM (558 mg L^{-1}) and detention times as short as 0.5 h. It was also found that temperature exerted a significant effect on oxidation rates, and that dissolved oxygen concentration should be maintained above about 2 mg L^{-1}. Supplementation with carbon dioxide did not result in increased oxidation rates.

Previous work (Chapter 3) documented the kinetics of iron precipitation in solutions typical of AMD. It was found that due to kinetic limitations and complexation of iron with sulfate, the lowest dissolved iron concentration which could probably be achieved in an engineered setting would be about 5 mg L^{-1}. The pH required to achieve low solubility but sufficiently slow precipitation would probably be in the range of pH 3.0 to 4.0, which corresponds to a base/Fe ratio of about 2.0 to 2.5. Above this range, it was suspected that particles would form and grow large too quickly to be removed effectively.

OBJECTIVES

It was the goal of this phase of the research to apply the knowledge gained in the prior studies of iron oxidation and iron precipitation kinetics to a lab-scale multi-stage treatment system. In Phase I, the performance of a stand-alone precipitation reactor was investigated. This reactor was fed synthetically prepared solutions (ferric sulfate and bicarbonate) free of particulates over a range of operating pH values. Once the reactor's performance was documented, Phase II investigated the performance of a multi-stage system at a variety of loadings. The feed solution to the precipitation reactor was the effluent from a bioreactor and water from a limestone bed was used to provide pH adjustment for the precipitation reactor. Such influents were expected to contain particulate matter which might have a significant impact on performance. It was also hoped that an examination of the iron coatings which developed on the seed particles in the reactor would provide some insight into the mechanism of iron removal by the reactor system.

Specifically, some questions posed in this study were:
1. Is there a pH range for iron-oxide surface precipitation which optimizes rate of iron removal while minimizing the concentration of suspended iron?
2. What is the maximum iron loading which minimizes suspended iron particle concentration?
3. Does the presence of particulates in the feed to a multi-stage system prevent adequate removal performance?

METHODOLOGY

Simulated Acid Mine Drainage, Chemicals, and Water

The feed solution, referred to as "simulated AMD", was prepared with tap water in volumes of 18 L at a time (about 5 gal) as given in Table 4.1. The simulated AMD was allowed to sit before use at room temperature for at least 15 hours to allow chlorine to volatilize. Ferrous iron was then added from a stock solution (0.2 M ferrous sulfate acidified to < pH 2.5 with nitric acid). All chemicals used to prepare solutions were reagent grade except for aluminum sulfate, which was technical grade. Water used for purposes other than preparation of simulated AMD was deionized. Acids such as nitric, sulfuric and hydrochloric were "Plus" grade by Fisher Chemical Company.

Table 4.1. Simulated acid mine drainage (after adjustment to pH 2.3 with sulfuric acid).

Constituent	Molarity	mg L^{-1}
Iron	0.010	558
Aluminum	0.002	54
Calcium	0.002	80
Magnesium	0.001	24
Sodium	0.0075	175
Potassium	0.0005	20
Ammonium (as N)	0.0005	7
Sulfate	0.025	2400
Phosphate (as P)	0.0005	16

AMD Treatment system

Bioreactor

The first stage of the treatment system (Figure 4.1) was a bioreactor of 1 L total volume, containing ~ 0.55 L of EPS beads coated with jarosite, an iron sulfato-hydroxide mineral, and iron-oxidizing microorganisms, as described previously (Chapter 2). The bacteria converted ferrous (Fe II) to ferric (Fe III), using the energy available in this oxidation for growth. Being lithotrophic, these organisms used carbon dioxide as a sole carbon source, and thus required no extraneous nutrient solution. The drainable liquid volume in the bioreactor was 0.6 L.

Fluidized Bed Reactor

The second treatment stage employed a fluidized bed reactor (FBR) for chemical precipitation of iron. This reactor consisted of a column (both 0.1 L and 0.25 L were used at various times) containing medium quartz sand (mean diameter = 1.26 mm, surface area assuming spheres = 1.8 m^2g^{-1}) with an external reservoir and pump for re-circulation to fluidize the sand. The external reservoir (not shown in Figure 4.1) protected the pump from the jamming effects of sand which was occasionally washed out with the effluent from the fluidized bed column, especially on start-up.

During the synthetic feed phase, the iron feed solution was introduced by peristaltic pump into the suction side of the centrifugal pump which re-circulated water through the FBR at a rate of about 2 L min^{-1}. Based on flow rate and tubing configuration, injected iron feed was transported into the reactor within a second. A bicarbonate solution of various concentrations was injected by a peristaltic pump at the same point in the pump inlet tubing. Later, when the integrated system was assembled, the bioreactor effluent replaced the synthetic iron feed solution and flowed by gravity. At that time, the sodium bicarbonate solution was replaced by effluent from the carbonate bed described below, with the flow controlled by a pH controller commanding a peristaltic pump.

The diagram in Figure 4.1 indicates that media is added from above and withdrawn from the bottom of the FBR. In the lab-scale version, sand was manually replaced on several occasions. As with pellet reactors used for water softening in Europe (Scholler et al., 1991, Wilms et al., 1992), an automated method for replacing sand media which had increased in density due to iron coating growth would facilitate on-going operation.

Initially, to protect the pump from becoming jammed by sand grains upon shutdown, the sand media within the column was supported by a layer of small gravel, similar to the configuration of a rapid sand filter. It was found that after several weeks of operation iron-oxide solids would accumulate on the surfaces of the gravel, eventually constricting passages through the gravel bed. Once the flow became sufficiently restricted, the sand bed would no longer fluidize and particulates would proliferate in the liquid. After the gravel bed was replaced by a perforated plate, the problem appeared to be solved so long as the perforations did not become clogged. In a large-scale system, the hydrodynamics of the system would become an important part of the overall system design process. It was not possible within the constraints of a small lab-scale system to explore these issues more fully.

Carbonate Bed

Effluent from the FBR flowed into the third stage, a calcium carbonate bed (CB) for pH neutralization. Liquid was re-circulated from the discharge end of this bed back to the FBR by a pH control system. The CB had a total volume of 2 L, with a liquid volume of about 1 L.

Trickling Filter

Water was pumped from the discharge end of the CB into the final stage, where it trickled down through a gravel-filled column (0.25 L) along with added caustic soda (NaOH) solution so as to maintain a pH in the effluent from the column of 9-10. In a full scale system, effluent from the trickling filter (TF) would be recirculated to the influent end of the CB. In order to simplify analysis during lab studies, effluent from the TF was not recirculated, but discharged as final effluent.

Digestion of Iron Oxide Coatings

Total Dissolution of Coatings

Samples of sand grains were removed from the FBR at various times for mineral analysis. Total mineral dissolution was achieved by digestion with hot HCl as recommended by Schwertmann and Cornell (1991). Triplicate samples (~0.3 g) were placed in 15 mL of 6 M hydrochloric acid in test tubes which had been previously acid cleaned. The test tubes were placed in a boiling water bath for 1 h, and stored for later analysis of iron and sulfate.

Oxalate Dissolution of Amorphous Iron

Oxalate-soluble iron ($[Fe]_o$) is that iron mineral which dissolves when placed in 0.2 M ammonium oxalate acidified to pH 3 with 0.2 M oxalic acid, according to the method of Schwertmann and Cornell (1991). Oxalate solubility is generally presumed to relate to the degree of crystallinity of the mineral, with more crystalline iron minerals such as goethite and hematite not dissolving during this extraction. Triplicate ~0.3 g samples of oxide coated sand were placed in 25 mL of oxalate solution in flasks. The flasks were stoppered, and place on a shaker table in the dark for 2 h. The solution was then removed, filtered through 0.2 µm membranes, and stored for later analysis of iron and sulfate.

Ferrous Iron Determinations

Ferrous iron was determined immediately after sampling and appropriate dilution with acidified deionized water (deionized water to which a few drops of 6 M nitric acid had been added). Acidified deionized water was used for diluting samples before ferrous iron determinations to prevent oxidation of the iron. A DR700 HACH colorimeter was used along with HACH ferrous iron reagent powder pillows (HACH Corporation, Loveland, CO), which conformed to the 1, 10 phenanthroline method (Method 3500-Fe D.) as detailed in Standard Methods for the Examination of Water and Wastewater (APHA, AWWA,WEF, 1992). This method is approved by USEPA. The pre-programmed conversion factor of the colorimeter was checked with freshly prepared Fe II standard solutions.

Total Iron Analysis

Total iron was assayed using flame atomic absorption spectrophotometry (Method 3500-Fe B.) as detailed in Standard Methods for the Examination of Water and Wastewater (APHA, AWWA,WEF 1992).

Sulfate Analysis

The presence of iron in all samples made analysis by ion chromatography impractical due to iron precipitation within the column. Therefore, Method 4500-SO_4^{2-} E. (Turbidimetric) as described in Standard Methods for the Examination of Water and Wastewater (APHA, AWWA,WEF 1992) was selected for use. The method used the precipitation of barium sulfate by the addition of barium chloride to create turbidity in the sample, which was measured in a nephalometer (Monitek Model TA1). Samples were diluted prior to addition of the barium chloride based on estimates of sulfate concentration so as to yield acceptable absorbance values. Blanks and standards (Na_2SO_4) were carried through the procedure to generate a standard curve as stipulated in the method.

Statistical Methods and Calculations

Where appropriate, means, standard deviations, linear regression, and analysis of variance (ANOVA) were accomplished using the data analysis features of Microsoft

Excel 7.0. These calculations were consistent with traditional statistical methods as reported in the literature (Sokal and Rolf, 1995). The standard level of significance was set at $\alpha = 0.05$.

Scanning Electron Microscopy

Electron micrographs were produced using a scanning electron microscope (CAMSCAN Series 2 by Cambridge Instruments) operated by the Department of Geological Sciences, Virginia Polytechnic Institute and State University, in Blacksburg, Virginia. Images were recorded by a thermal printer and digitally scanned for inclusion in this document. The sample sand grains were dried and coated with carbon vapor prior to introduction into the device. Micrographs were printed on thermal paper and later digitized for incorporation into this document.

RESULTS AND DISCUSSION

Phase I - Performance of FBR with Synthetic Feed

The FBR was operated as a stand-alone reactor receiving a synthetic iron feed solution and sodium bicarbonate solution. Various configurations of sand mass, gravel under-layer and flow rates were used as ranging studies. A representative period useful to illustrate the FBR performance is provided in Figure 4.2.

During this period, the flow rate was held constant at 2 mL min^{-1}, and the influent [Fe] was about 5 mM (279 mg L^{-1}). With a total liquid volume of 0.5 L, the hydraulic retention time (HRT) within the system was 5 h. Except for a few occasions, during this time span the pH of the system was about 3.5, and the specific loading to the system ranged from 0.1 to 0.25 (mg Fe m^{-2} surface area h^{-1}). The data points indicating effluent [Fe] of 58 and 46 mg L^{-1} occurred on days 7 and 8 when the pH of the system dropped to 2.75 and 2.98, respectively. Otherwise, the effluent iron concentration ranged from 6 to 20 mg L^{-1}.
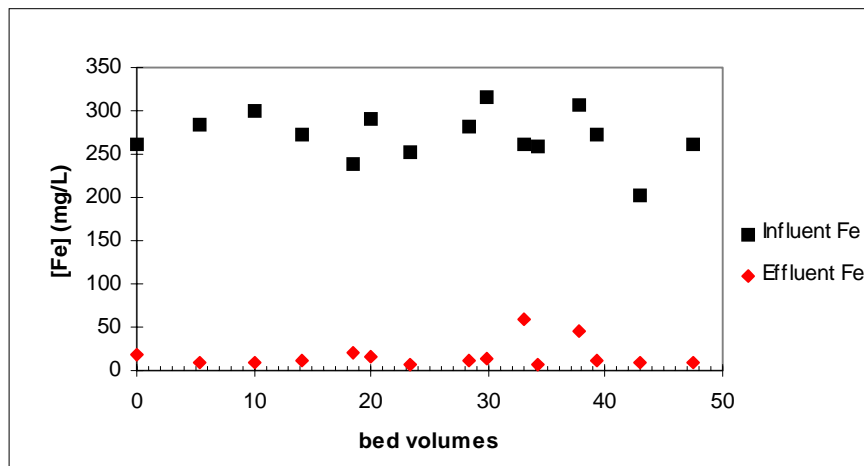

Figure 4.2. Example of performance of FBR over a 10 d period. Each data point represents an individual measurement.

When data from other periods of operation were combined including those with an HRT of 2.5 h, a better picture of performance emerged. The data in Figure 4.3 show effluent [Fe] as a function of pH. The pattern below pH ~3 is not unexpected in that iron solubility increases sharply in that pH range. There appeared to be a plateau region between pH 3 and pH 4 in which effluent [Fe] was at its minimum. Above pH 4, the total iron increased as iron particulates appeared in the effluent.
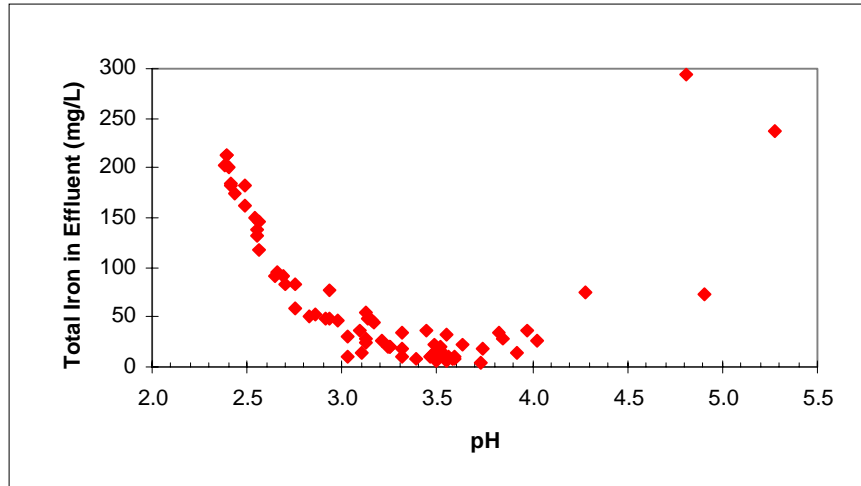

Figure 4.3. Effluent iron concentration as a function of pH in FBRs. Each data point represents an individual measurement.

When the reactor pH was increased above about 3.5, turbidity increased (Figure 4.4). It was found that once turbidity in the system had increased above about 50 NTUs, a clear effluent could not be restored by just reducing pH to a lower value. It was necessary to shutdown the system, remove the reactor liquid, and flush the entire system to remove particulates. Apparently, suspended particulate iron in the reactor served as nucleii for surface precipitation as dissolved iron was fed into the reactor.

When the removal efficiency was plotted as a function of pH (Figure 4.5), the reactor performance efficiency mirrored the effluent [Fe] plot, as expected. It was concluded therefore that optimum reactor pH was in the range of pH 3.3 to 3.7. Within this range, removal efficiencies of 95 to 98% could be achieved. Below an optimum pH range, the effluent was clear but with increased dissolved [Fe]. Above the optimum pH range, the effluent became turbid with an increase in total iron concentration due to particulate iron. Other variables such as loading (to be discussed later) and hydrodynamics also affected effluent quality.
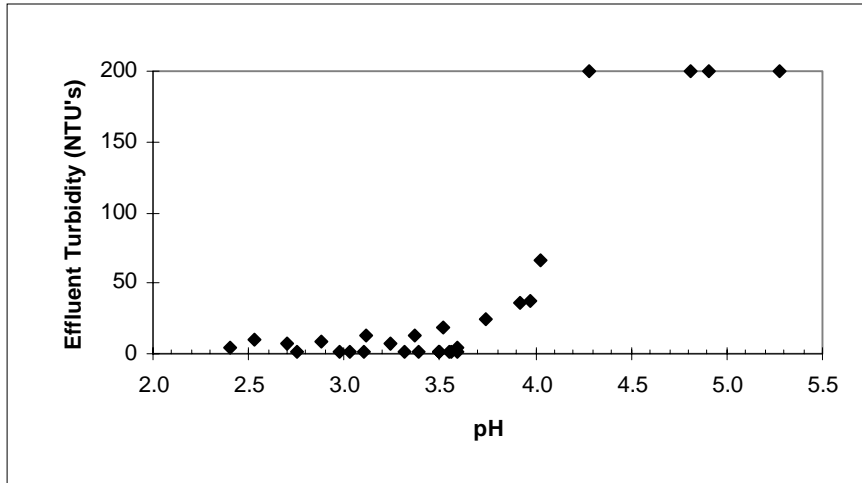
Figure 4.4. Effluent turbidity as a function of pH in FBRs; note: indicated value of 200 indicates true value > 200 NTUs. Each data point represents an individual measurement.
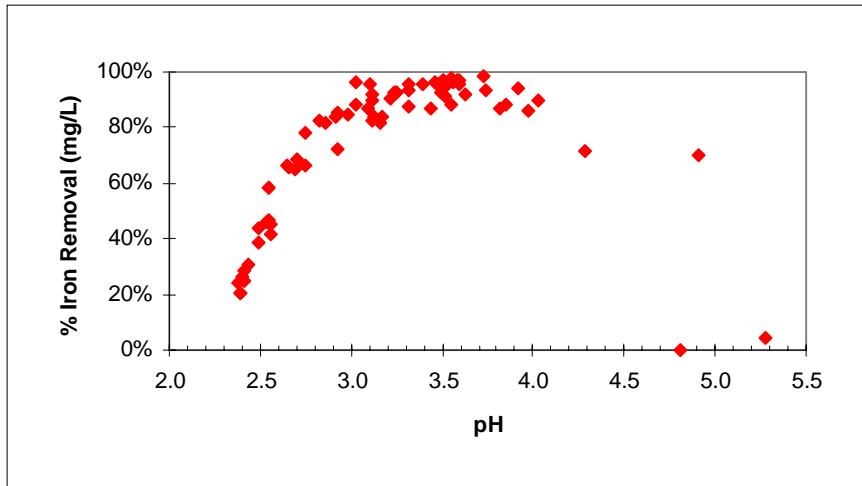
Figure 4.5. Iron removal efficiency as a function of pH in FBRs. Each data point represents an individual measurement.

Phase II - Performance of a Multi-Stage Iron Removal System

The integrated system was operated for a total of six weeks under various configurations. The final 2 weeks of operation included the addition of heavy metals other than iron to the feed, with results reported elsewhere (Chapter 5). Simulated AMD was prepared as described above using ferrous iron concentrations ranging from 250 to 700 mg/L. The flow rate was varied to investigate the response of the system to increased mass loading.

Stage 1: Bioreactor Performance

Figure 4.6 presents a history of the bioreactor performance over a 17 day period. Notice that the vertical axis is plotted as a log scale in order to see the response in effluent [Fe II] resulting from increased influent concentrations. Effluent ferrous iron was typically below 10 mg/L until influent concentration and flow rate were increased over the final few days of operation. The oxidation efficiency was 98-99% until the final 2 days.
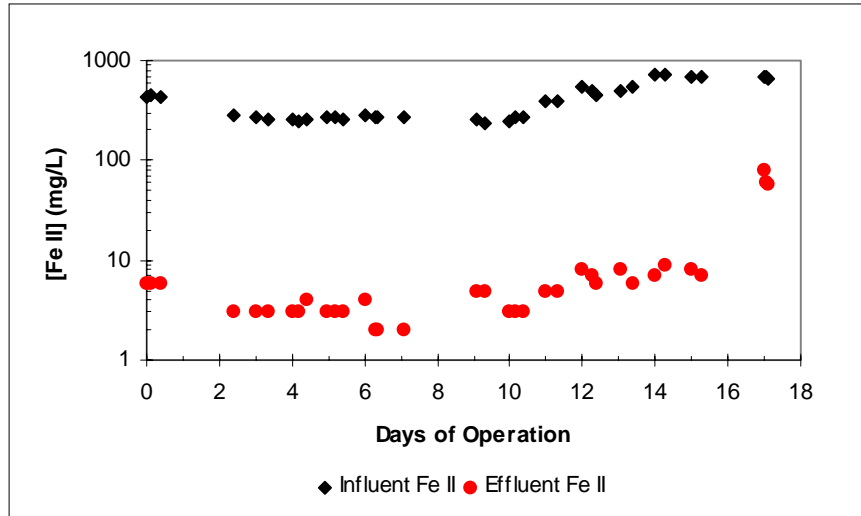

Figure 4.6. Ferrous iron oxidation performance by a bioreactor as the 1st stage of a multi-stage AMD treatment system. Each data point represents an individual measurement.

The response of the bioreactor is seen more clearly when effluent [Fe II] is plotted as a function of ferrous iron loading (mg L^{-1} h^{-1}) in Figure 4.7. There was very little change in effluent [Fe II] until the loading exceeded about 125 mg L^{-1} h^{-1} at a dilution rate of 0.2 h^{-1} (HRT = 5 h). Also shown in Figure 4.7 are the data points fit ($R^2 = 0.989$) to predictions by the biokinetic model presented in Wichlacz and Unz (1985) using kinetic coefficients ($\mu_{max} = 0.142$ h^{-1}, $Y_{obs} = 0.011$, $X = 26$ mg L^{-1}, and $K_s^* = 6$ mg L^{-1}) determined or estimated in earlier studies (Chapter 2). The model tended to over-predict substrate concentration at high loadings and slightly under-predict substrate at low loadings.
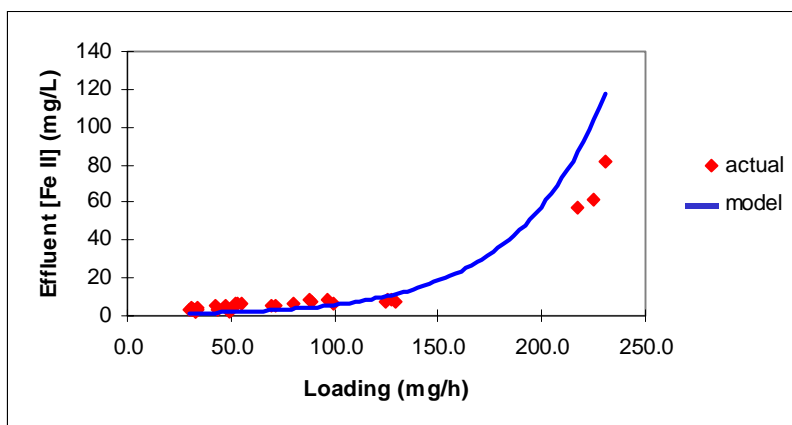
Figure 4.7. Effluent ferrous iron as a function of ferrous iron loading. Model is the Wichlacz and Unz (1985) model with parameters adjusted for use in a packed bed column reactor. Kinetic coefficients used were μ_{max} = 0.142 h^{-1}, Y_{obs} = 0.011, X = 26 mg L^{-1}, and K_s^* = 6 mg L^{-1}. Each actual data point represents an individual measurement.

Stage 2: Fluidized Bed Reactor Performance

Effluent from the bioreactor flowed by gravity into the FBR. The pH control system maintained the FBR within the range of pH 3.5 - 4.0 using effluent from the carbonate bed, which typically had a pH of between 6 and 7. The pH controller functioned in a simple on/off mode. The total iron flux (mg h^{-1}) from the bioreactor into the FBR is presented in Figure 4.8, as well as the FBR effluent and the final iron flux. Mass flux instead of concentration was presented to account for changes in flow rate, which were made on day 7 and day 16.

Iron removal averaged 94 % in the FBR over this period. Effluent quality was relatively constant until day 16 when total iron loading exceeded about 100 mg h^{-1}, which was equivalent to a specific loading of about 0.22 mg h^{-1} m^{-2} media surface. Effluent [Fe] flux (mg Fe h^{-1}) increased with specific iron loading as shown in figure 4.9a. Once the specific loading exceeded about 0.20 mg h^{-1} m^{-2} the effluent iron flux increased.

The turbidity data reinforced the observation that a loading of 0.20 mg h^{-1} m^{-2} constituted a system limit. As shown in Figure 4.9c, effluent turbidity remained between 1 and 50 NTUs until the loading exceeded 0.20 mg h^{-1} m^{-2}, above which an increase in turbidity was noted with increased loading. It is speculated that below a loading of 0.20, turbidity was due primarily to iron precipitation onto imported particles, mainly from the carbonate bed (the bioreactor effluent appeared to be clear). But above that loading level, incremental turbidity may have been the result of spontaneous iron nucleation.
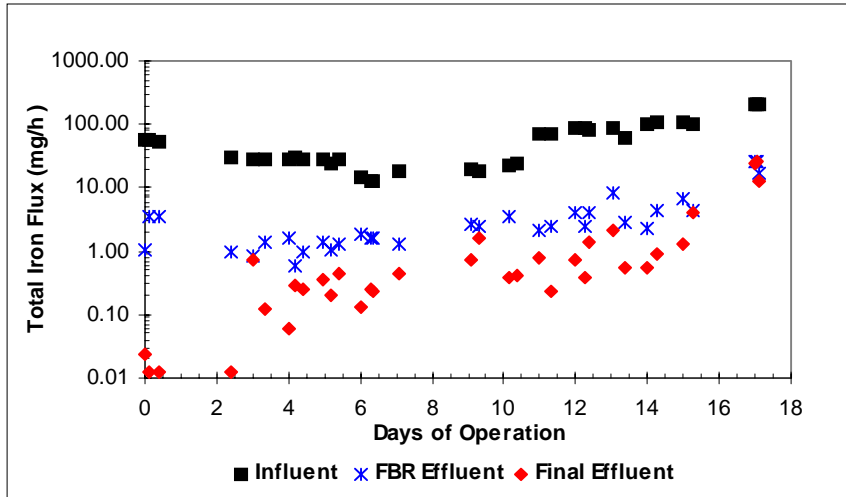
67

Figure 4.8. Total iron in influent, FBR effluent, and in final effluent of multi-stage AMD treatment system. Each data point represents an individual measurement.

The precipitation of iron onto imported particles would be reflected in the effluent iron concentration and flux data, and would help to explain the scatter seen in these data sets when compared to the results for the stand-alone FBR receiving synthetic feed solutions with no particulates.

Final Effluent Quality and Overall Performance

Effluent flowed from the FBR into the CB. The CB was an open top rectangular tank filled with previously washed crushed limestone. Iron in the FBR effluent did precipitate at the entrance end of the CB, resulting in some accumulation of reddish-orange precipitate. However, it did not appear that the carbonate gravel became coated.

It is possible that a different configuration for this reactor stage would result in better performance, but the kinetics of carbonate dissolution and pH neutralization of the flow were not investigated. Possibly some other design for the CB would result in an effluent more free of particulate matter.

The CB effluent iron concentration was typically less than 3 mg/L, except when the system was overloaded during the last several days of the test period. The pH of the final effluent was between 6.5 and 7.2. Overall iron removal efficiency was 99% not including the last 2 days of overload.
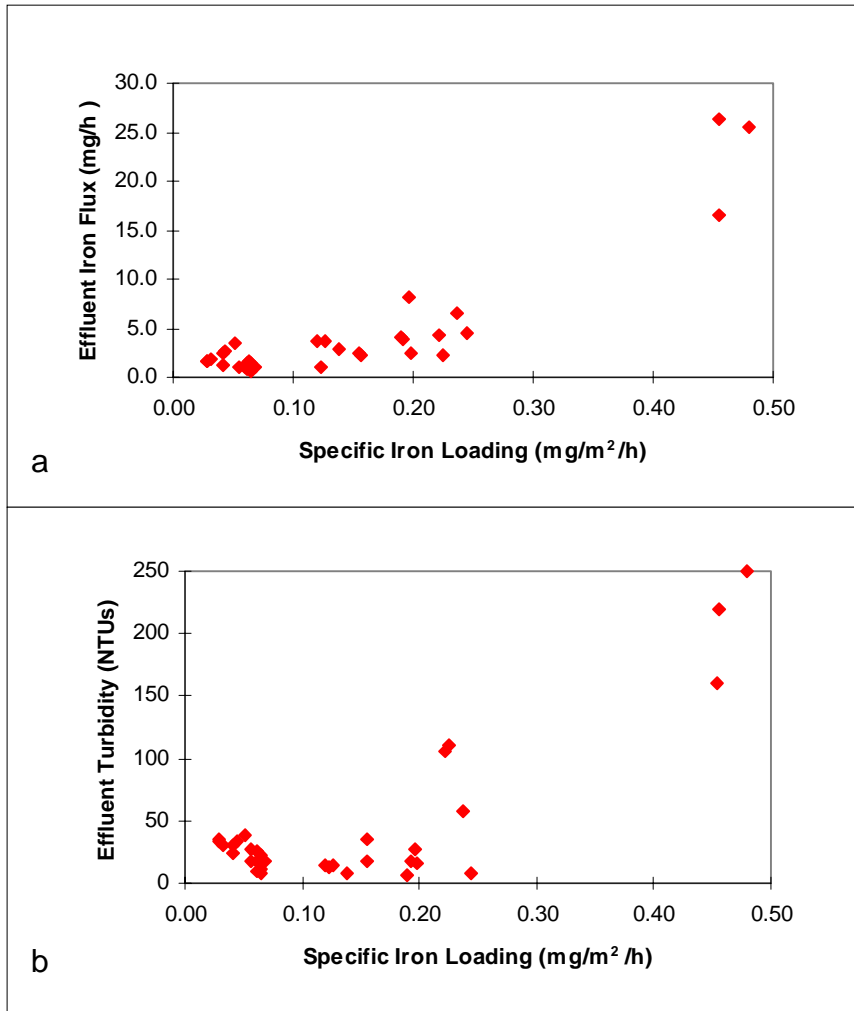
Figure 4.9. Effluent iron (a) concentration and (b) mass flux and (c) turbidity as a function of specific iron loading in the FBR stage of a multi-stage AMD treatment system. Each data point represents an individual measurement.

Elemental Analysis of Iron Oxide Coating

Oxide coating from sand grains was digested and analyzed for oxalate soluble mineral, total acid soluble mineral, iron content and sulfate content. Essentially all of the iron mineral coating sand grains was oxalate soluble, with an Fe/SO_4 molar ratio of 6.7. Based on iron mineral characteristics reported by Schwertmann and Cornell (1991), it appears that most if not all of the mineral coating was schwertmannite $[Fe_{16}O_{16}(OH)_{12}(SO_4)_2]$, an iron oxyhydroxysulfate mineral precipitated from acidic iron sulfate solutions in the pH range of 3.0 to 4.5 (Bigham et al., 1994).

Scanning Electron Microscopic (SEM) Examination of Coated Sand

SEM micrographs (Figure 4.10) revealed that the coating on sand grains was composed of bead-like structures with a diameter of ~ 0.2 to 1 μm. In areas protected from abrasion, the size of the beads appeared to be greater than on flat surfaces. The flat areas had a coating in which many small spheres appeared to be consolidated. It was not determined if the beads were formed within the bulk solution and subsequently attached to the surface, or if the beads grew in place on the surface.

The presence of mineral beads may be explained by a review of the steps leading to precipitation of schwertmannite (Chapter 3, Bigham et al., 1996). Small particles (perhaps 50 nm) resulting from nucleation agglomerate. Agglomeration results if particles are sufficiently small and forces of attraction (van der Waals forces) overcome shear and gravitational forces (Mullin, 1993). Walton (1969) made a theoretical estimate that a solute with a solubility of 10^{-4} M with an initial concentration of 10^{-2} M (values appropriate to these studies) would produce agglomerated particles with terminal diameters of about 1 to 10 μm. Bigham et al., (1996) reported that schwertmannite formed spherical particles with diameters ranging from 0.4 to 0.6 μm. This is a similar size range to the bead-like structures observed in the oxide coating on grains in the FBR.

The conditions within the FBR are not unlike those within a rapid sand filter, except that both sand and water are in motion in the FBR. Yao et al. (1971) described three mechanisms by which particles were removed in a rapid sand filter: interception and sedimentation for particles with diameters(d) > 1 μm, and diffusion for particles of d < 1 μm. They reported that removal efficiency was at a minimum for particles with d = 1 μm, but increased as size increased or decreased.

It seems reasonable to suggest that the sand grains in the FBR acted as particle collectors, and that the efficiency of the collection process was related to particle size. When particles grew too large (perhaps →1 μm), their removal by the sand grain surfaces diminished and turbidity in the reactor effluent increased. Higher shear forces exist in a fluidized bed than in a rapid sand filter bed, and may have led to a continued decrease in collector efficiency with increased particle size. Continuing surface precipitation of dissolved iron onto the attached particles may have resulted in consolidation of the particles, resulting in the coating pictured in the micrographs.
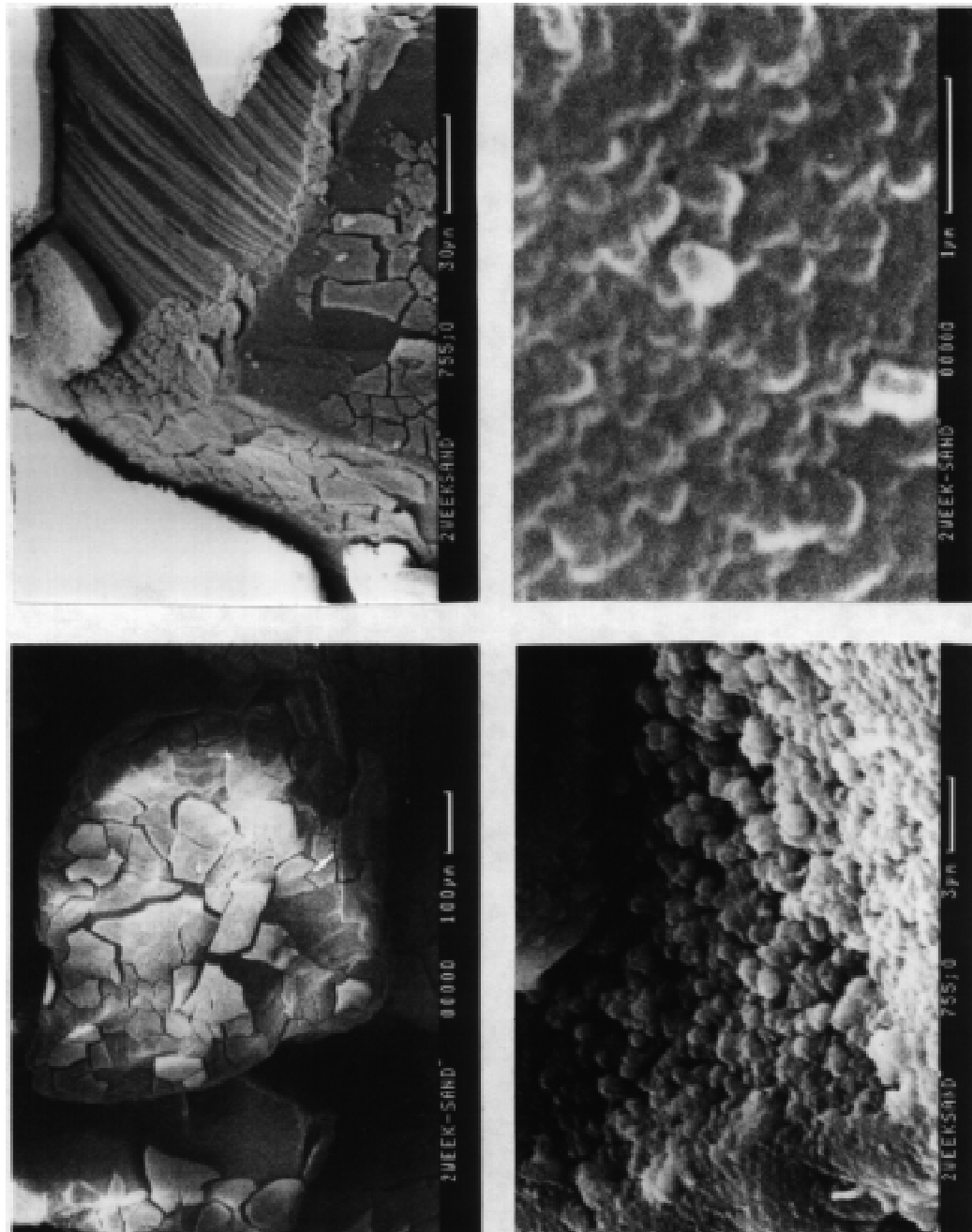
Figure 4.10. Scanning electron micrographs of oxide-coated sand which had remained in the FBR for 2 weeks. Cracking and scaling of coating are believed to be artifacts of preparation; after rotating page: top left micrograph is an individual sand grain, bar = 100 μm; top right is a close-up (bar = 30 μm) of the grain showing two layers of coating which have both become loosened from the underlying quartz grain; bottom left is a view of a protected area with individual beads attached to the grain and one another (bar = 3 μm); bottom right is a close-up (bar = 1 μm) of the surface of the coating, showing a consolidated bead-like structure.

CONCLUSIONS

The goal of this research was to design and evaluate a prototype multi-stage system to remove iron and acidity from acid mine drainage without the necessity for a sedimentation basin. It was found that the precipitation of iron could be controlled, with most of the iron being removed from solution as a coating on sand grains. The performance of the FBR was better when fed synthetically prepared solutions than when fed effluent from the bioreactor and alkaline water from a limestone bed, possibly due to particulate matter in those effluents. In the integrated system, 99% iron removal efficiency was achieved without the formation of iron hydroxide sludge, with effluent iron concentration remaining less than 3 mg L^{-1}, and pH >6.

Additionally, it was found that:

1. The optimum pH for iron removal while minimizing the concentration of particulate iron was about pH 3.5.
2. The maximum iron loading which minimizes suspended iron particle concentration while permitting maximum iron removal was about 0.20 mg Fe h^{-1} m^{-2} reactor surface area.
3. Particulates in the feed had an adverse impact on the removal performance of the system. Thus control of particulates entering the FBR should be an important design consideration.
4. The predominant mineral formed in the precipitation reactor appeared to be an iron sulfate oxyhydroxide mineral known as schwertmannite. It appeared likely that spherical particles formed in the bulk solution which were subsequently removed by attachment and consolidation onto the surface of the sand media.

LITERATURE CITED

APHA, AWWA, WEF. (1992) Standard Methods for the Examination of Water and Wastewater, 18th Edition. American Public Health Association. Washington, DC.

Bigham, J. M., L. Carlson, and E. Murad. 1994. Schwertmannite, a New Iron Oxyhydroxysulphate from Pyhasalmi, Finland, and Other Localities. Mineralog. Mag. 58:641-648.

Bigham, J. M., U. Schwertmann, S. J. Traina, R. L. Winland, and M. Wolf. 1996. Schwertmannite and the Chemical Modeling of Iron in Acid Sulfate Waters. Geochim. Cosmochim. Acta, 60(12):2111-2121.

Bourne, J.R. and R.J. Davey. 1976. J. Crystal Growth 36:278.

Dousma, J. and P.L. de Bruyn. 1979. Hydrolysis-Precipitation Studies of Iron Solutions. III. Application of Growth Models to the Formation of Colloidal αFeOOH from Acid Solutions. J. Colloid Interface Sci. 72(2):314-320.

Hedin, R. S. and G. R. Watzlaf. 1992. The Effects of Anoxic Limestone Drains on Mine Water Chemistry. Proceedings of the International Land Reclamation and Mine Drainage Conference, Pittsburgh, PA. April 24-26, 1994. Pp. 185-194.

Mullin, J. W. 1993. Crystallization, Third Edition. Butterworth-Heinemann Ltd., Oxford.

Murayama, T., Y. Konno, T. Sakata, and T. Imaizumi. 1987. Application of Immobilized *Thiobacillus ferrooxidans* for Large-Scale Treatment of Acid Mine Drainage. Meth. Enzymol. 36:530-49.

Scholler, M., J. C. van Dijk, and D. Wilms. Fluidized Bed Pellet Reactor to Recover Metals or Anions. Metal Finishing, November, 1991.

Schwertmann, U., and R.M. Cornell. 1991. Iron Oxides in the Laboratory: Preparation and Characterization. Verlagsgesellschaft mbH, Weinheim. pp.137.

Sokal, R. R. and F. J. Rolf. 1995. Biometry: The Principles and Practice of Statistics in Biological Research, 3rd Edition. W. H. Freeman and Company. New York.

Tarutis, Jr., W. J. and R. F. Unz. 1995. Iron and Manganese Release in Coal Mine Drainage Wetland Microcosms. Wat. Sci. Technol. 32(3):187-192.

Unz, R. F. and J. M. Dietz. 1986. Biological Applications in the Treatment of Acidic Mine Drainages. in Biotechnology for the Mining, Metal-Refining, and Fossil Fuel Processing Industries. H. L. Erhlich and D. S. Holmes, Eds. John Wiley & Sons, Inc. New York. pp. 163-170.

USEPA. 1976. Development Document for Interim Final Effluent Limitations Guidelines and New Source Performance Standards for the Coal Mining Point Source Category. EPA 440/1-76/057a. pp.288.

Vatcharapijarn, Y., B. Graves, and J. Bender. 1994. Remediation of Mining Water with Microbial Mats. in Emerging Technology for Bioremediation of Metals. J. L. Means and R. E. Hinchee, Eds. Lewis Publishers, Boca Raton. pp.124-129.

Walton, A. G. 1967. The Formation and Properties of Precipitates, Interscience, New York.

Walton, A. G. 1969. Principles of Precipitation of Fine Particles. In Dispersion of Powders in Liquids, G.D. Parfitt (ed.), Elsevier, Amsterdam.

Whitesell, Jr., L. ., R. L. Huddleston, and R. C. Allred. 1971. Microbiological Treatment of Acid Mine Waters. Water Pollution Control Research Series 14010 ENW 09/71, USEPA. p 78.

Wichlacz, P. L. and R. F. Unz. 1985. Growth Kinetics of Attached Iron-Oxidizing Bacteria. Appl. Environ. Microbiol. 50:460-467.

Wildeman, T. R., D. M. Updegraff, J. S. Reynolds, and J. L. Bolis. 1994. Passive Bioremediation of Metals from Water Using Reactors or Constructed Wetlands. in Emerging Technology for Bioremediation of Metals. J. L. Means and R. E. Hinchee, Eds. Lewis Publishers, Boca Raton. pp.13-25.

Wilms, D., K. Vercaemst, and J. C. Van Dijk. 1992. Recovery of Silver by Crystallization of Silver Carbonate in a Fluidized-Bed Reactor. Wat. Res. 26(2): 235-239.

Yao, K., M. T. Habibian, and C. R. O'Melia. 1971. Water and Waste Water Filtration: Concepts and Applications. Environ. Sci. Technol. 5(11): 1105-1112.

Chapter 5 . Heavy Metal Removal in an Innovative Treatment System for Acid Mine Drainage

INTRODUCTION

Heavy metals are frequently found in streams affected by acid mine drainage (AMD) which continues to be an important water pollution problem in regions of the United States and around the world. Current treatment technologies are either inadequate or too expensive to be employed at numerous abandoned mine land sites which are sources of untreated AMD. For example, limestone used for pH adjustment becomes coated with iron oxyhydroxide, reducing its solubility (Hedin and Watzlaf, 1992.). Constructed wetlands have sometimes been successful, but create metal-contaminated soils and potentially contaminate groundwater (Tarutis and Unz, 1995). The treatment employed for acidic iron wastewaters from active mines and certain industrial processes involves rapid neutralization with lime or caustic soda followed by sedimentation. The iron sludge created requires dewatering and has a high cost for ultimate disposal, particularly if classified as a hazardous waste.

This paper addresses the removal of certain heavy metals (Cu, Mn, Ni, and Zn) in a new process designed to remove iron and acidity from AMD and industrial wastewaters without the creation of metal hydroxide sludge. The reactor environment enhances the preferential formation of a surface coating while avoiding dispersed iron particles. Of considerable interest in this study was how various metals would behave in the series of environments which constitute the treatment system. Therefore, four metals (copper, manganese, nickel, and zinc) were selected due to differing chemical behavior and concerns about their presence in AMD and water supplies.

METHODOLOGY

Simulated Acid Mine Drainage

The feed solution, referred to as "simulated AMD", was prepared as given in Table 5.1 with tap water. The simulated AMD was allowed to sit at room temperature for at least 15 hours to allow chlorine to volatilize. Ferrous iron was then added from a stock solution (0.2 M ferrous sulfate acidified to $< $ pH 2.5 with nitric acid). Copper and zinc were added to the feed solution at final concentrations of approximately 1×10^{-4} M, nickel at about 2.5×10^{-4} M, and manganese at 1×10^{-3} M. Stock solutions of 0.02 M cuprous sulfate ($CuSO_4 \cdot 5H_2O$), manganous sulfate ($MnSO_4 \cdot H_2O$), nickel chloride ($NiCl_2 \cdot 6H_2O$), and zinc sulfate ($ZnSO_4 \cdot 7H_2O$) were prepared from Certified ACS reagent grade chemicals (Fisher Scientific).

Table 5.1. Simulated AMD (after pH adjustment to 2.3 with sulfuric acid).

Constituent	Molarity	mg L^{-1}
Iron	0.010	558
Aluminum	0.002	54
Calcium	0.002	80
Magnesium	0.001	24
Sodium	0.0075	175
Potassium	0.0005	20
Ammonium (as N)	0.0005	7
Sulfate	0.025	2400
Phosphate (as P)	0.0005	16

Inoculum

The microorganisms used in this study were obtained from an AMD site near Galax, Virginia, during January, 1996. Simulated AMD was inoculated with Galax sediments with mixing and aeration. Once the liquid became turbid, the sediment was discarded. Periodically, the culture was centrifuged and decanted, followed by replacement of the simulated AMD. During June, 1996, expanded polystyrene (EPS) beads of approx. 2-3 mm diameter were submerged in the culture medium with added feed and recirculation so as to begin development of a mineral coating. After about two months, a yellow coating later identified by x-ray diffraction to be jarosite $[(H,K,Na)Fe_3(OH)_6(SO_4)_2]$ appeared on the beads. Over time, this coating turned orange. Coated beads were maintained submerged in simulated AMD with either periodic or continuous feed of ferrous iron.

AMD Treatment system

The first stage of the treatment system (Figure 5.1) was a bioreactor of 1 L total volume, containing ~ 0.55 L of EPS beads coated with jarosite, an iron sulfato- hydroxide mineral, and iron-oxidizing microorganisms. The bacteria converted ferrous (Fe II) to ferric (Fe III) iron and utilized the energy available in this oxidation. Being lithotrophic, they used carbon dioxide as a sole carbon source, and thus required no extraneous nutrient solution. The drainable liquid volume in the bioreactor was 0.6 L. At a flow rate of 0.162 L/h, the detention time in the bioreactor was about 3.7 h.

The second treatment stage employed a fluidized bed reactor (FBR) for iron removal. It consisted of a 0.25 L column containing 200 g (about 0.15 L) of fine quartz sand (mean diameter: 0.6 mm, surface area assuming spheres: 3.6 m^2g^{-1}) with an external reservoir and pump for recirculation to fluidize the sand.

Effluent from the FBR flowed into the third stage, a calcium carbonate bed (CB) for pH neutralization. Liquid was recirculated from the discharge end of this bed back into the FBR by the pH control system. The CB had a total volume of 2 L, with a liquid volume of about 1 L. Since the FBR and the CB were hydraulically integrated by the pH control system, it was impossible to determine the detention time for each stage separately, but the total detention time for the FBR and the CB together was about 9 h.

Water was pumped from the discharge end of the CB into the final stage, where it trickled down through a coarse sand filled column (0.25 L) along with added caustic soda (NaOH) solution. In a full scale system, effluent from the trickling filter (TF) would be recirculated to the influent end of the CB. In order to simplify analysis during lab studies, effluent from the TF was not recirculated, but discharged as final effluent.
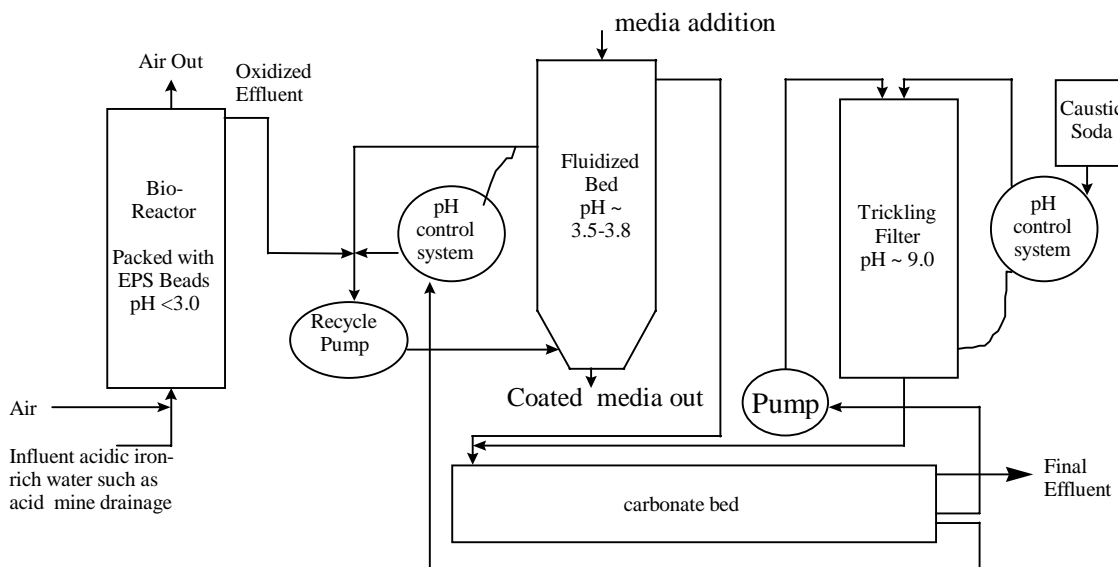

Figure 5.1. Schematic of a new multi-stage AMD treatment system.

Sampling and metal analysis

Samples were removed from each stage daily over a 8 day period after the system had stabilized (which took about 4 days) and diluted 1:10 with a sulfuric acid solution (0.1 N) to which had been added 0.5% hydroxylamine sulfate (NH_2OH). Samples were not filtered. Diluted samples were then allowed to remain at room temperature for at least a day and were checked for clarity before analysis. Total metals were assayed using acetylene-air flame atomic absorption spectrophotometry (Perkin-Elmer Model 703). Wavelengths used for each metal were: copper at 324.8 nm; manganese at 280.1 nm; nickel at 232 nm; and zinc at 213.9 nm. Standards prepared from stock solutions (1000 mg/L, Fisher Scientific) were used to calibrate the instrument and for quality control during and after analysis.

Statistical Methods and Calculations

Where appropriate, means and standard deviations were produced using the data analysis features of Microsoft Excel 7.0. These calculations were consistent with traditional methods as reported in the literature (Sokal and Rolf, 1995). The standard level of significance was set at $\alpha = 0.05$.

Hydrogen ion concentration

The mean pH of the stages of treatment were as follows: bioreactor - pH 2.5 with a standard deviation (sd.) of 0.2; FBR - pH 3.8 (sd. 0.16) ; CB - pH 6.4 (sd. 0.37); TF - pH 10.2 (sd. 0.30).

Iron

While iron removal is not the direct focus of this paper, an understanding of the fate of iron in the engineered system is helpful to understanding the behavior of the other metals. Essentially all (99%) of the iron in the feed solution was oxidized in the bioreactor. The mean total iron concentration of the feed solution was 279 mg/L (0.005 M) over the period, with the bioreactor effluent averaging 246 mg/L. There was a mean 94% removal of iron in the FBR over the period. The mean effluent iron concentration from the CB over this time period was 5 mg/L total iron (sd. 5.1, n = 7), for a removal of 98%. Iron was not analyzed in the TF effluent.

Copper

The mean value for copper in the feed solution was 5.4 mg/L (0.85×10^{-4} M). There was no removal within the bioreactor, but the FBR effluent copper value was 1.2 mg/L (sd. 0.2, n = 7), for a 79% removal at pH 3.8. The [Cu] decreased to a mean of 0.5 mg/L (sd. 0.3, n = 7) in the CB, and to 0.2 mg/L (sd. 0.02, n = 7) in the TF (Figure 5.2a and b).
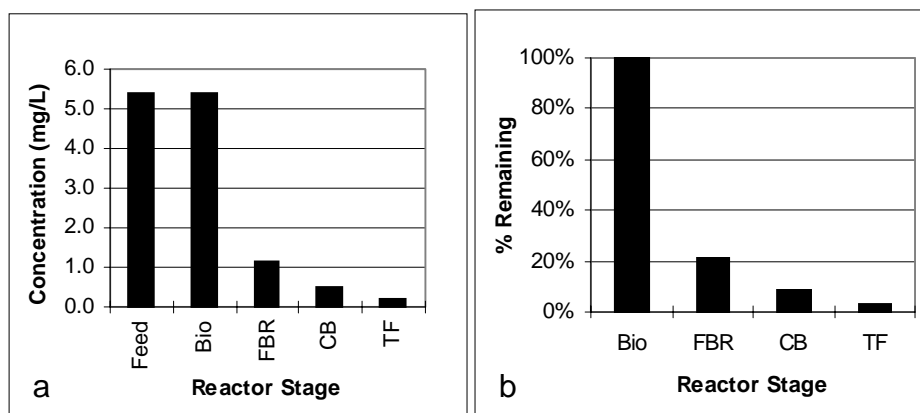

Figure 5.2 (a) Copper concentrations and (b) % copper remaining during multi-stage treatment of simulated AMD; Bio = bioreactor, FBR = fluidized bed reactor, CB = carbonate bed, and TF = trickling filter.

Manganese

There was no removal of manganese in the bioreactor stage of treatment. Average [Mn] in the feed was 60 mg/L (1.1×10^{-3} M), while mean FBR effluent [Mn] was 55.6 mg/L (sd. 1.3, n = 7), a removal of 7%. There was essentially no removal in the CB, but considerable removal in the TF at pH > 9, where mean effluent [Mn] was 2.4

mg/L (sd. 1.8, n = 7). Thus, 96% of the initial Mn had been removed (Figure 5.3a and b). The lowest final effluent [Mn] recorded was 0.2 mg/L.
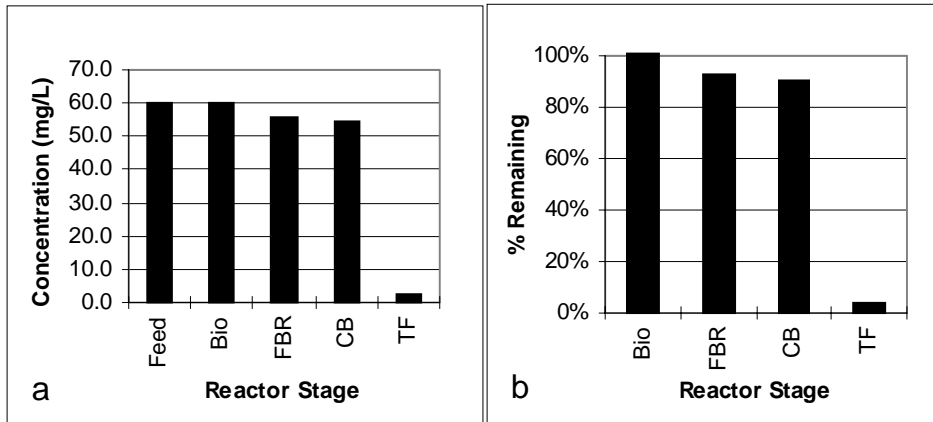

Figure 5.3. (a) Manganese concentration and (b) % manganese remaining during multi-stage treatment of simulated AMD; Bio = bioreactor, FBR = fluidized bed reactor, CB = carbonate bed, and TF = trickling filter.

Nickel

Nickel showed the lowest removals of all the metals evaluated. The nickel concentration steadily declined as the water flowed through each stage of the treatment following the bioreactor (Figure 5.4). The mean feed nickel concentration was 14.5 mg/L (2.5×10^{-4} M). The [Ni] declined by 9% after passing through the FBR, and then decreased to 59% of the original concentration (8.6 mg/L, sd. 1.4, n = 8) in the CB effluent. A further decline to 37% (5.3 mg/L, sd. 1.0, n = 8) of the original feed concentration occurred in the TF.
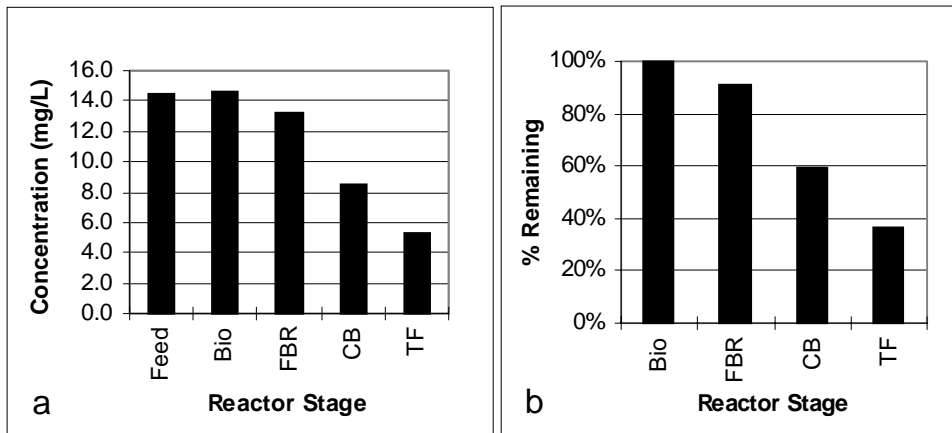

Figure 5.4. (a) Nickel concentration and (b) % nickel remaining during multi-stage treatment of simulated AMD; Bio = bioreactor, FBR = fluidized bed reactor, CB = carbonate bed, and TF = trickling filter.

Zinc

Feed solution [Zn] was 7.2 mg/L (1.1×10^{-4} M). Figure 5.5a and b show that there was a slight removal in the bioreactor (~ 2%), but the effluent concentration from the FBR decreased to 4.0 mg/L (sd. 0.8, n = 7), or 55% of the feed concentration. A further decrease in concentration occurred in the CB to 45% of the original strength. A final removal occurred in the TF, with a mean effluent [Zn] of 0.5 mg/L (sd. 0.3, n = 7), which was 6% of the original concentration.
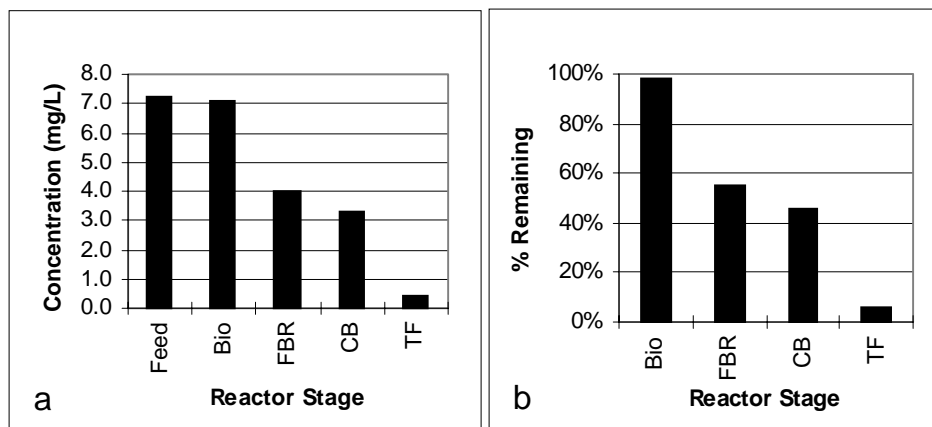

Figure 5.5a, b. (a) Zinc concentration and (b) % zinc remaining during multi-stage treatment of simulated AMD; Bio = bioreactor, FBR = fluidized bed reactor, CB = carbonate bed, and TF = trickling filter.

DISCUSSION

Iron Removal

The kinetics and chemistry of iron removal is to be the topic of another paper. In brief, the process was based on the observation that when less than the stoichiometric requirement of hydroxyl ions (assuming a formula of $Fe(OH)_3$) was added to an acidic ferric sulfate solution, precipitation was not instantaneous. The induction period ranged from seconds to hours, depending on the ratio of added hydroxyl ions to Fe (III) in solution. The length of the induction period was affected by the sulfate concentration, but was not affected by the presence of the cations Al (III) and Mn (II) (data not shown). Taking advantage of this delay phenomenon, it was possible to introduce the iron-rich solution into the fluidized bed reactor without the instantaneous formation of iron floc so long as the pH of the system was maintained in the proper range, and the flow regime did not allow for any hydraulic dead zones.

Copper Removal

The more oxidized Cu II ion tends to dominate in natural waters over the Cu I valence (Cotton and Wilkinson, 1988.). Copper forms complexes with many ligands, but in this treatment environment with relatively low organic matter, the most likely ligands for complexation are the hydroxyl and carbonate ions. Copper II solubility decreases with

increase in pH due to the formation of malachite ($Cu_2(OH)_2CO_3$) and tenorite (CuO), reaching a minimum solubility at about pH 11 (Figure 5.6). However, solubility considerations cannot explain why copper would decrease in the FBR, which was operated at a pH well within the solubility field of Cu II. Likely explanations would be sorption and/or surface precipitation. Surface precipitation is the result of the substitution of the foreign cation for the main metal (Fe III in this case) in the growing crystal structure.   A number of factors determine the likelihood of such substitution, including ionic radius and charge, rate of crystal surface growth, and degree of crystallinity (Stumm, 1992.). The concentration of Cu II in the CB is located just at the border of solubility and thus may be controlled by the solubility of malachite. The TF effluent contains more copper than would be predicted by solubility alone. Since the analysis of effluents was for total metals, it may be that most of the copper in the TF effluent was particulate, either sorbed to MnO_x particles or in the form of tenorite.
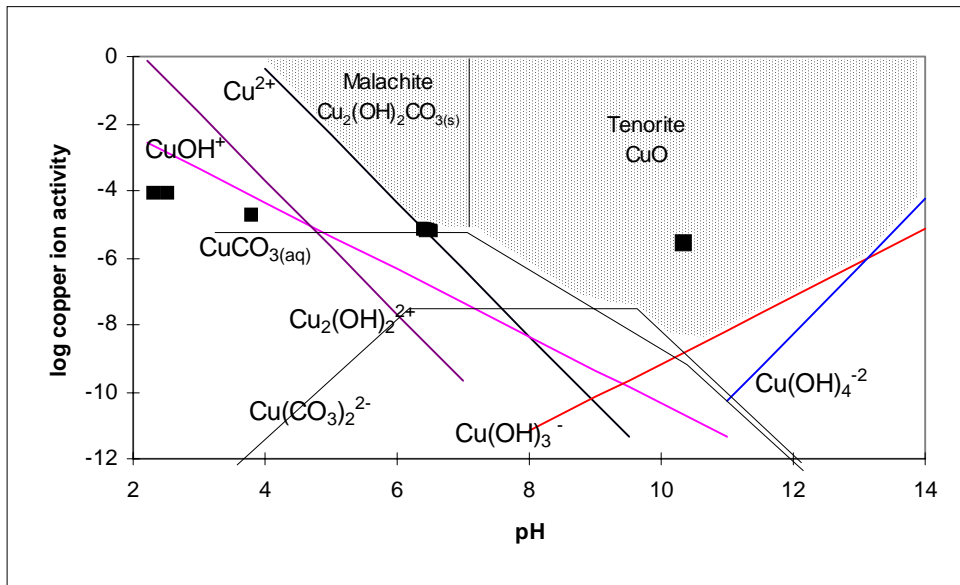

Figure 5.6. Copper solubility diagram. Black squares indicate copper concentration in various stages of treatment..

Manganese Removal

While manganese can theoretically exist in numerous oxidation states, only the II and IV valences are relatively stable in natural waters (Stumm and Morgan, 1970). Oxidation of the manganous ion (Mn II) is pH dependent, being quite slow below pH 9 even though thermodynamically favored. It also proceeds more rapidly when the ions become adsorbed to an MnO_x surface (Stumm and Morgan, 1970). Manganese forms oxides, hydroxides, or carbonates depending on pH and p$\in$ (Ehrlich, 1990). As can be seen in Figure 5.7a and b, there is little removal of manganese except in the TF, where high pH accelerates the oxidation of Mn II to Mn IV. Since this process is rapid above pH 9, and since Mn IV is essentially insoluble, it can be assumed that Mn removal is the result of oxidation and precipitation of manganese oxide. This phenomenon is important

to the performance of the TF stage since MnO_x surfaces are known to be strong scavengers of other heavy metals (Singh and Subramanian, 1986).
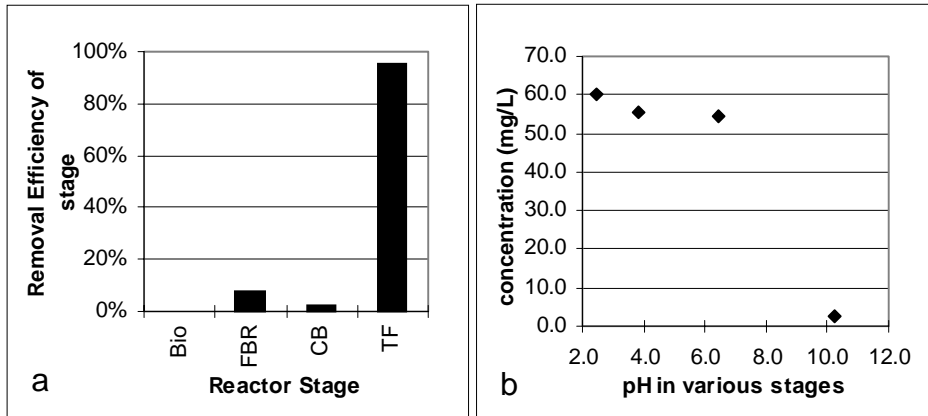

Figure 5.7a, b. (a) Manganese removal efficiency and (b) effluent manganese concentration as a function of pH in various stages of AMD treatment.

Nickel Removal

Among the predominant aqueous forms of nickel in natural waters (Morel and Hering, 1993), those of interest here are Ni^{2+} and $Ni(OH)_3^-$. As can be seen in the solubility diagram (Figure 5.8), the reduction in nickel concentration in the treatment system shown by the black squares corresponding to successive treatment stages can not be explained by the formation of nickel hydroxide below pH 7, where the dissolved forms should be soluble. At a pH above 10, the most efficient stage was the TF as shown in Figure 5.9. The measurement of metals in the TF effluent was for total metals, and may
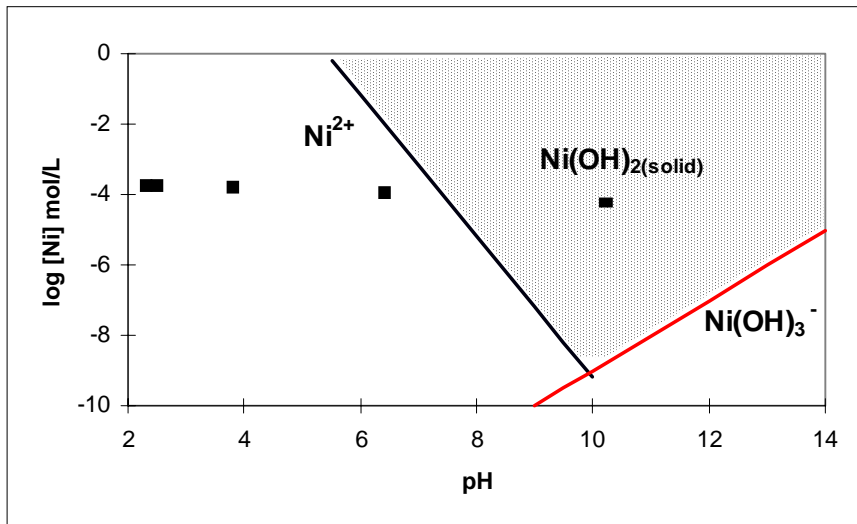

Figure 5.8. Nickel solubility as a function of pH. Black squares indicate [Ni] in various stages of AMD treatment. Equilibrium constants from Baes and Mesmer (1976).

82

explain the presence of nickel at a level higher than predicted by solubility constants for nickel species. With continued operation or different design, it may be possible to improve nickel removal based on its reported solubility.
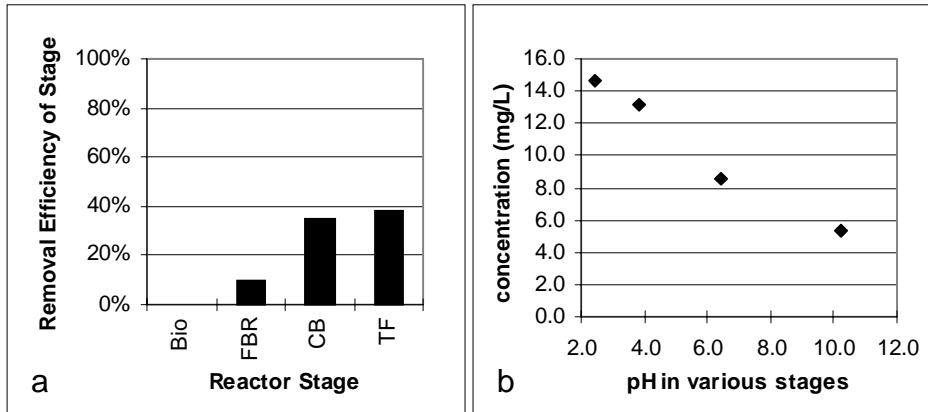

Figure 5.9a, b. (a) Removal efficiency for nickel and (b) effluent nickel concentration as a function of pH in various stages of AMD treatment.

Zinc Removal

Zinc forms complexes with numerous anions in aerobic natural waters, including Cl^-, SO_4^{2-}, OH^-, and CO_3^{2-} (Morel and Hering, 1993). Those which influence solubility are the carbonate and the hydroxyl ions. Below pH of about 7.5, zinc carbonate is the most insoluble form; as pH is increased, a hydroxy-carbonate mineral (hydrozincite) becomes controlling (Figure 5.10a).

The highest removal efficiency for zinc occurred in the TF, followed by the FBR, and then in the CB (Figure 5.10b). At the low pH of the FBR, sorption/surface precipitation to the growing oxide surface was the most likely mechanism for removal. The pH within the CB was too low (pH ~ 6) to result in the formation of zinc carbonate or hydrozincite and thus explain the decrease in zinc concentration in the CB. However, within the carbonate bed there probably existed locally high carbonate and pH zones in which hydrozincite may have formed. In the TF, hydrozincite solubility may have been the controlling factor since the solubility product of hydrozincite depends on $[OH^-]^6$ and $[CO_3^{2-}]^2$. Thus, NaOH added to the TF would have a pronounced effect on its formation.
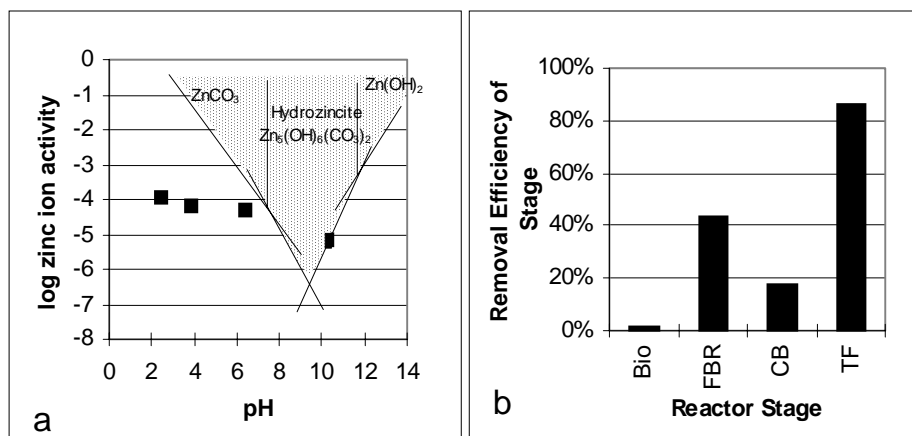
Figure 5.10a, b. (a) Zinc solubility (from [5]); black squares indicate experimental data. (b) Zinc removal efficiency in various stages of AMD treatment.

CONCLUSIONS

The lab-scale treatment system for the removal of metals and acidity from AMD achieved iron removal of better than 98% without the generation of metal hydroxide sludge. Removal efficiencies for other metals were 97% for copper, 96% for manganese, 70% for nickel, and 94% for zinc. The mechanism of removal for iron and manganese was by precipitation as the hydrous oxides, and it was speculated that the other metals were removed primarily by sorption onto either iron or manganese-oxide surfaces. The pilot-scale and full-scale performance of the system is yet to be determined. Further studies may provide insight into removal mechanisms for individual heavy metals which would lead to optimization strategies.

ACKNOWLEDGEMENT

LITERATURE CITED

Baes, C. F., Jr. and R. E. Mesmer. 1976. The Hydrolysis of Cations. Wiley. New York.

Cotton, f. A. and G. Wilkinson. 1988. Advanced Inorganic Chemistry, Fifth Edition. Wiley-Interscience, New York.

Ehrlich, H.L. 1990. Geomicrobiology, 2nd Edition. Marcel Dekker, Inc. New York.

Hedin, R. S. and G. R. Watzlaf. 1992. The Effects of Anoxic Limestone Drains on Mine Water Chemistry. Proceedings of the International Land Reclamation and Mine Drainage Conference, Pittsburgh, PA.

Morel, F.M.M. and J.G. Hering. 1993. Principles and Applications of Aquatic Chemistry. John Wiley & Sons, New York.

Singh, S. K., and V. Subramanian. 1986. Hydrous Fe and Mn Oxides: Scavengers of Heavy Metals in the Aquatic Environment. CRC Critical Reviews Environmental Control 14(1): 33-90.

Sokal, R. R. and F. J. Rolf. 1995. Biometry: The Principles and Practice of Statistics in Biological Research, 3rd Edition. W. H. Freeman and Company. New York.

Stumm, W. 1992. Chemistry of the Solid-Water Interface - Processes at the Mineral-Water and Particle-Water Interface in Natural Systems. John Wiley & Sons, Inc., New York.

Stumm, W. and J.J. Morgan. 1970. Aquatic Chemistry - An Introduction Emphasizing Chemical Equilibria in Natural Waters. Wiley Interscience, New York.

Tarutis, Jr., W. J. and R. F. Unz. 1995. Iron and Manganese Release in Coal Mine Drainage Wetland Microcosms. Water Science and Technology, 32(3):187-192.

Chapter 6 Summary

The goal of this research project has been to devise a new treatment technology for acid mine drainage (AMD). The need for this new technology exists because current approaches are either inadequate, impractical, or too expensive to be used at the source of AMD at abandoned mine lands (AML). Contaminated water continues to be discharged from many AML sites day after day with no treatment at all. The negative impact on the aquatic habitat is significant. The Commonwealth of Pennsylvania, for instance, has identified AMD as the number one water quality problem in its waters. While there are many dispersed releases of AMD from abandoned surface mines, there are typically a few localized point sources in each affected area which account for most of the mass of the pollution released. These sources are often of modest hydraulic flow but are quite concentrated, and once intermingled with adjacent waters contaminate the entire downstream aquatic system. Therefore, a point-source system may be useful in treating these polluted waters.

The new process presented in this dissertation is relatively simple in design and operation. The unit operations of the system include a bioreactor for the oxidation of ferrous iron, a fluidized bed reactor for the precipitation of iron onto the surfaces of seed particles, and a trickling filter for the oxidation and precipitation of manganese at high (>9) pH, with final neutralization of the effluent by passage through a calcium carbonate bed. There is a removal of heavy metals (Cu, Ni, Zn were evaluated) at various stages in the system. The technology avoided the generation of iron sludge and the necessity for sedimentation basins. Other than electrical power to operate the system, the only maintenance requirements would be the replacement of sand media in the fluidized bed, the periodic replenishment of the concentrated caustic soda (NaOH) for the trickling filter stage, and the addition of limestone (or dolomite) to the carbonate bed. The requirement for caustic soda would be much lower than in conventional treatment, since most of the acid-neutralizing power is provided by the carbonate bed, a much cheaper source of alkalinity. Also, when the water reaches the trickling filter, there is little buffer capacity left. Thus, the consumption of caustic soda would be low since relatively little would be required to increase the pH from about 7 to above 9. An additional cost and operational advantage is that it would not be necessary to remove the iron-coated sand from the site unless there was some productive use for it elsewhere. It is, after all, simply rust-coated sand, and in this form poses no threat to aquatic life.

The study found that the performance of the bioreactor (Chapter 2) could be predicted with a relatively simple set of kinetic expressions. For design purposes, a detention time of about 0.5 to 1 h (dilution rate = 1 to 2 h^{-1}) would be sufficient to oxidize essentially all of the influent ferrous iron (up to a concentration of 10 mM). Depending on the specific AMD characteristics of the site, the detention time could possibly be even shorter. The bacteria which inhabit the system are naturally occurring, grow slowly, require no artificial input of nutrients, and produce very little biomass. Thus, the disposal of biomass would not appear to be necessary. Since the oxidation rate was affected by

dissolved oxygen (DO) concentration, the aeration system would need to be properly sized to maintain DO at a minimum of about 2 mg L^{-1}. Since temperature did have a major impact on rates, it would be important to maintain the reactor temperature as high as practical,. If the system could be located close to where the AMD emerged from below ground (at the mean annual sub-surface temperature), reactor temperature would probably remain in an acceptable range. Otherwise, supplemental heating might be necessary.

Iron loading to the fluidized bed reactor was the most important design parameter. Sufficient surface area (a function of the mass and diameter of seed sand grains) would be required to prevent iron loading from exceeding 0.20 mg Fe m^{-2} h^{-1}. Above this loading, dispersed iron particulates formed, resulting in a turbid effluent. The limiting loading rate was probably a function of the collector efficiency of the seed particles and the growth rate of the particles after being exposed to the reactor environment.

Based on precipitation rate studies in ferric sulfate solutions (Chapter 3), a detention time of less than 1 h within the fluidized bed would result in a dissolved iron concentration of less than 10 mg L^{-1} at pH 3.5. Particulates in the influent may cause effluent iron to be higher than this value.

While the minimum iron concentration in the effluent was determined by pH as reported in Chapter 3, the solubility and rate of precipitation of iron is closely related to the sulfate concentration and the initial iron concentration itself. The multiple regression expression (multiple $R^2 = 0.84$) was

$$\log t_{ind} = 6.7(\pm 0.30) - 1.29(\pm 0.10)\text{pH} + 0.94(\pm 0.07)\log [SO_4] - 0.36(\pm 0.05)\log[Fe]$$

Site-specific AMD characteristics would therefore influence the optimal operating values for the system. Below the optimal pH value, the dissolved iron concentration increased in a clear effluent; above this value, a turbid effluent developed due to the presence of particulate iron. Due to the limitations imposed by laboratory-scale vessels, it was not possible to fully investigate the proper positioning of the injection points for the oxidized-iron feed stream or the point of addition of the base solution. Further testing during pilot-scale studies would establish the best location for each fluid injection to optimize iron precipitation onto the sand grains.

The automated addition of seed particles and their removal after having grown too dense to remain fluidized were not addressed in this study. These issues would be important components of pilot-scale research. Also not investigated were alternatives to sand as the seed particles. It is conceivable that particles such as polyethylene beads could serve as seeds. In such a case, the fluidization would necessarily be in a downward direction since plastic beads are less dense than water. With appropriate downward fluid velocity, plastic beads which had achieved a target density due to accumulated iron could be ejected from the main reactor and trapped in a secondary chamber for subsequent removal.

Iron remaining in the fluidized bed effluent was largely removed in the carbonate bed, and a final effluent iron concentration of less than 3 mg/L was routinely produced.

Alternative configurations for the carbonate bed and the detention time within it were not thoroughly investigated in this study.

As discussed in Chapter 5, certain heavy metals (Cu, Ni, and Zn) were removed in the fluidized bed reactor as well as in the trickling filter, where pH >9 caused manganese to oxidize and precipitate (96% removal); removals of copper, nickel, and zinc (initial concentrations ranging from 5 to 15 mg L^{-1}) appeared to be due primarily to sorption onto oxide surfaces. Removals averaged 97% for copper, 70% for nickel and 94% for zinc. During pilot-scale studies, more information could be obtained relating to the configuration of the trickling filter and the optimization of its performance.

It is also conceivable that this system could be employed to remove heavy metals in wastewaters which are not rich in iron and/or manganese. Low concentrations of iron, manganese, and acid could be added to the influent at a rate just sufficient to slowly generate new oxide surfaces. The alternating environments of low pH in the fluidized bed and high pH in the trickling filter would provide a combination of environments which would strongly sorb both anions and cations, in a fashion similar to sequential anion/cation -exchange resins. Several toxic elements form oxyanions, such as arsenate, selenate and chromate, and may be efficiently removed in the fluidized bed where iron oxides at low pH would have positively charged surfaces. Cationic heavy metals would be strongly attracted to the negatively charged MnO_x surfaces of the trickling filter. A drawback to ion-exchange resins is that they require periodic regeneration by flushing with concentrated saline or acid/base solutions, thus creating contaminated backwash waters. This new treatment system would not require such a step. For example in the case of the removal of radionuclides from low-level radioactive wastewaters, this new process might operate over long periods of time without the generation of radioactive backwash waters. Since the additions of iron and manganese would be modest, the seed particles also might not require replacement over long periods.

Although it is difficult to scale-up from lab-scale studies, it is estimated that for pilot-scale studies to treat an AMD source with 500 mg L^{-1} ferrous iron at a flow rate of about 7.5 L min^{-1} (2,880 gpd), the bioreactor could be a 375 L (100 gal) tank reactor containing about 250 L of beads and holding about 225 L of liquid, for a 30 min detention time. The FBR would be a 750 L vessel (about 200 gal) for a 1 h detention time, with the CB twice that volume at 1,500 L. It is difficult to estimate the size of the TF at this time, but a volume about equal to the TF would probably be sufficient. With associated controls, pumps, and piping, the entire system would occupy a space of about 2.5 m x 4 m (about 8 by 12 ft).

The feasibility of this technology for AMD is yet to be established but it offers the promise of a compact economical treatment technology suitable for AMD seeps, drainage from acidic tailings ponds, active mine effluent, and acidic iron-rich industrial wastewater. Its applicability to other contaminated waters is yet to be investigated, but it is the hope of the author that sufficient interest by potential research sponsors will allow further investigation of this new technology at both AML sites, at active mining sites, and with other contaminated waters of great concern to society.

Chapter 7 Vita

Harry R. Diz was graduated from Duke University in Durham, North Carolina, with an A.B. in zoology. After several years as a secondary school science teacher, he entered graduate school at Northern Arizona University in Flagstaff, Arizona, where he earned a Master of Arts degree in teaching biology. He returned to high school teaching until leaving academia to enter business. After achieving his business career goals by serving as President and CEO of a multi-location construction materials manufacturing and distribution company, he returned to graduate school and earned a Master of Science degree in environmental engineering, an ABET accredited program at Virginia Polytechnic Institute and State University in 1994 and continued study there, earning a Doctor of Philosophy degree in Civil Engineering in 1997.

Dr. Diz passed the Fundamentals of Engineering examination in the spring of 1994. His academic awards include election to Chi Epsilon, the national civil engineering honor society, Phi Kappa Phi, a national academic honor society, and selection by the United States Environmental Protection Agency for a doctoral fellowship in the inaugural year of their Science to Achieve Results (STAR) Graduate Fellowship program.